

Interactions of air quality and climate: Consequences of US emission controls

A dissertation presented

by

Eric M. Leibensperger

to

The School of Engineering and Applied Sciences

in partial fulfillment of the requirements
for the degree of
Doctor of Philosophy
in the subject of
Applied Physics

Harvard University
Cambridge, Massachusetts

April 2011

© 2011 by Eric M. Leibensperger

All rights reserved.

Dissertation Advisor

Author

Professor Daniel J. Jacob

Eric M. Leibensperger

Interactions of air quality and climate: Consequences of US Emission Controls

Abstract

This thesis applies global chemical transport (CTM) and general circulation models (GCM), along with chemical and meteorological observations, to investigate the interactions between US air quality and climate.

The frequency of summertime mid-latitude cyclones tracking across eastern North America at 40-50°N is shown to be a strong predictor of stagnation and ozone pollution days in the eastern United States. Analyses of the NCEP/NCAR Reanalysis dataset, NASA Goddard Institute for Space Studies (GISS) GCM simulations, and daily weather maps show a significant long-term decline in the number of summertime cyclones in this track starting in 1980 (-0.15 a^{-1}). Using observed correlations between ozone pollution days and cyclone frequency, it is shown that this trend has offset by half the ozone air quality gains in the northeastern US from reductions in anthropogenic emissions. Without this trend in cyclones the northeastern US would have been largely compliant with the ozone air quality standard by 2001.

Aerosol distributions derived from the GEOS-Chem CTM using historical and projected emissions are used with the NASA GISS GCM to estimate the radiative forcing and

climate effects of US anthropogenic aerosols. Aerosol forcing in the eastern US peaked in 1970-1990 (direct effect: -2.0 W m^{-2} ; indirect effects: -2.0 W m^{-2}) and has strongly declined since then due to air quality regulation. This regional radiative forcing is found to elicit a strong regional climate response, cooling the central and eastern US by $0.5\text{-}1.0^\circ\text{C}$ on average during 1970-1990. Aerosol cooling reduces surface evaporation and thus decreases precipitation along the US east coast, but increases the southerly flow of moisture from the Gulf of Mexico resulting in increased cloud cover and precipitation in the central US. Observations over the eastern US show a lack of warming in 1960-1980 followed by very rapid warming, which is attributed here to trends in US anthropogenic aerosol sources. It is shown that US aerosol concentrations are by now sufficiently low that projected air quality regulations will cause little further warming (0.1°C over 2010-2050). Most of the potential warming from aerosol source controls in the US has thus already been realized.

In an additional study, it is shown that anthropogenic emissions of nitrogen oxides ($\text{NO}_x \equiv \text{NO} + \text{NO}_2$) and carbon monoxide (CO) affect particulate matter (PM) air quality on an intercontinental scale by changing background concentrations of oxidants (OH, ozone, H_2O_2) and thus the local oxidation rate of SO_2 to sulfate and NO_x to nitrate. Simulations with GEOS-Chem reveal that the intercontinental influences of NO_x and CO emissions on PM can be greater than those from SO_2 emissions (the direct PM precursor). Effects are largest (up to $0.3 \mu\text{g m}^{-3}$) in receptor regions with large domestic SO_2 , NO_x , and ammonia emissions and hence already high concentrations of PM.

Contents

Abstract	iii
Table of Contents	v
List of Figures	vii
List of Tables	ix
Citations to Previously Published Work	x
1 Overview	1
1.1 Effect of Climate Change on Air Quality	2
1.2 Effect of Air Pollutants on Climate	3
1.3 Summary of Results	4
Bibliography	6
2 Sensitivity of US air quality to mid-latitude cyclone frequency and implications of 1980-2006 climate change	9
2.1 Introduction	10
2.2 Data and methods	13
2.2.1 Detection and tracking of mid-latitude cyclones	13
2.2.2 Detection of stagnation episodes	18
2.2.3 Surface ozone data	19
2.2.4 GCM simulations	21
2.3 Mid-latitude cyclones as predictors of stagnation and ozone pollution	22
2.4 Long-term trends in mid-latitude cyclone frequency and ozone pollution	24
2.5 Effect of 1980-2006 climate change on ozone air quality	27
2.6 Conclusions	29
Bibliography	32
3 Intercontinental influence of NO_x and CO emissions on particulate matter air quality	37
3.1 Introduction	38
3.2 Model simulations	39
3.3 Intercontinental PM enhancements	43
3.3.1 Effect of US emissions	43

3.3.2	Effect of Asian emissions	46
3.4	Discussion	49
	Bibliography	50
4	Climatic effects of 1950-2050 changes in US anthropogenic aerosols	
	Part 1: Aerosol trends and radiative forcing	56
4.1	Introduction	57
4.2	Methods	59
4.2.1	Global aerosol simulation	59
4.2.2	Direct aerosol radiative forcing	63
4.2.3	Indirect aerosol radiative forcing	64
4.3	Evaluation of 1980-2010 US aerosol trends	66
4.4	Aerosol direct radiative forcing from US anthropogenic sources	75
4.5	Aerosol indirect radiative forcing from US anthropogenic sources	79
4.6	Conclusions	81
	Bibliography	83
5	Climatic effects of 1950-2050 changes in US anthropogenic aerosols	
	Part 2: Climate Response	91
5.1	Introduction	92
5.2	Methods	95
5.2.1	Aerosol simulations	95
5.2.2	Climate simulations	96
5.3	Climate response to US anthropogenic aerosols	100
5.3.1	Radiation	100
5.3.2	Temperature	102
5.3.3	Hydrology and dynamics	107
5.4	Aerosol effects on 1950-2050 trends in US surface air temperature	110
5.5	Conclusions	114
	Bibliography	117

List of Figures

2.1	Evolution of surface ozone during a mid-latitude cyclone passage	11
2.2	July climatology of North American mid-latitude cyclones	15
2.3	Summertime mid-latitude cyclone tracks in eastern North America	16
2.4	Time series of summer mid-latitude cyclone frequency in the southern North American climatological storm track	17
2.5	Average number of summertime stagnant days in the US	19
2.6	Average number of summertime ozone pollution days in the US	20
2.7	Interannual correlation between mid-latitude cyclones, stagnation days, and ozone pollution	23
2.8	1948-2006 time series of mid-latitude cyclones	24
2.9	Long-term trend and correlation of ozone pollution days and mid-latitude cyclones	26
2.10	Observed and climate change-corrected 1980-2006 time series of ozone pollution days	28
3.1	Annual mean enhancement of surface PM in Europe and Asia from US anthropogenic SO ₂ , NO _x , and CO emissions	42
3.2	Speciation and seasonality of sulfate-nitrate-ammonium enhancements in Europe and China from US anthropogenic SO ₂ , NO _x , and CO emissions .	44
3.3	Annual mean enhancement of surface PM in North America and Europe from Asian anthropogenic SO ₂ , NO _x , and CO emissions	47
3.4	Speciation and seasonality of sulfate-nitrate-ammonium enhancements in North America and Europe from US anthropogenic SO ₂ , NO _x , and CO emissions	48
4.1	Global and US trends in SO ₂ , NO _x , BC, and POA emissions	61
4.2	Simulated and observed 1980-2010 sulfate wet deposition fluxes and surface air concentrations	67
4.3	Simulated and observed trends of wet deposition fluxes and surface air concentrations	69
4.4	Simulated and observed 1980-2010 ammonium wet deposition fluxes and surface air concentrations	70

4.5	Simulated and observed 1980-2010 nitrate wet deposition fluxes and surface air concentrations	72
4.6	Simulated and observed black carbon and organic carbon surface air concentrations	74
4.7	Spatial distribution of radiative forcing of 1980 US anthropogenic aerosols .	76
4.8	Time series of the aerosol direct and indirect radiative forcing of US anthropogenic aerosols	77
4.9	Change in cloud properties due to US anthropogenic aerosols	80
5.1	Observed 1930-1990 change in annual mean temperature in the US	93
5.2	Changes in net TOA and surface solar radiation due to US anthropogenic aerosol sources	100
5.3	Changes in annual mean surface air and 500 hPa temperature due to US anthropogenic aerosol sources	103
5.4	Change in US annual mean surface air temperature due to US anthropogenic aerosol sources	105
5.5	Seasonal changes in mid-Atlantic US surface air temperatures due to US anthropogenic aerosol sources	106
5.6	Change in hydrological quantities due to US anthropogenic aerosols	108
5.7	Change in summer mean 850 geopotential height due to US anthropogenic aerosols	109
5.8	Change in annual mean mid-Atlantic surface air temperature due to US anthropogenic aerosols	111
5.9	1950-2050 trends in annual mean surface air temperatures over the mid-Atlantic US	112

List of Tables

4.1	Global mean cloud properties	78
5.1	Trends in surface air temperature in the mid-Atlantic US	113

Citations to Previously Published Work

Chapters 2 and 3 have appeared previously in the following papers:

Leibensperger, E. M., Mickley, L. J., Jacob, D. J. (2008). Sensitivity of US air quality to mid-latitude cyclone frequency and implications of 1980-2006 climate change, *Atmos Chem and Phys*, 8(23):7075-7086.

Leibensperger, E. M., Mickley, L. J., Jacob, D. J., Barrett, S. R. H. (in press). Intercontinental influence of NO_x and CO emissions on particulate matter air quality, *Atmospheric Environment*.

Chapter 1

Overview

Increasing energy consumption has driven global economic growth and development. The combustion of fossil fuels, mainly coal, oil, and natural gas has provided most of this energy, while unintentionally emitting pollutants that have instigated global climate change and air quality degradation. Climate change and air quality problems thus have a common source: fossil fuel combustion. However, these concurrent environmental problems additionally influence each other. Surface air pollutant concentrations are influenced by local meteorology, which control pollutant chemistry and transport. Anthropogenic climate change is expected to alter many of the air quality relevant meteorological parameters (Jacob and Winner, 2009; Weaver et al., 2009). These same air pollutants affect the climate system by enhancing the greenhouse effect, scattering solar radiation, and modifying cloud properties (Forster et al., 2007).

Ongoing emission regulations have significantly improved air quality in the US over the last 30 years (US Environmental Protection Agency (US EPA), 2010). In the same period, the climate of the US has experienced 0.8°C of warming (Hansen et al., 2010). This

thesis uses observations and models of global composition and climate to better understand the efficacy of recent emission reductions given recent climate change and to quantify the influence of air quality pollutants on recent observed US climate change.

1.1 Effect of Climate Change on Air Quality

The main air pollutants in the US are ozone and particulate matter (PM; US EPA, 2010). The chemical formation of both pollutants is sensitive to changes in temperature and humidity, while circulation patterns affect the export of pollution from the boundary layer. Pollution episodes in the eastern US are typically associated with stagnant air masses and warm, cloud-free conditions (Logan, 1989). The cold front of a migrating mid-latitude cyclone terminates a pollution episode by ventilating the boundary layer and replacing the air mass with cooler, cleaner air (Cooper et al., 2001; Li et al., 2005). Simulations of 21st-century climate change have found a reduction in the frequency of mid-latitude cyclones. Such decreases have been shown to negatively affect US air quality (Mickley et al., 2004; Murazaki and Hess, 2006; Wu et al., 2008), an effect termed the climate change penalty on air quality.

When I began my thesis, no study had quantified the effects of the rapidly changing US climate on air quality mitigation strategies. Previous studies had identified a decreasing trend in mid-latitude cyclones in the observational record for winter (Zishka and Smith, 1980; McCabe et al., 2001; Wang et al., 2006), but no study had determined the trend in summertime cyclones relevant to US ventilation or quantified from observations the sensitivity of US air quality to mid-latitude cyclone frequency. To better understand the effect of climate on air quality and improve constraints on the projected climate change

penalty for air quality, I addressed the following questions:

- What cyclone track is of most importance for ventilation of the eastern US?
- Has there been a trend in summertime mid-latitude cyclones in that track, and can it be related to increasing greenhouse gases?
- What is the impact of this trend on air quality?

I answered these questions by using correlated observations of surface ozone and meteorological variables, together with GCM simulations.

1.2 Effect of Air Pollutants on Climate

Aerosols directly affect the climate system by scattering and absorbing solar radiation, and indirectly by altering cloud microphysical properties. The net effect is to cool the surface. The cooling effect of anthropogenic aerosols has partly mitigated 20th-century greenhouse warming (Hegerl et al., 2007). In the US, aerosol concentrations rose in the 20th-century, peaked in the 1980s, and have been decreasing rapidly since due largely to a 56% reduction of SO₂ emissions between 1980 and 2008 to improve air quality (PM; US EPA, 2010). Thus the US provides an interesting testbed to examine the unintended regional climate response from air quality regulations. My work addressed the following questions:

- What is the climate impact of US anthropogenic aerosols? Is the impact localized to the US or does it extend throughout the Northern Hemisphere?
- What impact have trends in US anthropogenic aerosols had on the climate of the US?

I answered these questions by using the GEOS-Chem CTM to simulate 1950-2050 time series of aerosol distributions and radiative forcing with and without US anthropogenic

aerosol sources. The aerosol distributions were used to conduct 1950-2050 transient-climate simulations with the NASA Goddard Institute for Space Studies (GISS) GCM 3 in order to isolate the effect of US anthropogenic aerosols. I used these simulations to investigate the regional climate effects of historical and projected changes in US anthropogenic aerosol sources, and compared to the long-term observational record.

1.3 Summary of Results

In Chapter 2, I show that the frequency of summertime mid-latitude cyclones tracking across eastern North America at 40-50°N (the southern climatological storm track) is a strong predictor of stagnation and ozone pollution days in the eastern United States. I analyze data from the NCEP/NCAR Reanalysis and daily weather maps from NOAA to identify a significant long-term decline in the number of summertime mid-latitude cyclones in the southern climatological track starting in 1980 (-0.15 a^{-1}). A GISS GCM simulation including historical forcing by greenhouse gases reproduces this decreasing cyclone trend starting in 1980. I find that such a long-term decrease in mid-latitude cyclone frequency over the 1980-2006 period may have offset by half the ozone air quality gains in the northeastern US from reductions in anthropogenic emissions. I show that if mid-latitude cyclone frequency had not declined, the northeastern US would have been largely compliant with the ozone air quality standard by 2001.

Chapter 3 presents the results of a side project in which I analyzed the intercontinental effects of NO_x and CO emissions on PM air quality. I find that anthropogenic emissions of NO_x and CO affect PM air quality on an intercontinental scale by changing background concentrations of oxidants (OH , ozone, H_2O_2) and thus increasing the oxidation rate of sulfur dioxide (SO_2) to sulfate and NO_x to nitrate. I use sensitivity simulations with the

GEOS-Chem chemical transport model to show that these intercontinental influences of NO_x and CO emissions on PM can be greater than those from SO_2 emissions (a direct PM precursor). I find that the intercontinental impact of oxidant precursors is greatest in receptor regions with high domestic SO_2 , NO_x , and ammonia emissions and hence already high levels of PM. US NO_x and CO emissions increase annual mean PM in northern Europe and eastern China by up to $0.25 \mu\text{g m}^{-3}$. The increase in Europe is mostly as sulfate, whereas in China it is mostly as nitrate. East Asian NO_x and CO emissions have a weaker intercontinental influence ($0.2 \mu\text{g m}^{-3}$ in northern Europe, $0.1 \mu\text{g m}^{-3}$ in the eastern US).

In Chapter 4, I use the GEOS-Chem CTM combined with the GISS GCM to calculate the aerosol direct and indirect (cloud) radiative forcings from US anthropogenic sources over the 1950-2050 period, based on historical emission inventories and future projections from the IPCC A1B scenario. I evaluate the aerosol simulation with observed spatial distributions and 1980-2010 trends of aerosol concentrations and wet deposition in the contiguous US. I find that the radiative forcing from US anthropogenic aerosols is strongly localized over the eastern US and peaked in 1970-1990, with values over the eastern US (east of 100°W) of -2.0 W m^{-2} for direct forcing including contributions from sulfate (-2.0 W m^{-2}), nitrate (-0.2 W m^{-2}), organic carbon (-0.2 W m^{-2}), and black carbon ($+0.4 \text{ W m}^{-2}$). The aerosol indirect effect is of comparable magnitude to the direct forcing. I find that the forcing declined sharply from 1990 to 2010 (by 0.8 W m^{-2} direct and 1.0 W m^{-2} indirect), mainly reflecting decreases in SO_2 emissions, and project that it will continue declining post-2010 but at a much slower rate since US SO_2 emissions have already declined by almost 60% from their 1980 peak. This suggests that much of the warming effect from reducing US anthropogenic aerosol sources may have already been realized. The small positive radiative forcing from US BC emissions ($+0.3 \text{ W m}^{-2}$ over the eastern

US in 2010) suggests that an emission control strategy focused on BC would have only limited climate benefit.

Chapter 5 presents the results from climate simulations using the aerosol and radiative forcing distributions of US anthropogenic aerosols analyzed in Chapter 4. I find that the regional radiative forcing from US anthropogenic aerosols elicits a strong regional climate response, cooling the central and eastern US by 0.5-1.0°C on average during 1970-1990, with the strongest effects on maximum daytime temperatures in summer and fall. Aerosol cooling is evenly split between direct and indirect radiative effects. Absorbing aerosols (mainly black carbon) have little offsetting effect. Aerosol cooling reduces surface evaporation and thus decreases precipitation along the US east coast, but also increases the southerly flow of moisture from the Gulf of Mexico resulting in increased cloud cover and precipitation in the central US. Observations over the eastern US show a lack of warming in 1960-1980 followed by very rapid warming since, and we attribute this to trends in US anthropogenic aerosol sources. Present US aerosol concentrations are sufficiently low that future air quality regulations are projected to cause little further warming (0.2°C over 2010-2050). I find that most of the potential warming from aerosol source controls in the US has in fact already been realized.

Bibliography

- Cooper, O., Moody, J., Parrish, D., Trainer, M., Ryerson, T., Holloway, J., Hubler, G., Fehsenfeld, F., Oltmans, S., and Evans, M. (2001). Trace gas signatures of the airstreams within North Atlantic cyclones: Case studies from the North Atlantic Regional Experiment (NARE '97) aircraft intensive. *J Geophys Res-Atmos*, 106(D6):5437–5456.
- Forster, P., Ramaswamy, V., Artaxo, P., Berntsen, T., Betts, R., Fahey, D. W., Haywood, J., Lean, J., Lowe, D. C., Myhre, G., Nganga, J., Prinn, R., Raga, G., Schulz, M., and Dorland, R. V. (2007). *Climate Change 2007: The Physical Science Basis*, chapter

- Changes in Atmospheric Constituents and in Radiative Forcing. Cambridge University Press.
- Hansen, J., Ruedy, R., Sato, M., and Lo, K. (2010). Global surface temperature change. *Rev Geophys*, 48(4):RG4004.
- Hegerl, G. C., Zwiers, F. W., Braconnot, P., Gillett, N. P., Luo, Y., Orsini, J. A. M., Nicholls, N., Penner, J. E., and Stott, P. A. (2007). *Climate Change 2007: The Physical Science Basis*, chapter Understanding and Attributing Climate Change. Cambridge University Press.
- Jacob, D. and Winner, D. (2009). Effect of climate change on air quality. *Atmos Environ*, 43(1):51–63.
- Li, Q., Jacob, D. J., Park, R. J., Wang, Y., Heald, C. L., Hudman, R., Yantosca, R. M., Martin, R. V., and Evans, M. (2005). North American pollution outflow and the trapping of convectively lifted pollution by upper-level anticyclone. *J Geophys Res-Atmos*, 110(D10):D10301.
- Logan, J. (1989). Ozone in rural areas of the United States. *J Geophys Res-Atmos*, 94(D6):8511–8532.
- McCabe, G., Clark, M., and Serreze, M. (2001). Trends in Northern Hemisphere surface cyclone frequency and intensity. *J Climate*, 14(12):2763–2768.
- Mickley, L., Jacob, D., Field, B., and Rind, D. (2004). Effects of future climate change on regional air pollution episodes in the United States. *Geophys Res Lett*, 31(24):1–4.
- Murazaki, K. and Hess, P. (2006). How does climate change contribute to surface ozone change over the United States? *J Geophys Res-Atmos*, 111(D5):D05301.
- US Environmental Protection Agency (2010). *Our Nation's Air - Status and Trends Through 2008*. Washington, DC.
- Wang, X. L., Wan, H., and Swail, V. R. (2006). Observed changes in cyclone activity in Canada and their relationships to major circulation regimes. *J Climate*, 19(6):896–915.
- Weaver, C. P., Liang, X. Z., Zhu, J., Adams, P. J., Amar, P., Avise, J., Caughey, M., Chen, J., Cohen, R. C., Cooter, E., Dawson, J. P., Gilliam, R., Gilliland, A., Goldstein, A. H., Grambsch, A., Grano, D., Guenther, A., Gustafson, W. I., Harley, R. A., He, S., Hemming, B., Hogrefe, C., Huang, H. C., Hunt, S. W., Jacob, D. J., Kinney, P. L., Kunkel, K., Lamarque, J. F., Lamb, B., Larkin, N. K., Leung, L. R., Liao, K. J., Lin, J. T., Lynn, B. H., Manomaiphiboon, K., Mass, C., McKenzie, D., Mickley, L. J., O'Neill, S. M., Nolte, C., Pandis, S. N., Racherla, P. N., Rosenzweig, C., Russell, A. G., Salathe, E., Steiner, A. L., Tagaris, E., Tao, Z., Tonse, S., Wiedinmyer, C., Williams, A., Winner,

- D. A., Woo, J. H., Wu, S., and Wuebbles, D. J. (2009). A preliminary synthesis of modeled climate change impacts on US regional ozone concentrations. *B Am Meteorol Soc*, 90(12):1843–1863.
- Wu, S., Mickley, L. J., Leibensperger, E. M., Jacob, D. J., Rind, D., and Streets, D. G. (2008). Effects of 2000-2050 global change on ozone air quality in the United States. *J Geophys Res-Atmos*, 113(D6):D06302.
- Zishka, K. and Smith, P. (1980). The climatology of cyclones and anticyclones over North America and surrounding ocean environs for January and July, 1950-77. *Mon Weather Rev*, 108(4):387–401.

Chapter 2

Sensitivity of US air quality to mid-latitude cyclone frequency and implications of 1980-2006 climate change

Abstract

We show that the frequency of summertime mid-latitude cyclones tracking across eastern North America at 40°-50°N (the southern climatological storm track) is a strong predictor of stagnation and ozone pollution days in the eastern United States. The NCEP/NCAR Reanalysis, going back to 1948, shows a significant long-term decline in the number of summertime mid-latitude cyclones in that track starting in 1980 (-0.15 a^{-1}). The more recent but shorter NCEP/DOE Reanalysis (1979-2006) shows similar interannual variability in cyclone frequency but no significant long-term trend. Analysis of NOAA daily weather maps for 1980-2006 supports the trend detected in the NCEP/NCAR Reanalysis 1. A GISS general circulation model (GCM) simulation including historical forcing by greenhouse gases reproduces this decreasing cyclone trend starting in 1980. Such a long-term decrease in mid-latitude cyclone frequency over the 1980-2006 period may have offset by half the ozone air quality gains in the northeastern US from reductions in anthropogenic emissions. We find that if mid-latitude cyclone frequency had not declined, the northeastern US would have been largely compliant with the ozone air quality standard by 2001. Mid-latitude cyclone frequency is expected to decrease further over the coming decades in response to greenhouse warming and this will necessitate deeper emission reductions to achieve a given air quality goal.

2.1 Introduction

Regional pollution episodes in the eastern US develop under summertime stagnant conditions with clear skies, a situation associated with weak high-pressure systems (Logan, 1989; Vukovich, 1995; Hegarty et al., 2007). The pollution episode ends when the warm, stagnant air mass is pushed to the Atlantic by the cold front of a passing mid-latitude baroclinic cyclone and replaced with cooler, cleaner air (Merrill and Moody, 1996; Dickerson et al., 1995; Cooper et al., 2001; Li et al., 2005). We show here with 1980-2006 data that interannual variability in the frequency of these mid-latitude cyclones is a major predictor of the interannual variability of pollution episodes, as measured by indices for stagnation and elevated surface ozone. Greenhouse-driven climate change is expected to decrease mid-latitude cyclone frequency, and we present evidence that such a decrease may have already taken place over the 1980-2006 period. As we show, this would have major implications for pollution trends in the eastern US and significantly offset the benefits of decreasing anthropogenic emissions.

Figure 2.1 illustrates the role of mid-latitude cyclones in ventilating the eastern US with an example from the summer of 1988. That summer experienced the worst regional air quality of the 1980-2006 record (Lin et al., 2001). On June 14, the daily maximum 8-h average ozone concentrations exceeded 100 ppb across most of the region, a result of accumulation over several days of stagnant high-pressure conditions. Over the next two days, a mid-latitude cyclone moved along a westerly track across southeastern Canada. The associated cold front swept the pollution eastward to the North Atlantic, leaving much cleaner air with lower ozone concentrations in its wake. The westerly track across southeastern Canada illustrated in Fig. 2.1 is typical of mid-latitude cyclones traveling across North

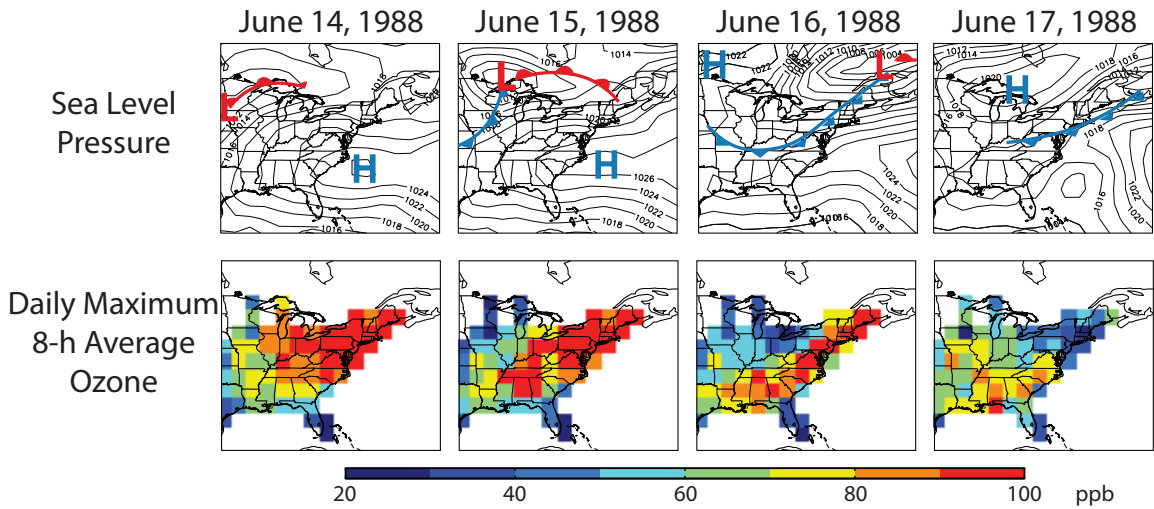


Figure 2.1: Evolution of surface ozone concentrations in the eastern US during the passage of a mid-latitude cyclone (June 14-17, 1988). The top row shows instantaneous sea-level pressure fields at 12Z from the NCEP/NCAR Reanalysis 1, while the bottom row shows daily maximum 8-h average ozone concentrations from monitoring sites of the US Environmental Protection Agency (<http://www.epa.gov/ttn/airs/airsaqs/>). The contour interval for sea level pressure is 2 hPa. The ozone data have been averaged on a $2.5^\circ \times 2.5^\circ$ grid.

America. The frequency of these cyclones varies considerably from year to year (Zishka and Smith, 1980; Whittaker and Horn, 1981).

General circulation model (GCM) simulations of greenhouse-forced 21st-century climate change indicate a poleward shift in the preferential storm tracks (Yin, 2005) and a decrease in the frequency of northern mid-latitude cyclones (Geng and Sugi, 2003; Yin, 2005; Lambert and Fyfe, 2006; Meehl et al., 2007). These effects result from a shift and reduction of baroclinicity forced by weakened meridional temperature gradients (Geng and Sugi, 2003; Yin, 2005). One would expect an adverse effect on US air quality. A GCM simulation by Mickley et al. (2004) including pollution tracers found a 20% decrease in the frequency of summertime mid-latitude cyclones ventilating the US by 2050 and an associated increase in the frequency and intensity of pollution episodes. Two subsequent studies

of US air quality in 21st-century climates, using global chemical transport models driven by GCM output, confirmed the increase of ozone pollution episodes due to decreased frequency of mid-latitude cyclones (Murazaki and Hess, 2006; Wu et al., 2008), but another study using a regional climate model did not (Tagaris et al., 2007).

Decreasing trends in mid-latitude cyclones over the past decades have been identified in the observational record. A study by Zishka and Smith (1980) using observational weather maps for North America found a significant decrease of 4.9 cyclones per decade in July and 9.0 cyclones per decade in December for 1950-1977. Another study by Wang et al. (2006) using surface pressure data for 1953-2002 identified a significant decreasing trend in cyclone activity along eastern Canada during the winter. Similar trends have been found in studies using meteorological reanalyses (i.e., assimilated meteorological data). Gulev et al. (2001) found a decrease of 12.4 cyclones per decade in the Northern Hemisphere and 8.9 cyclones per decade over the Atlantic Ocean during winter 1958-1999. McCabe et al. (2001) found a significant decrease in cyclones at mid-latitudes (30°-60°N) and an increase at high-latitudes (60°-90°N) during winter 1959-1997. Previous studies have generally focused on winter, the season with the strongest climate change signal. In this study we focus on summer, which is of most interest from an air quality standpoint.

A large number of statistical studies have related air quality to local meteorological variables such as temperature, humidity, wind speed, or solar radiation, often with the goal of removing the effect of interannual meteorological variability in the interpretation of air quality trends (Zheng et al., 2007; Bloomfield et al., 1996; Thompson et al., 2001; Camalier et al., 2007; Gégo et al., 2007). Ordóñez et al. (2005) found that the number of days since the last frontal passage was a significant predictor of ozone air quality in Switzerland. Hegarty et al. (2007) related the interannual frequency and intensity of sea level pressure

patterns over eastern North America to ozone, CO, and particulate matter concentrations. Mid-latitude cyclone frequency is an attractive meteorological predictor for air quality on several accounts. First, it encapsulates to some extent the information in the local meteorological predictors (temperature, solar radiation, wind speed), while additionally providing direct information on boundary layer ventilation. Second, it represents a non-local single metric to serve as explanatory variable for air quality on a regional scale. Third, since mid-latitude cyclones are an important aspect of the general circulation of the atmosphere, cyclone frequency can be expected to be robustly simulated by GCMs and thus provide a useful and general metric for probing the effect of climate change on air quality.

2.2 Data and methods

2.2.1 Detection and tracking of mid-latitude cyclones

Various metrics can be used to diagnose mid-latitude cyclone activity, including eddy kinetic energy (Hu et al., 2004), temporal variability of sea-level pressure, temperature or meridional wind (Harnik and Chang, 2003), the meridional temperature gradient, and the Eady growth rate (Paciorek et al., 2002). Some studies have used the probability distribution of sea-level pressure as a diagnostic of cyclone frequency (Murazaki and Hess, 2006; Lin et al., 2008; Racherla and Adams, 2008). A problem with these metrics for application to air quality is that they potentially convolve cyclone frequency and intensity, while air quality is most sensitive to cyclone frequency (i.e., the frequency of cold frontal passages). For example, Owen et al. (2006) found that both strong and weak warm conveyor belts effectively ventilate US pollution, although at different altitudes. In Sect. 2.3 we will show that mid-latitude cyclone is an excellent predictor of pollution episodes.

We constructed long-term cyclone frequency statistics for eastern North America in

June-August using two different methods and three different data sets (1) daily observed weather maps for 1980-2006 from the National Oceanic and Atmospheric Administration (NOAA) available from the NOAA Central Library (<http://www.lib.noaa.gov>) with labeled cyclones and cold fronts; (2) sea-level pressure data from the National Centers for Environmental Prediction/National Center for Atmospheric Research (NCEP/NCAR) Reanalysis 1 (<http://www.esrl.noaa.gov/psd/data/gridded/data.ncep.reanalysis.html>) (Kalnay et al., 1996; Kistler et al., 2001) for 1948-2006 and from the NCEP/Department of Energy (NCEP/DOE) Reanalysis 2 (<http://www.esrl.noaa.gov/psd/data/gridded/data.ncep.reanalysis2.html>) (Kanamitsu et al., 2002) for 1979-2006. Reanalysis 2 is a newer version of Reanalysis 1 incorporating updated physical parameterizations and various error fixes, but it does not cover as long a period. The reanalysis datasets have a spatial resolution of $2.5^\circ \times 2.5^\circ$ and a temporal resolution of six hours. The previously mentioned studies of long-term mid-latitude cyclone trends (McCabe et al., 2001; Gulev et al., 2001; Geng and Sugi, 2001) all used Reanalysis 1.

We generate cyclone tracks in the meteorological reanalyses by locating and following sea-level pressure minima following the algorithm of Bauer and Del Genio (2006), which is an upgraded version of the scheme by Chandler and Jonas (1999). For each 6-h time step the algorithm searches for sea-level pressure minima extending 720 km or more in radius. The low-pressure center is tracked through time by assuming that the strongest sea-level pressure minimum in the next 6-h time step within 720 km is the same system. In order to remove spurious minima, the system must be tracked for at least 24 hours and have a central pressure no higher than 1020 hPa.

Figure 2.2 shows 28-year July climatologies of cyclone density over North America. The compilation of Zishka and Smith (1980) for 1950-1977, produced from 6-h weather

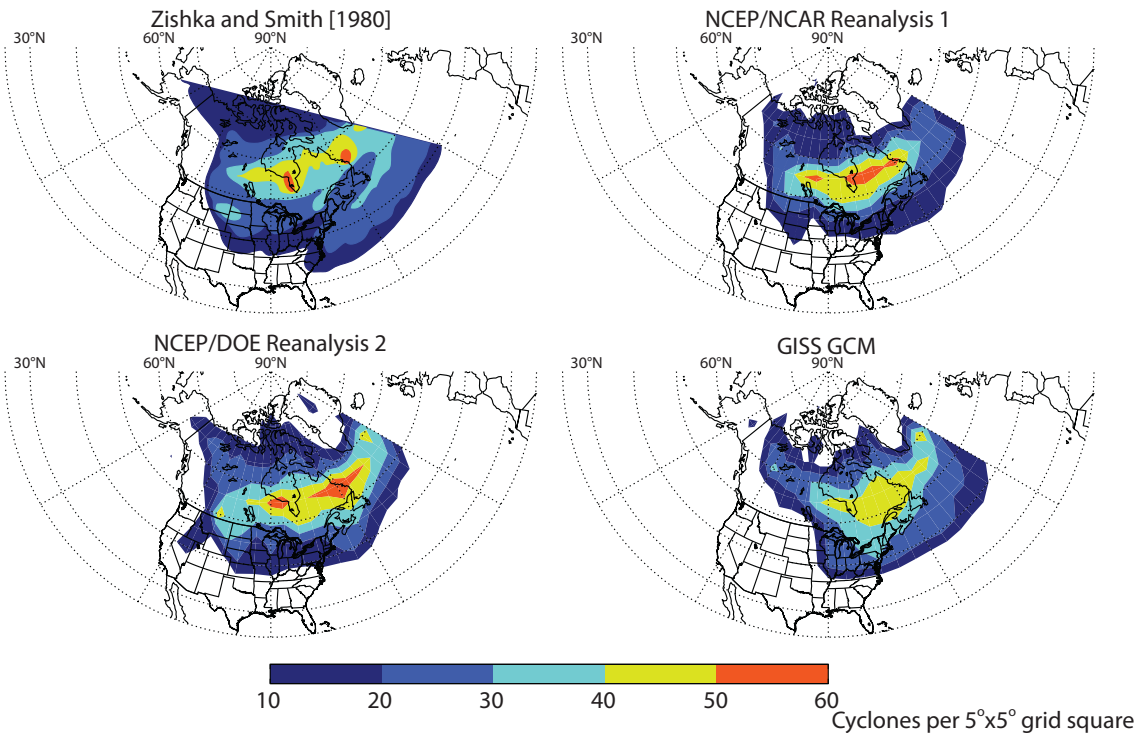


Figure 2.2: 28-year July climatologies of cyclone tracks across North America, counting all cyclone tracks that pass through $5^\circ \times 5^\circ$ grid squares. The Zishka and Smith (1980) climatology is for 1950-1977 and based on monthly compilations of 6-h weather maps; the data shown here are adapted from their Fig. 3. The NCEP/NCAR Reanalysis 1 and NCEP/DOE Reanalysis 2 climatologies are for 1950-1977 and 1979-2006, respectively. The GISS GCM climatology is for 1950-1977 in a transient-climate simulation including historical trends in greenhouse gases and aerosols.

maps, is compared to the climatologies produced by applying the algorithm of Bauer and Del Genio (2006) to Reanalysis 1 (1950-1977) and Reanalysis 2 (1979-2006). Patterns and magnitudes are in good agreement, showing that the cyclone tracking algorithm applied to the reanalysis data can reproduce the observed large-scale climatological distribution of mid-latitude cyclones. Inspection of 1979-2006 vs. 1950-1977 climatologies in Reanalysis 1 indicates no difference between these two periods in the large-scale cyclone patterns shown in Fig. 2.2, although there is a significant trend as discussed in Sect. 2.4.

We see from Fig. 2.2 that cyclone density is maximum over east-central Canada, cor-

responding to the two northern climatological cyclone tracks across North America previously identified by Zishka and Smith (1980) and Whittaker and Horn (1981). These studies also identified a less intense southern climatological track that begins in the central US and moves northeastward along the US- Canada border before merging with the northern tracks along the east coast of Canada. As we will see, it is this southern climatological track that is of most interest for US air quality.

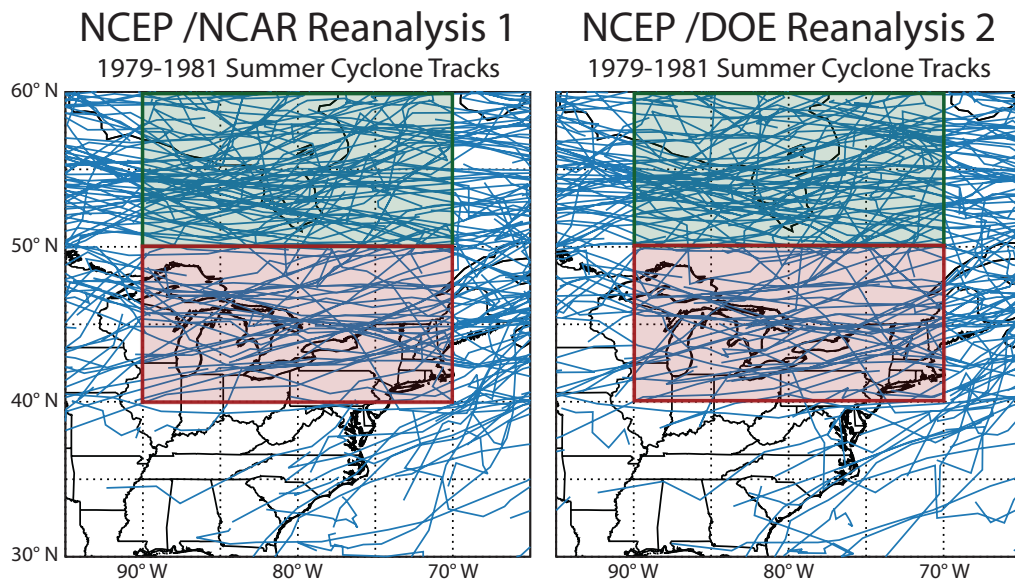


Figure 2.3: Mid-latitude cyclone tracks for June-August 1979-1981 in the NCEP/NCAR Reanalysis 1 (left) and NCEP/DOE Reanalysis 2 (right). The red box (70° - 90° W, 40° - 50° N) is used to diagnose the frequency of mid-latitude cyclones traveling along the southern climatological cyclone track. The green box (70° - 90° W, 50° - 60° N) is used for the northern climatological cyclone tracks.

Figure 2.3 shows individual cyclone tracks for June-August 1979-1981 over eastern North America in Reanalyses 1 and 2. A cluster over the Great Lakes region represents the southern climatological cyclone track. We will show in Sect. 2.3 that the frequency of cyclones moving along this track, identified by the red box (70° - 90° W, 40° - 50° N), is a strong seasonal predictor of the frequency of US pollution episodes. By contrast, we find

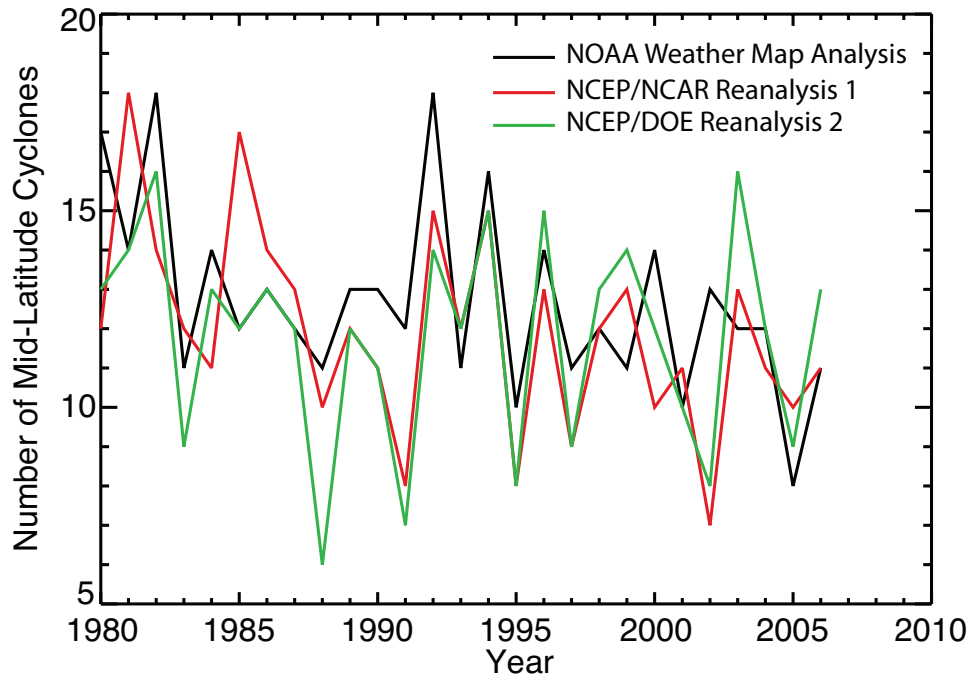


Figure 2.4: June-August 1980-2006 time series of the number of mid-latitude cyclones passing through the red box of Fig. 2.3, corresponding to the southern climatological cyclone track across North America. Results are shown for three different data sets: NOAA daily weather maps (black), NCEP/NCAR Reanalysis 1 (red) and NCEP/DOE Reanalysis 2 (green).

that the number of cyclones passing through the northern climatological tracks (70° - 90° W, 50° - 60° N, green box in Fig. 2.3) is not a successful predictor. We focus on the southern track in the rest of this paper.

Figure 2.4 shows the time series of the 1980-2006 summertime frequency of mid-latitude cyclones in the southern climatological cyclone track (number of cyclones tracking through 70° - 90° W, 40° - 50° N) from Reanalyses 1 and 2 as well as from our manual analysis of the NOAA weather maps. We tallied a system as a cyclone in the NOAA weather maps if it was marked as a Low on the map, contained a closed sea-level pressure contour, and was tracked for at least 24 hours. The three datasets have comparable climatological statistics (11.9 ± 2.6 cyclones summer $^{-1}$ in Reanalysis 1, 11.8 ± 2.7 in Reanalysis 2, 12.7

± 2.4 in NOAA weather maps). Reanalysis 1 and the NOAA weather maps show a significant decreasing trend for 1980-2006 but Reanalysis 2 does not. We discuss these long-term trends in Sect. 2.4.

Figure 2.4 shows strong interannual correlations between cyclone frequencies diagnosed from the three different data sets but also significant differences. Inspection of these differences for individual years shows that although the diagnosis of cyclones in Reanalyses 1 and 2 generally follows the cyclone identification in the daily weather maps, there are some differences in the intensity and position of the sea-level pressure minima for the three different data sets. These differences can result in displacement of the cyclone relative to the red box in Fig. 2.3 used to identify the southern climatological track, and can occasionally affect cyclone detection. Cyclone identification using the NOAA weather maps is closest to the actual observations but is subject to case-by-case human interpretation. The cyclone tracking algorithm applied to the meteorological reanalyses is more objective and can be applied to GCM fields (Sect. 2.4), but it is subject to errors both in the reanalyses and in the tracking algorithm. We will use the three datasets to overcome these problems in the reanalysis and weather map analyses.

2.2.2 Detection of stagnation episodes

We use stagnation frequency as a link to better understand the correlation between cyclone frequency and pollution events. The number of stagnant days was calculated from Reanalyses 1 and 2 data for June-August 1980-1998 with the metric described by Wang and Angell (1999), which is similar to the original version by Korshover and Angell (1982). A day is considered stagnant if the daily mean sea-level pressure geostrophic wind is less than 8 m s^{-1} , the daily mean 500 hPa wind is less than 13 m s^{-1} , and there is no precipita-

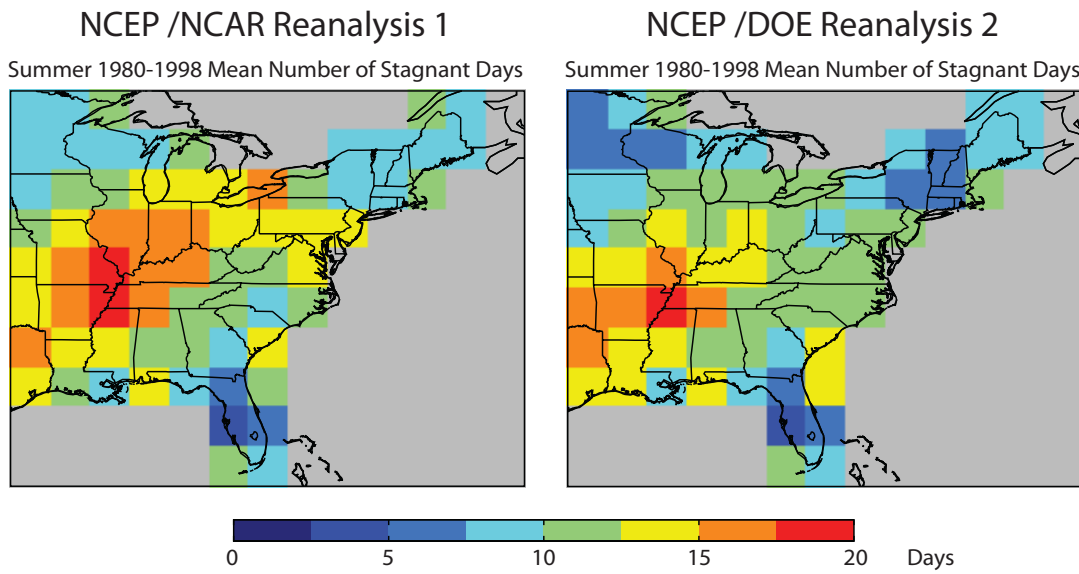


Figure 2.5: Seasonal mean number of June-August stagnant days in the 1980-1998 records from NCEP/NCAR Reanalysis 1 (left) and NCEP/DOE Reanalysis 2 (right).

tion. Precipitation was identified with daily gridded data ($0.25^\circ \times 0.25^\circ$) from the NOAA Climate Prediction Center (<http://www.cdc.noaa.gov/cdc/data.unified.html>) extending to 1998. For our purposes, the 1980-1998 period is sufficient to show the relationship between stagnation and ozone episodes. Figure 2.5 shows the mean number of stagnant days per summer for 1980-1998 from Reanalyses 1 and 2. The frequency of stagnant days in both datasets is highest in a band stretching from Texas to Ohio, as previously shown by Wang and Angell (1999).

2.2.3 Surface ozone data

We generated time series of daily maximum 8-h average ozone concentrations for June-August 1980-2006 from hourly observations of ozone concentrations retrieved from EPAs Air Quality System (AQS, <http://www.epa.gov/ttn/airs/airsaqs/>), representing a network of over 2000 sites in the contiguous United States. The average number of sites providing

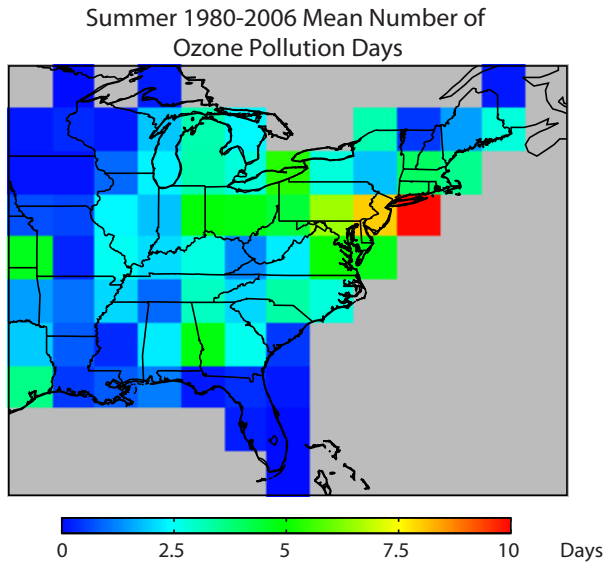


Figure 2.6: Seasonal average number of June-August ozone pollution days for the 1980-2006 period. A pollution day occurs when the mean daily maximum 8-h average ozone concentration averaged over observational sites within a $2.5^\circ \times 2.55^\circ$ grid square is greater than 84 ppb.

ozone data since 1980 is about 1000 per summer; this number has increased over time. The daily maximum 8-h average ozone concentrations from all AQS sites were averaged onto the $2.5^\circ \times 2.5^\circ$ grid of the NCEP Reanalyses, producing a daily time series for 1980-2006 (Fig. 2.1 was produced from that time series). The number of days with a daily maximum 8-h average ozone concentration greater than 84 ppb was tallied for each summer, creating a 27-year time series of the seasonal number of ozone pollution days for each grid square corresponding to an exceedance of the 0.08 ppm US air quality standard. Spatial averaging causes an underestimate of the number of ozone pollution days, but enhances statistical robustness by removing data extremes and improving continuity. Spatial averaging also enables comparison to the identically gridded reanalysis products. Not every grid square included measurements for all 27 years. A grid square was analyzed only if it had 5 or more years of data.

Figure 2.6 shows the mean number of summertime ozone pollution episodes for 1980-2006 on the $2.5^\circ \times 2.5^\circ$ grid. The highest values (>6 days) are in the New York City-Washington, D.C. corridor, but high values (2-6 days) extend over much of the industrial Midwest and Northeast, and in some areas of the Southeast.

2.2.4 GCM simulations

We conducted two simulations with the Goddard Institute for Space Studies (GISS) GCM 3 (Rind et al., 2007) to investigate the effect of 1950-2006 climate change on mid-latitude cyclone frequencies. The first simulation was conducted for 1950-2006 using reconstructed time-dependent concentrations of greenhouse gases, aerosol forcing, and solar radiation (Hansen et al., 2002). The second (control) simulation was conducted in radiative equilibrium (greenhouse gas and aerosol concentrations were held at their 1950 levels), also for 1950-2006. The GCM has a horizontal resolution of 4° latitude \times 5° longitude and 23 vertical layers extending from the surface to 0.002 hPa in a sigma-pressure coordinate system (Rind et al., 2007). It uses a qflux representation for ocean heat transport (Hansen et al., 1988), which allows temporal variation in sea surface temperature and sea ice, but holds constant the horizontal heat transport fluxes in the ocean to values derived from present-day sea surface temperature distributions. Mid-latitude cyclones are detected and tracked from the GCM sea-level pressure output with the same algorithm used for the reanalysis data (Sect. 2.2.1). The GCM cyclone climatology for 1950-1977 (1979-2006 shows the same climatological patterns) is compared to the observational and reanalyses data in Fig. 2.2. Agreement is excellent. The number of GCM cyclones passing through the southern climatological track (red box in Fig. 2.3) is 10.8 ± 2.4 per summer for the 1980-2006 period, consistent with the reanalyses (Sect. 2.2.1).

2.3 Mid-latitude cyclones as predictors of stagnation and ozone pollution

The data and methods of Sect. 2.2 provide totals for individual summers of the number of cyclones passing through the southern climatological cyclone track (1948-2006 for Reanalysis 1, 1979-2006 for Reanalysis 2, 1980-2006 for NOAA weather maps), as well as the numbers of stagnation days (1980-1998) and ozone pollution days (1980-2006) in each $2.5^\circ \times 2.5^\circ$ grid square of the eastern United States. We use the linear Pearson correlation coefficient to correlate these different variables on an interannual basis, and a Students t-test to determine the significance of the correlation. To avoid the aliasing effects of long-term trends on the correlations, we removed linear trends from all individual time series that had significant trends at the 95% level. Long-term trends in ozone pollution days and mid-latitude cyclones will be discussed in Sect. 2.4.

Figure 2.7 (top panels) shows the interannual correlation between the number of stagnant days and the number of mid-latitude cyclones derived from the reanalysis datasets. The correlation is generally significant and negative, indicating that less frequent mid-latitude cyclones in a given summer are associated with more frequent stagnant conditions. The negative correlation is strongest in the northeastern and midwestern United States. This is because the cold fronts associated with mid-latitude cyclones generally do not extend to the southern US (see Fig. 2.1); moist convection and inflow from the Gulf of Mexico are a more important ventilation pathways in that region (Li et al., 2005).

The middle panels of Fig. 2.7 show the interannual correlation between the number of stagnant days and the number of ozone pollution days. There is strong positive correlation throughout the eastern US, with the exception of grid squares on the edge of the domain

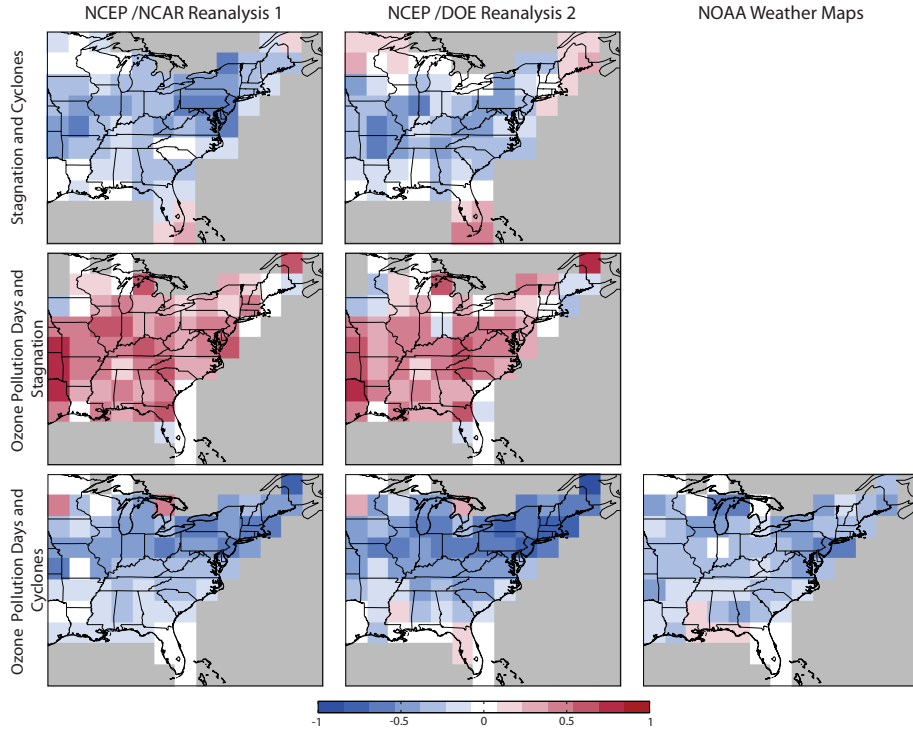


Figure 2.7: Interannual correlation coefficients (r) between the summer total numbers of mid-latitude cyclones, stagnation days, and ozone pollution days for 1980-1998 (top and middle panels) and 1980-2006 (bottom panels). The data are as described in Sect. 2.2. Numbers of cyclones are from the NCEP/NCAR Reanalysis 1 (left), the NCEP/DOE Reanalysis 2 (middle), and NOAA daily weather maps (right). Numbers of stagnation events are from the reanalyses only.

where wind direction (i.e., advection of pollution from upwind) is a more important predictor (Camalier et al., 2007).

The bottom panels of Fig. 2.7 show the interannual correlation between the number of ozone pollution days and the number of mid-latitude cyclones diagnosed from the reanalyses and from the NOAA weather maps. There is widespread negative correlation, stronger in the Midwest and Northeast than in the Southeast, consistent with the correlation of mid-latitude cyclones and stagnation days seen in the reanalyses. We thus see that there is a clear cause-to-effect link, at least in the Midwest and Northeast, between mid-latitudes cyclones, stagnation days, and ozone pollution days. The frequency of mid-latitude cyclones

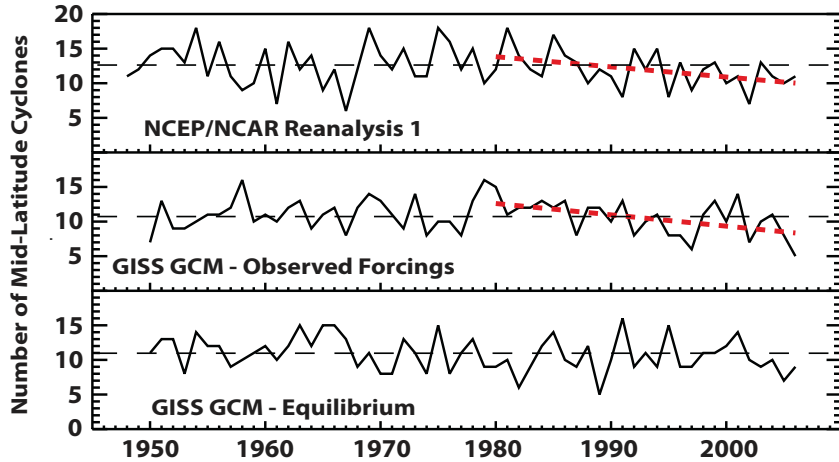


Figure 2.8: Time series of the number of June-August mid-latitude cyclones tracking through 40°-50°N, 70°-90°W (the southern climatological cyclone track, see Fig. 2.2) for 1948-2006. Results from the NCEP/NCAR Reanalysis 1 (top) are compared to the GISS GCM 3 simulation including historical radiative forcings (middle), and to a GISS GCM 3 simulation in radiative equilibrium (bottom). The dashed lines show the long-term means for each time series to aid in visual trend identification. Red dashed lines show 1980-2006 regressions for the top two panels, where the trends are significant.

can be used as an interannual predictor of air quality. An important implication, from a climate change perspective, is that long-term trends in cyclone frequency may be expected to drive corresponding trends in air quality.

2.4 Long-term trends in mid-latitude cyclone frequency and ozone pollution

Reanalysis 1 and the NOAA weather maps feature a statistically significant decreasing trend of the number of cyclones in the southern climatological track between 1980 and 2006 (-0.15 a^{-1} for Reanalysis 1, -0.14 a^{-1} for the NOAA weather maps, both with $p < 0.01$) (Fig. 2.4). Reanalysis 2 does not show a significant trend. Previously derived trends in mid-latitude cyclones have used the longer record of the Reanalysis 1 data (McCabe

et al., 2001; Gulev et al., 2001; Geng and Sugi, 2001). The consistent trend that we see here between the NOAA daily weather maps and Reanalysis 1 provides important corroboration with the earlier studies.

We used the entire 1948-2006 extent of Reanalysis 1 to extend our trend analysis and compare to our GISS GCM simulations of the same period. Results in Fig. 2.8 show that the trend in Reanalysis 1 is confined to 1980-2006. The 1948-1980 period shows strong interannual variability but no trend. The GISS GCM simulation with historical changes in greenhouse gases, aerosols, and solar forcing shows a 1980-2006 decreasing trend in the number of cyclones frequency (-0.16 a^{-1} , $p < 0.01$), consistent with Reanalysis 1 and the NOAA weather maps. It shows no trend prior to 1980, consistent with Reanalysis 1. The GCM control simulation, conducted in radiative equilibrium, with greenhouse gas and aerosol concentrations and solar activity held at their 1950 levels, does not exhibit any significant trend over the 1950-2006 record. Thus we see that the 1980-2006 trend in cyclone frequency in the GISS GCM is driven by increase in greenhouse gases.

Figure 2.9 shows the trend in the number of ozone pollution days in the Northeast (defined as the New England and mid-Atlantic regions; see inset of Fig. 2.9). We focus on the Northeast because of its high number of ozone pollution days (Fig. 2.6) and the strong relationship of these pollution days to mid-latitude cyclone frequency (Fig. 2.7). The data in black represent the number of days over the course of the summer where one of the $2.5^\circ \times 2.5^\circ$ grid squares in the Northeast experienced a daily maximum 8-h average ozone concentration exceeding 84 ppb. The number of ozone pollution days decreased at a rate of 0.84 a^{-1} over the 1980-2006 period, a trend that can be credited to reduction of anthropogenic emissions of ozone precursors including nitrogen oxides ($\text{NO}_x \equiv \text{NO} + \text{NO}_2$) and volatile organic compounds (VOCs) (Lin et al., 2001; Gégo et al., 2007).

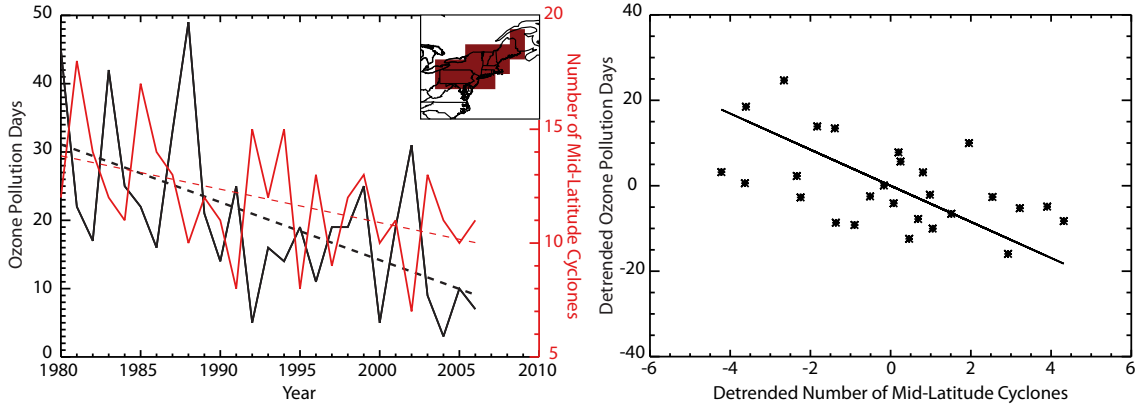


Figure 2.9: Long-term trends and correlations of the number of ozone pollution days in the Northeast (inset) and the number of mid-latitudes cyclones in the southern climatological track. The left panel shows the number of ozone pollution days (black) and the number of mid-latitude cyclones passing through the southern climatological track (red). Ozone pollution days are defined as in Sect. 2.2.3. Cyclone data are from the NCEP/NCAR Reanalysis 1 and are as in Fig. 2.4. Dashed lines show the linear trends ($p < 0.01$). The right panel shows a scatterplot of the number of ozone pollution days (n) vs. the number of mid-latitude cyclones in the southern climatological track (C) after removal of the long-term linear trend.

This improvement in ozone air quality occurred despite the concurrent decreasing trend of mid-latitude cyclones diagnosed from Reanalysis 1 (also shown in Fig. 2.9) and the daily NOAA daily weather maps. The detrended anomalies of the cyclone and ozone time series are strongly anticorrelated, as previously shown in Fig. 2.7; the corresponding scatterplot is shown in the bottom panel of Fig. 2.9. A reduced major axis linear regression of the detrended anomalies (Fig. 2.9) indicates a dependence of the number n of ozone pollution days on the number C of mid-latitude cyclones, $\frac{dn}{dC}$, of -4.6 for the time series derived from daily weather maps and -4.2 for Reanalysis 1. This points to a major effect of 1980-2006 climate change on the observed ozone trends, as discussed below.

2.5 Effect of 1980-2006 climate change on ozone air quality

A long-term decreasing trend in mid-latitudes cyclones over the 1980-2006 period, as indicated by Reanalysis 1, the NOAA daily weather maps, and the GISS GCM simulation, would imply increasing stagnation and thus a more favorable meteorological environment for ozone pollution days. This could have offset some of the gains from decreases in anthropogenic emissions of ozone precursors, so that the return from emission controls would have been less than expected. Understanding such an effect is of great importance for the accountability of air quality policy (National Research Council, 2004).

We estimate here how the 1980-2006 trend in mid-latitude cyclones as indicated by Reanalysis 1 and the NOAA weather maps may have affected the 1980-2006 trend in ozone air quality in the Northeast. The observed trend in the number of ozone pollution days per summer, $\frac{dn}{dt}$, is -0.84 a^{-1} (Fig. 2.9). Let us assume that this observed trend is driven by trends in emissions E and in the number of cyclones C . We can then decompose the observed total derivative into partial derivatives:

$$\frac{dn}{dt} = \left[\frac{dn}{dt} \right]_E + \left[\frac{dn}{dt} \right]_C \quad (2.1)$$

with

$$\left[\frac{dn}{dt} \right]_E = \frac{\partial n}{\partial E} \frac{\partial E}{\partial t} \quad (2.2)$$

$$\left[\frac{dn}{dt} \right]_C = \frac{\partial n}{\partial C} \frac{\partial C}{\partial t} \quad (2.3)$$

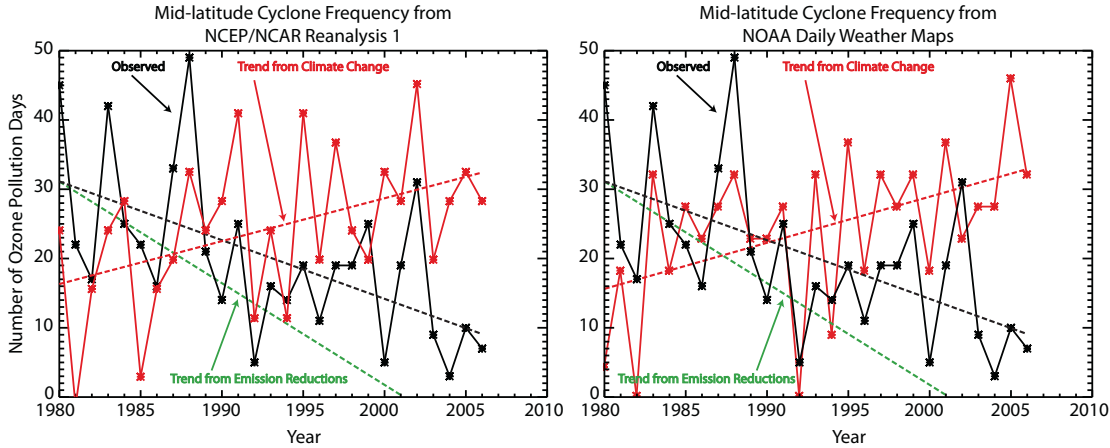


Figure 2.10: 1980-2006 time series of the number of ozone pollution days in the northeast United States (inset of Fig. 2.9). Observations are shown in black and are as in Fig. 2.9. The red line shows the number of ozone pollution days predicted from the number of mid-latitude cyclones in the NOAA weather maps (right) and in the NCEP/NCAR Reanalysis 1 (left) if anthropogenic emissions had not changed over the period (see text for derivation). Regression lines are shown and represent the observed trend ($\frac{dn}{dt}$, in black) and the trend expected from climate change in the absence of change in anthropogenic emissions ($[\frac{dn}{dt}]_E$, in red). The green dashed line shows the trend expected from reductions in anthropogenic emissions in the absence of climate change, $[\frac{dn}{dt}]_C = \frac{dn}{dt} [\frac{dn}{dt}]_E$.

where $[\frac{dn}{dt}]_E$ describes the trend due to changing emissions in the absence of climate change, and $[\frac{dn}{dt}]_C$ describes the trend due to climate change in the absence of change in emissions. We previously derived $\frac{\partial n}{\partial C} = -4.2$ from Reanalysis 1 (-4.6 for the weather map analysis) and $\frac{\partial C}{\partial t} = -0.15 \text{ a}^{-1}$ (-0.14 a^{-1}) in Sect. 2.4. Thus the trend in number of ozone pollution days due to climate change is $[\frac{dn}{dt}]_C = 0.63 \text{ a}^{-1}$ (0.64 a^{-1}). Replacing into Eq. 2.1 yields a trend in the number of ozone pollution days due to changing anthropogenic emissions, $[\frac{dn}{dt}]_E = -1.5 \text{ a}^{-1}$ (-1.5 a^{-1}). The analysis thus indicates that decreasing mid-latitude cyclone frequency over the 1980-2006 period has offset the benefit of emission controls almost by half.

Figure 2.10 shows this result graphically for the cyclone trends from the NOAA weather maps and from Reanalysis 1. The time series of the number of ozone pollution days ob-

served in the Northeast, as previously displayed in Fig. 9, is shown in black with the corresponding regression line $\frac{dn}{dt} = -0.84 \text{ a}^{-1}$. The time series predicted from the number of mid-latitude cyclones (Fig. 2.9) and the dependence, $\frac{\partial n}{\partial C} = -4.2(-4.6)$, derived in Sect. 2.4 is shown in red, with the corresponding regression line $[\frac{dn}{dt}]_C = 0.63 \text{ a}^{-1}$ (0.64 a^{-1}) representing the expected trend in ozone pollution days from climate change had emissions remained constant. We see that the frequency of ozone pollution days would have doubled over the 1980-2006 period as a result of climate change, were it not for concurrent decreases in anthropogenic emissions. The green line in Fig. 10 shows the trend in ozone pollution days that would have been realized from the decrease in anthropogenic emissions in the absence of climate change, i.e., $[\frac{dn}{dt}]_E = \frac{dn}{dt} [\frac{dn}{dt}]_C = -1.5 \text{ a}^{-1}$ (-1.5 a^{-1}). We see that the expected number of ozone pollution days would have dropped to zero by 2001, instead of remaining a significant problem (expected value of 10) by 2006.

2.6 Conclusions

We showed that the frequency of mid-latitudes cyclones tracking across eastern North America in the 40° - 50°N latitudinal band (southern climatological track) is a strong predictor variable of the frequency of summertime pollution episodes in the eastern United States. Cold fronts associated with these cyclones effectively ventilate the US boundary layer. We constructed cyclone tracks using the algorithm of Bauer and Del Genio (2006) applied to assimilated meteorological data from the NCEP/NCAR Reanalysis 1 (1948-2006) and the NCEP/DOE Reanalysis 2 (1979-2006); the two reanalyses agree closely in the locations and frequencies of cyclone tracks, and also agree well with cyclone statistics constructed directly from NOAA weather maps. Statistical analysis of 1980-2006 summer data shows large interannual variability in the number of cyclones in the southern climatological track

(11.9 ± 2.6 for Reanalysis 1) and reveals strong negative interannual correlations between the number of cyclones and both the number of stagnation days and the number of ozone pollution days.

The frequency of mid-latitude cyclones in the 40° - 50° N band is of particular interest as a predictor variable for US air quality. First, it encapsulates in a single synoptic-scale variable the effects of known local predictor variables including temperature, wind speed, and solar radiation. Second, mid-latitude cyclones are a feature of the general circulation of the atmosphere and are therefore amenable to trend analysis and prediction using GCMs. They can thus be used to diagnose and project the effects of climate change on US air quality.

Greenhouse warming is expected to decrease mid-latitude cyclone frequencies (Geng and Sugi, 2003; Yin, 2005; Lambert and Fyfe, 2006; Meehl et al., 2007), and such a decrease has been observed in climatological analyses of 1950-2000 data (Zishka and Smith, 1980; Gulev et al., 2001; McCabe et al., 2001; Wang et al., 2006). We examined more specifically the historical trend in the number of summer cyclones in the North American southern climatological track (40° - 50° N) responsible for ventilating the eastern United States. The NCEP/NCAR Reanalysis 1 and the NOAA daily weather maps both show significant decreasing trends for 1980-2006, with consistent slopes (-0.15 a^{-1} and -0.14 a^{-1} , respectively). The NCEP/DOE Reanalysis 2 shows no significant trend.

The NCEP/NCAR Reanalysis 1 starts in 1948. Analysis of the complete 1948-2006 record shows no cyclone trend prior to 1980. We compared this result to a transient-climate simulation for 1950-2006 with the GISS GCM 3 including historical greenhouse and aerosol forcing. This simulation shows a decrease in the number of cyclones for 1980-2006 (-0.16 a^{-1}), and no trend prior to 1980, consistent with Reanalysis 1. A control

GCM simulation for 1950-2006 with no greenhouse and aerosol forcing shows by contrast no trend over the whole period. The cyclone trend for the 1980-2006 period can thus be attributed to greenhouse forcing.

A 1980-2006 decrease in cyclone frequency as indicated by the NCEP/NCAR Reanalysis 1 and by the NOAA daily weather maps has important implications for the success and accountability of emission control strategies directed at improving US air quality. Our analysis of the surface ozone data indicates a decrease in the observed number of summertime ozone pollution days in the Northeast by 0.84 a^{-1} over the 1980-2006 period, from an expected value of 31 (1980) to 10 (2006). This decrease can be credited to reduction of anthropogenic emissions, but we find that the benefit of these reductions may have been significantly offset by climate change. Taking the relationship between the number of summertime cyclones and the number of ozone pollution days from our correlation analysis, combined with the cyclone trend derived from either Reanalysis 1 or the NOAA daily weather maps, we deduce that the number of ozone pollution days would have doubled over the 1980-2006 period as a result of climate change if anthropogenic emissions had remained constant. Correcting the observed decrease of ozone pollution days for this climate trend, we find that the number of ozone pollution days would have dropped to an expected value of zero by 2001 in the absence of climate change.

We conclude from this analysis that the decrease in mid-latitude cyclones over the 1980-2006 has offset half of the air quality gains in the Northeast US that should have been achieved from reduction of anthropogenic emissions over that period. This suggests that climate change has had already a major effect on the accountability of emission control strategies over the past 2-3 decades, preventing achievement of the ozone air quality standard. It demonstrates the potential of climate change to dramatically affect air quality

on decadal scales relevant to air quality policy. Future attention to this issue is necessary in view of the consistent predictions from GCMs that 21st-century climate change will decrease the frequency of mid-latitude cyclones (Lambert and Fyfe, 2006).

Our analysis has focused on ozone air quality because of the availability of long-term records with high spatial density. We would expect mid-latitude cyclone frequency to also be a good predictor of particulate matter (PM) air quality, which is similarly affected by stagnation, but further analysis using PM observational records is necessary. Also, our analysis has focused on the eastern US, but similar analyses would be of value for western Europe and China, where mid-latitudes cyclones are also major agents for pollutant ventilation (Liu et al., 2003; Ordóñez et al., 2005). We have found in the eastern US that although mid-latitude cyclone frequency is a good predictor of pollution episodes in the Northeast and Midwest, it is less effective in the South. Other large-scale meteorological metrics should be sought there and in the West to enable assessments of the effect of climate change on air quality.

Bibliography

- Bauer, M. and Del Genio, A. D. (2006). Composite analysis of winter cyclones in a GCM: Influence on climatological humidity. *J Climate*, 19:1652–1672.
- Bloomfield, P., Royle, J., Steinberg, L., and Yang, Q. (1996). Accounting for meteorological effects in measuring urban ozone levels and trends. *Atmos Environ*, 30(17):3067–3077.
- Camalier, L., Cox, W., and Dolwick, P. (2007). The effects of meteorology on ozone in urban areas and their use in assessing ozone trends. *Atmos Environ*, 41(33):7127–7137.
- Chandler, M. and Jonas, J. (1999). Atlas of Extratropical Storm Tracks (1961-1998). <http://data.giss.nasa.gov/stormtracks/>.
- Cooper, O., Moody, J., Parrish, D., Trainer, M., Ryerson, T., Holloway, J., Hubler, G., Fehsenfeld, F., Oltmans, S., and Evans, M. (2001). Trace gas signatures of the airstreams

- within North Atlantic cyclones: Case studies from the North Atlantic Regional Experiment (NARE '97) aircraft intensive. *J Geophys Res-Atmos*, 106(D6):5437–5456.
- Dickerson, R. R., Doddridge, B. G., KELLEY, P., and Rhoads, K. P. (1995). Large-scale pollution of the atmosphere over the remote Atlantic Ocean - Evidence from Bermuda. *J Geophys Res-Atmos*, 100(D5):8945–8952.
- Gégo, E., Porter, P. S., Gilliland, A., and Rao, S. T. (2007). Observation-based assessment of the impact of nitrogen oxides emissions reductions on ozone air quality over the eastern United States. *J Appl Meteorol Clim*, 46(7):994–1008.
- Geng, Q. and Sugi, M. (2001). Variability of the North Atlantic cyclone activity in winter analyzed from NCEP-NCAR reanalysis data. *J Climate*, 14(18):3863–3873.
- Geng, Q. and Sugi, M. (2003). Possible change of extratropical cyclone activity due to enhanced greenhouse gases and sulfate aerosols - Study with a high-resolution AGCM. *J Climate*, 16(13):2262–2274.
- Gulev, S., Zolina, O., and Grigoriev, S. (2001). Extratropical cyclone variability in the Northern Hemisphere winter from the NCEP/NCAR reanalysis data. *Clim Dynam*, 17(10):795–809.
- Hansen, J., Sato, M., Nazarenko, L., Ruedy, R., Lacis, A., Koch, D., Tegen, I., Hall, T., Shindell, D., Santer, B., Stone, P., Novakov, T., Thomason, L., Wang, R., Wang, Y., Jacob, D., Hollandsworth, S., Bishop, L., Logan, J., Thompson, A., Stolarski, R., Lean, J., Willson, R., Levitus, S., Antonov, J., Rayner, N., Parker, D., and Christy, J. (2002). Climate forcings in Goddard Institute for Space Studies SI2000 simulations. *J Geophys Res-Atmos*, 107(D18):4347.
- Harnik, N. and Chang, E. (2003). Storm track variations as seen in radiosonde observations and reanalysis data. *J Climate*, 16(3):480–495.
- Hegarty, J., Mao, H., and Talbot, R. (2007). Synoptic controls on summertime surface ozone in the northeastern United States. *J Geophys Res-Atmos*, 112(D14):D14306.
- Hu, Q., Tawaye, Y., and Feng, S. (2004). Variations of the Northern Hemisphere atmospheric energetics: 1948–2000. *J Climate*, 17(10):1975–1986.
- Kalnay, E., Kanamitsu, M., Kistler, R., Collins, W., Deaven, D., Gandin, L., Iredell, M., Saha, S., White, G., Woollen, J., Zhu, Y., Chelliah, M., Ebisuzaki, W., Higgins, W., Janowiak, J., Mo, K., Ropelewski, C., Wang, J., Leetmaa, A., Reynolds, R., Jenne, R., and Joseph, D. (1996). The NCEP/NCAR 40-year reanalysis project. *B Am Meteorol Soc*, 77(3):437–471.
- Kanamitsu, M., Ebisuzaki, W., Woollen, J., Yang, S., Hnilo, J., Fiorino, M., and Potter, G. (2002). NCEP-DOE AMIP-II reanalysis (R-2). *B Am Meteorol Soc*, 83(11):1631–1643.

- Kistler, R., Kalnay, E., Collins, W., Saha, S., White, G., Woollen, J., Chelliah, M., Ebisuzaki, W., Kanamitsu, M., Kousky, V., van den Dool, H., Jenne, R., and Fiorino, M. (2001). The NCEP-NCAR 50-year reanalysis: Monthly means CD-ROM and documentation. *B Am Meteorol Soc*, 82(2):247–267.
- Korshover, J. and Angell, J. K. (1982). A review of air-stagnation cases in the Eastern United States during 1981 - Annual summary. *Mon Wea Rev*, 110(10):1515–1518.
- Lambert, S. and Fyfe, J. (2006). Changes in winter cyclone frequencies and strengths simulated in enhanced greenhouse warming experiments: results from the models participating in the IPCC diagnostic exercise. *Clim Dynam*, 26(7-8):713–728.
- Li, Q., Jacob, D., Park, R., Wang, Y., Heald, C., Hudman, R., Yantosca, R., Martin, R., and Evans, M. (2005). North American pollution outflow and the trapping of convectively lifted pollution by upper-level anticyclone. *J Geophys Res-Atmos*, 110(D10):D10301.
- Lin, C., Jacob, D., and Fiore, A. (2001). Trends in exceedances of the ozone air quality standard in the continental United States, 1980-1998. *Atmos Environ*, 35(19):3217–3228.
- Lin, J.-T., Patten, K. O., Hayhoe, K., Liang, X.-Z., and Wuebbles, D. J. (2008). Effects of future climate and biogenic emissions changes on surface ozone over the United States and China. *J Appl Meteorol Clim*, 47(7):1888–1909.
- Liu, H., Jacob, D., Bey, I., Yantosca, R., Duncan, B., and Sachse, G. (2003). Transport pathways for Asian pollution outflow over the Pacific: Interannual and seasonal variations. *J Geophys Res-Atmos*, 108(D20):8786.
- Logan, J. A. (1989). Ozone in rural areas of the United States. *J Geophys Res-Atmos*, 94(D6):8511–8532.
- McCabe, G., Clark, M., and Serreze, M. (2001). Trends in Northern Hemisphere surface cyclone frequency and intensity. *J Climate*, 14(12):2763–2768.
- Meehl, G., Stocker, T., Collins, W., Friedlingstein, P., Gregory, A. G. J., Kitoh, A., Knutti, R., Murphy, J., Raper, A. N. S., Watterson, I., Weaver, A., and Zhao, Z.-C. (2007). *Climate Change 2007: The Physical Science Basis*, chapter Global Climate Projections, pages 747–846. Cambridge University Press.
- Merrill, J. and Moody, J. (1996). Synoptic meteorology and transport during the North Atlantic Regional Experiment (NARE) intensive: Overview. *J Geophys Res-Atmos*, 101(D22):28903–28921.
- Mickley, L. J., Jacob, D. J., Field, B. D., and Rind, D. (2004). Effects of future climate change on regional air pollution episodes in the United States. *Geophys Res Lett*, 31(24):L24103.

- Murazaki, K. and Hess, P. (2006). How does climate change contribute to surface ozone change over the United States? *J Geophys Res-Atmos*, 111(D5):D05301.
- National Research Council (2004). *Air Quality Management in the United States*. National Academies Press, Washington, DC.
- Ordóñez, C., Mathis, H., Furger, M., Henne, S., Huglin, C., Staehelin, J., and Prevot, A. (2005). Changes of daily surface ozone maxima in Switzerland in all seasons from 1992 to 2002 and discussion of summer 2003. *Atmos Chem Phys*, 5:1187–1203.
- Owen, R. C., Cooper, O. R., Stohl, A., and Honrath, R. E. (2006). An analysis of the mechanisms of North American pollutant transport to the central North Atlantic lower free troposphere. *J Geophys Res-Atmos*, 111(D23):D23S58.
- Paciorek, C., Risbey, J., Ventura, V., and Rosen, R. (2002). Multiple indices of Northern Hemisphere cyclone activity, winters 1949–99. *J Climate*, 15(13):1573–1590.
- Racherla, P. N. and Adams, P. J. (2008). The response of surface ozone to climate change over the Eastern United States. *Atmos Chem Phys*, 8(4):871–885.
- Rind, D., Lerner, J., Jonas, J., and McLinden, C. (2007). Effects of resolution and model physics on tracer transports in the NASA Goddard Institute for Space Studies general circulation models. *J Geophys Res-Atmos*, 112(D9):D09315.
- Tagaris, E., Manomaiphiboon, K., Liao, K.-J., Leung, L. R., Woo, J.-H., He, S., Amar, P., and Russell, A. G. (2007). Impacts of global climate change and emissions on regional ozone and fine particulate matter concentrations over the United States. *J Geophys Res-Atmos*, 112(D14):D14312.
- Thompson, M., Reynolds, J., Cox, L., Guttorp, P., and Sampson, P. (2001). A review of statistical methods for the meteorological adjustment of tropospheric ozone. *Atmos Environ*, 35(3):617–630.
- Vukovich, F. M. (1995). Regional-scale boundary layer ozone variations in the Eastern United States and their association with meteorological variations. *Atmos Environ*, 29(17):2259–2273.
- Wang, J. and Angell, J. (1999). Air Stagnation Climatology for the United States. NOAA/Air Resource Laboratory ATLAS No. 1.
- Wang, X., Wan, H., and Swail, V. (2006). Observed changes in cyclone activity in Canada and their relationships to major circulation regimes. *J Climate*, 19(6):896–915.
- Whittaker, L. and Horn, L. (1981). Geographical and seasonal distribution of North American cyclogenesis, 1958–1977. *Mon Wea Rev*, 109(11):2312–2322.

- Wu, S., Mickley, L. J., Leibensperger, E. M., Jacob, D. J., Rind, D., and Streets, D. G. (2008). Effects of 2000-2050 global change on ozone air quality in the united states. *J Geophys Res-Atmos*, 113(D6):D06302.
- Yin, J. (2005). A consistent poleward shift of the storm tracks in simulations of 21st century climate. *Geophy Res Lett*, 32(18):L18701.
- Zheng, J., Swall, J. L., Cox, W. M., and Davis, J. M. (2007). Interannual variation in meteorologically adjusted ozone levels in the eastern united states: A comparison of two approaches. *Atmos Environ*, 41(4):705–716.
- Zishka, K. M. and Smith, P. J. (1980). The climatology of cyclones and anticyclones over North America and surrounding ocean environs for January and July, 1950-77. *Mon Wea Rev*, 108(4):387–401.

Chapter 3

Intercontinental influence of NO_x and CO emissions on particulate matter air quality

Abstract

Anthropogenic emissions of nitrogen oxides ($\text{NO}_x \equiv \text{NO} + \text{NO}_2$) and carbon monoxide (CO) affect particulate matter (PM) air quality on an intercontinental scale by changing background concentrations of oxidants (OH, ozone, H_2O_2) and thus increasing the oxidation rate of sulfur dioxide (SO_2) to sulfate and NO_x to nitrate. We conduct sensitivity simulations with the GEOS-Chem chemical transport model and find that these intercontinental influences of NO_x and CO emissions on PM can be greater than those from SO_2 emissions (a direct PM precursor). The intercontinental impact of oxidant precursors is greatest in receptor regions with high domestic SO_2 , NO_x , and ammonia emissions and hence already high levels of PM. US NO_x and CO emissions increase annual mean PM in northern Europe and eastern China by up to $0.25 \mu\text{g m}^{-3}$. The increase in Europe is mostly as sulfate, whereas in China it is mostly as nitrate. East Asian NO_x and CO emissions have a weaker intercontinental influence ($0.2 \mu\text{g m}^{-3}$ in northern Europe, $0.1 \mu\text{g m}^{-3}$ in the eastern US). These intercontinental effects of NO_x and CO emissions on PM depend in a complex way on the chemical environment of receptor regions. Intercomparison of results from different models would be of great interest.

3.1 Introduction

Developed countries worldwide regulate domestic sources of particulate matter (PM) to meet air quality goals designed to protect public health and visibility. These regulations may involve neighboring countries to address transboundary transport. However, PM can also be transported on intercontinental scales with significant implications for air quality in the receptor continent (Park et al., 2006; Liu et al., 2009a). Here we show that this intercontinental influence on PM does not only involve emissions of PM and its direct precursors from the source continent, but also emissions of nitrogen oxides ($NO_x \equiv NO + NO_2$) and CO that affect PM through global perturbations to oxidant concentrations.

There has been much recent interest in quantifying the intercontinental transport of PM pollution (Jaffe et al., 1999; Park et al., 2004; Heald et al., 2006; Chin et al., 2007; Liu et al., 2009b). Intercontinental transport of desert dust and of plumes from large forest fires has long been recognized as a contributor to surface PM (Prospero, 1999; Forster et al., 2001; Husar et al., 2001; Fairlie et al., 2007). Surface, aircraft, and satellite observations have identified episodic transport of anthropogenic PM across the Pacific (Jaffe et al., 1999, 2003; Yu et al., 2008). Global models indicate annual mean sulfate enhancements in US surface air of up to $0.2 \mu\text{g m}^{-3}$ from anthropogenic Asian SO_2 emissions (Park et al., 2004; Heald et al., 2006; Chin et al., 2007). Direct intercontinental transport of anthropogenic organic and nitrate aerosols appears to be far less important based on both observational and modeling evidence (Heald et al., 2006; Peltier et al., 2008; Donkelaar et al., 2008).

Sulfate, nitrate, and organic aerosol form in the atmosphere by oxidation of their precursor gases SO_2 , NO_x , and volatile organic compounds (VOCs). Oxidant levels affect the rate of aerosol production. Previous global model studies have found that global changes in

anthropogenic emissions of oxidant precursors (NO_x, CO, VOCs) affect surface PM concentrations and radiative forcing by perturbing background concentrations of the oxidants OH, H₂O₂, and ozone (Unger et al., 2006; Rae et al., 2007; Kloster et al., 2008; Shindell et al., 2008, 2009). A recent study by Barrett et al. (2010) found that NO_x emissions from aircraft at cruising altitudes enhance surface sulfate PM production by increasing background oxidant levels such that surface sulfate concentrations increase linearly with aircraft NO_x emissions.

Current understanding of intercontinental pollution influence on PM air quality has been assessed by the Task Force on Hemispheric Transport of Air Pollutants (TF-HTAP, 2007) of the United Nations Environmental Program (UNEP). The assessment presents global multi-model estimates of intercontinental source-receptor relationships for PM and its precursors. These estimates can be made with either of two methods. In the first, PM or precursors from a given region are tagged and tracked as they undergo transport and chemical evolution. This method is applicable only for linear problems. In the second, more general method, sensitivity simulations with perturbed emissions in the source continent are compared to a control simulation. The TF-HTAP (2007) multi-model assessment used the second method but did not investigate the role of oxidant precursor emissions in contributing to intercontinental PM influences. We do so here.

3.2 Model simulations

We conducted detailed simulations of coupled tropospheric ozone-NO_x-VOC-aerosol chemistry with the GEOS-Chem chemical transport model (version 8-01-01; <http://geos-chem.org>) driven by assimilated meteorological data from the Goddard Earth Observing System (GEOS)-4. The model has a horizontal resolution of 2° latitude × 2.5° longitude and

30 vertical levels. GEOS-Chem simulates gas-phase oxidant chemistry together with the mass concentrations of the major aerosol types including sulfate-nitrate-ammonium (SNA), black carbon, primary organic carbon, secondary organic carbon, fine and coarse mode sea salt, and dust in four size classes (Park et al., 2003; Alexander et al., 2005; Park et al., 2006; Fairlie et al., 2007; Liao et al., 2007). Gas-phase and aerosol chemistry are coupled by in-cloud SO₂ oxidation, gas-aerosol thermodynamic partitioning of SNA and secondary organic aerosol (SOA), aerosol effects on photolysis rates (Martin et al., 2003), and heterogeneous chemistry (Jacob, 2000).

The model forms sulfate aerosol from SO₂ through gas-phase oxidation by OH and in-cloud oxidation by H₂O₂ and ozone (Park et al., 2004). The MARS-A aerosol thermodynamic equilibrium model is used to calculate SNA aerosol formation (Binkowski and Roselle, 2003). Nitric acid is formed by the gas phase reaction of NO₂ with OH and ozone, the latter leading to formation of N₂O₅ which hydrolyzes to HNO₃ in aqueous aerosol (Evans and Jacob, 2005). SOA is formed by oxidation of VOCs by ozone and OH, following the work of Chung and Seinfeld (2002), as implemented in GEOS-Chem by Liao et al. (2007).

Successive versions of GEOS-Chem have been extensively evaluated with surface, aircraft, and satellite observations of tropospheric oxidants, aerosols, and related species. Recent worldwide evaluations with satellite data are presented by Zhang et al. (2010) for ozone, Kopacz et al. (2010) for CO, and van Donkelaar et al. (2010) for aerosol. Comparisons to OH and H₂O₂ vertical profiles measured on aircraft missions have been presented by Hudman et al. (2007) and Mao et al. (2010). Air quality relevant evaluations with surface data for ozone and aerosols have been presented for North America and China (Choi et al., 2009; Wang et al., 2009). In addition, a number of GEOS-Chem studies have eval-

uated the model with observations specifically in the context of intercontinental influences on surface PM (Park et al., 2004; Heald et al., 2006; Donkelaar et al., 2008) and surface ozone (Fiore et al., 2009; Zhang et al., 2009a). GEOS-Chem results contributed to the TF HTAP (2007) multi-model assessment were within the ranges of results from other models.

We conducted a control simulation for year 2000 and six sensitivity simulations where we removed individually anthropogenic emissions of CO, NO_x, and SO₂ from the contiguous US and East Asia. Anthropogenic emissions include fuel and industry, not open fires. We define East Asia as the emission inventory domain of Streets et al. (2003), which extends from Pakistan to Japan in the west-east direction and from Indonesia to Mongolia in the south-north direction. Each simulation used meteorological data for 2000-2001. The first year (2000) was used for model initialization and the second year (2001) for analysis. The model does not allow for aerosols or ozone to affect meteorology. Changes in PM concentrations are thus solely due to atmospheric chemistry.

Anthropogenic emissions of NO_x and SO₂ are from the EDGAR 3.2 FT inventory for 2000 (Olivier and Berdowski, 2001). These include 4.8 Tg N a⁻¹ and 7.5 Tg S a⁻¹ from the contiguous US and 10 Tg N a⁻¹ and 27 Tg S a⁻¹ from East Asia. US anthropogenic emissions of CO are from the EPA National Emissions Inventory 1999 (NEI99; <http://www.epa.gov/ttn/chief/net/1999inventory.html>) and amount to 82 Tg CO a⁻¹. East Asian fossil anthropogenic emissions of CO are from Streets et al. (2006), and amount to 250 Tg CO a⁻¹. Ammonia emissions are from Bouwman et al. (1997). Additional source information for the model is available from Donkelaar et al. (2008).

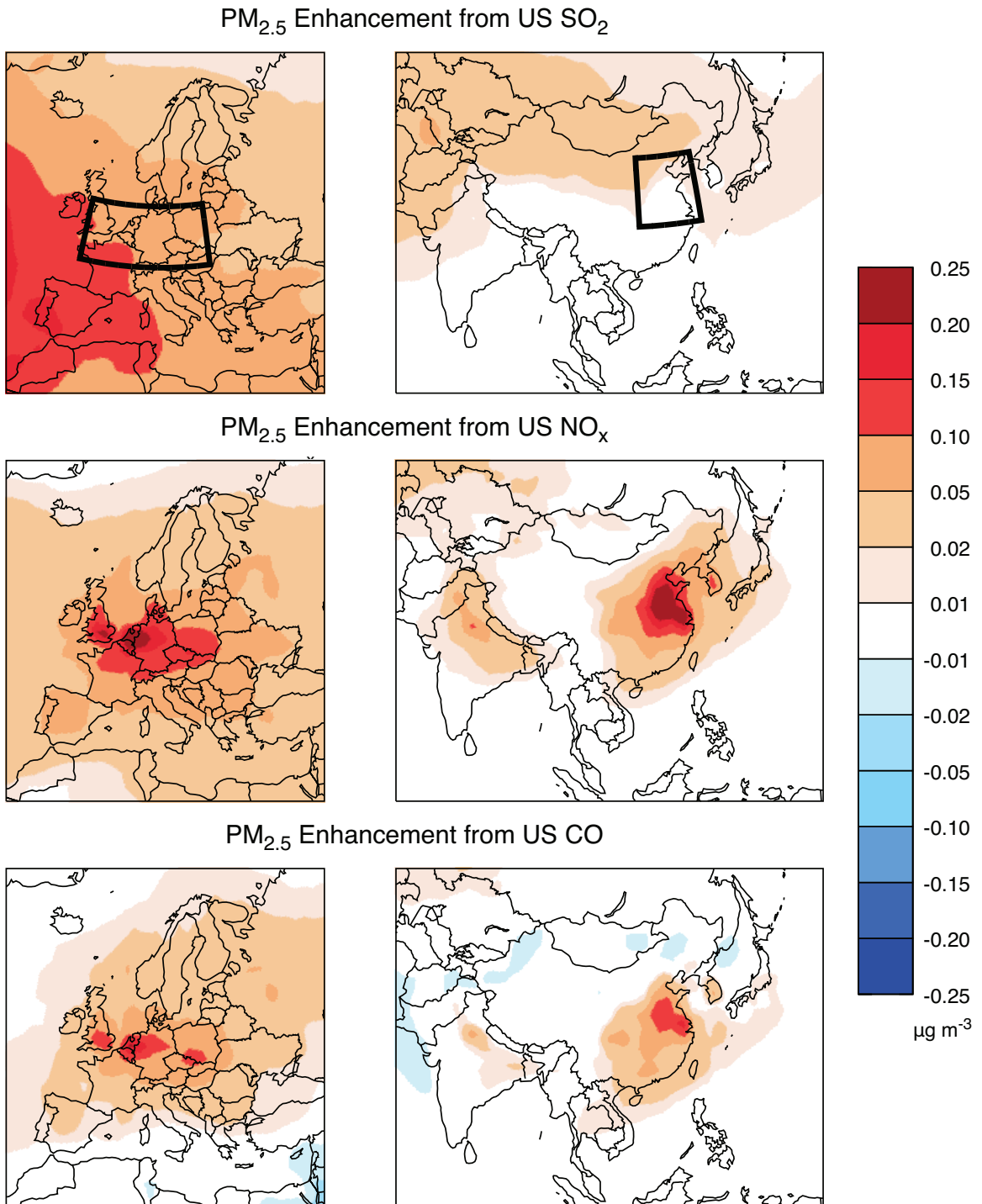


Figure 3.1: Annual mean enhancements of surface PM concentrations in Europe and Asia from US anthropogenic emissions of SO₂ (top), NO_x (middle), and CO (bottom). Values are differences between the control GEOS-Chem simulation and a sensitivity simulation with US anthropogenic emissions shut off. Boxes in the top panels outline receptor regions in northern Europe and eastern China for which speciation and seasonality are shown in Figure 3.2.

3.3 Intercontinental PM enhancements

3.3.1 Effect of US emissions

Figure 3.1 shows the annual mean PM enhancements in Europe and Asia from US anthropogenic sources of SO_2 , NO_x , and CO as calculated by GEOS-Chem. $PM_{2.5}$ enhancements are diagnosed as the differences in surface air concentrations of dry sulfate, nitrate, ammonium, and organic aerosol between the control simulation and a simulation with the corresponding emissions shut off. Fig. 3.2 shows the SNA speciation and seasonality of this enhancement for receptor regions (outlined as boxes in Fig. 3.1). Intercontinental enhancements in organic aerosol concentrations are small ($<5\text{ ng m}^{-3}$) and will not be discussed further.

The intercontinental effects of SO_2 emissions arise from the direct transport of SO_2 and sulfate, and decrease rapidly with distance downwind due to wet and dry removal. US SO_2 emissions thus mainly influence western Europe, by up to $0.2\text{ }\mu\text{g m}^{-3}$ on an annual mean basis. This enhancement is comparable to the results of Park et al. (2004), but larger than those of Chin et al. (2007) and Liu et al. (2009b). Increases in sulfate are partly offset by decreases in nitrate due to competition for ammonium (West et al., 1999; Park et al., 2004). US SO_2 emissions actually induce a net decrease in PM over eastern China in winter because the replacement of $2NH_4NO_3$ by $(NH_4)_2SO_4$ results in net loss of PM mass.

We find that US NO_x emissions enhance European and Asian $PM_{2.5}$ concentrations by up to $0.25\text{ }\mu\text{g m}^{-3}$ on an annual basis. The patterns in Fig. 3.1 show that this is not due to direct intercontinental transport of nitrate and its precursors, but to an increase in background oxidant levels that promotes formation of sulfate and nitrate from local sources of SO_2 and

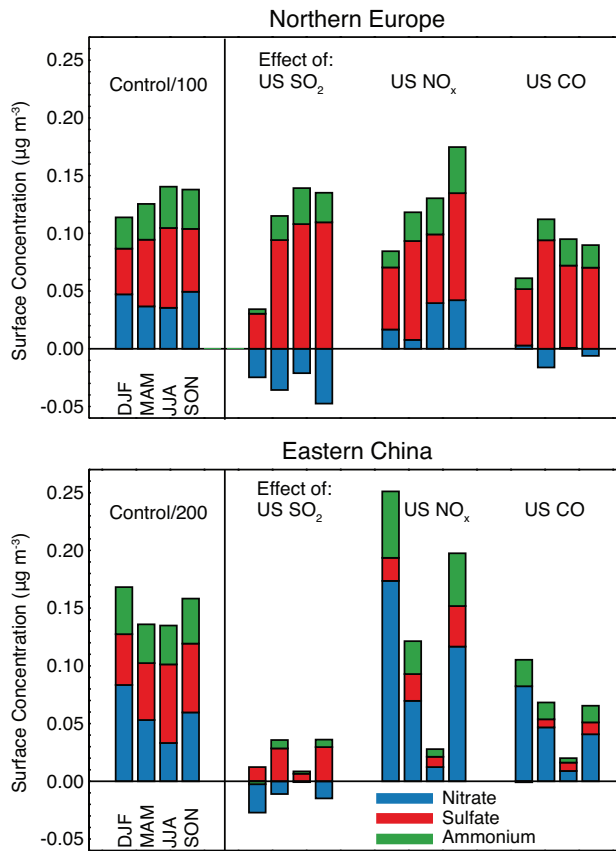


Figure 3.2: Speciation of sulfate-nitrate-ammonium (SNA) PM concentrations in surface air for the receptor regions of Fig. 3.1 (left panels) and corresponding intercontinental enhancements from US anthropogenic emissions of SO_2 , NO_x , and CO (right panels). Values are seasonal means from the GEOS-Chem model. Seasonal concentrations have been divided by 100 (Northern Europe) and 200 (Eastern China) to fit on scale.

NO_x in the receptor regions. US NO_x emissions increase annual mean tropospheric ozone by 3.3%, OH by 3.3%, and H_2O_2 by 0.2% in the Northern Hemisphere, with larger effects in Europe, which is directly downwind.

Figure 3.2 shows that the intercontinental PM enhancement from US NO_x emissions is mostly driven by sulfate in northern Europe but by nitrate in eastern China. Conversion of SO_2 to sulfate in the model is mostly by in-cloud oxidation by H_2O_2 and ozone. The process by H_2O_2 is faster than that by ozone, and in the presence of excess H_2O_2 , SO_2 oxidation is insensitive to increases in oxidants. At the high latitudes of northern Europe,

H_2O_2 production is slow so that SO_2 in-cloud oxidation is H_2O_2 -limited over SO_2 source regions for most of the year; thus increases of ozone and H_2O_2 result in increased sulfate. The sulfate increase is largest in fall due to a combination of extensive cloud cover and significant enhancement of oxidants. Cloud cover is also extensive in winter but the increase in oxidants is then less. In eastern China, by contrast to northern Europe, H_2O_2 -limited conditions prevail only in winter, and cloud cover is then infrequent due to the winter monsoon.

The large enhancement of nitrate PM in eastern China compared to northern Europe in Fig. 3.2 reflects the regional presence of excess ammonia for NH_4NO_3 formation. We find that increases in total inorganic nitrate (gas-phase HNO_3 plus aerosol nitrate) are comparable in the two regions, but northern Europe has less excess ammonia so that this inorganic nitrate remains in the gas phase as HNO_3 . The effect of increased oxidants on nitrate PM in eastern China is largest in winter, when cold temperatures promote nitrate partitioning into the aerosol and when oxidation of NO_x is relatively slow. In summer, oxidation of NO_x by OH in the region is sufficiently fast that the effect of added oxidants is small. This is not the case for northern Europe where OH concentrations are much lower because of the higher latitude.

CO emissions in the US decrease annual mean tropospheric OH by 1.9% in the Northern Hemisphere, but increase ozone by 1.3% and H_2O_2 by 3.4%. The effect on PM is qualitatively similar to that of US NO_x emissions, but not as large due to the decrease in OH concentrations. Speciation and seasonal patterns in Fig. 3.2 are similar to those for the effect of US NO_x emissions. The decrease in OH, affecting NO_x oxidation, results in some negative effects on nitrate in northern Europe. Nitrate concentrations still increase over China in seasons outside of summer, when oxidation of NO_x by ozone is a significant

nitrate formation pathway (Dentener and Crutzen, 1993).

3.3.2 Effect of Asian emissions

Figure 3.3 shows the intercontinental increases in PM from Asian emissions. The intercontinental influence of Asian SO_2 emissions are strongest in the western US where subsidence from the free troposphere brings Asian outflow to the surface. The enhancement of $0.1\text{--}0.25 \mu\text{g m}^{-3}$ in this region is comparable to the results of Park et al. (2004); Heald et al. (2006); Chin et al. (2007). The effect on Europe is weaker and more uniform than that of US SO_2 emissions, which are closer upwind (Fig. 3.1). Increases in sulfate cause lower levels of nitrate due to competition for ammonium, similar to the effects of US SO_2 emissions previously discussed.

The intercontinental influence of Asian NO_x on PM shown in Fig. 3.3 is weaker than that of US emissions (Fig. 3.1). Asian NO_x emissions increase annual mean tropospheric ozone by 8.8%, OH by 12.7%, and H_2O_2 by 1.1%. These increases are much larger than those from US emissions (Section 3.3.1), but the effect on PM is also contingent on emissions in the receptor continent. Thus the effect on the US is relatively weak, up to $0.1 \mu\text{g m}^{-3}$ over the central US where excess ammonia from agricultural emissions promotes ammonium nitrate formation. The effect on northern Europe (up to $0.2 \mu\text{g m}^{-3}$) is also weaker than for US emissions, which are closer upwind (Fig. 3.1). Figure 3.4 shows that sulfate accounts for most of the overall increase in PM over the eastern US and northern Europe. The increase is weakest in summer when Asian NO_x emissions actually cause H_2O_2 concentrations to decrease over the US and Europe. This reflects the large Asian source of NO_x and complicated effects of NO_x emissions on H_2O_2 . On the one hand, NO_x leads to ozone production and from there to H_2O_2 production. On the other hand, NO_x increases

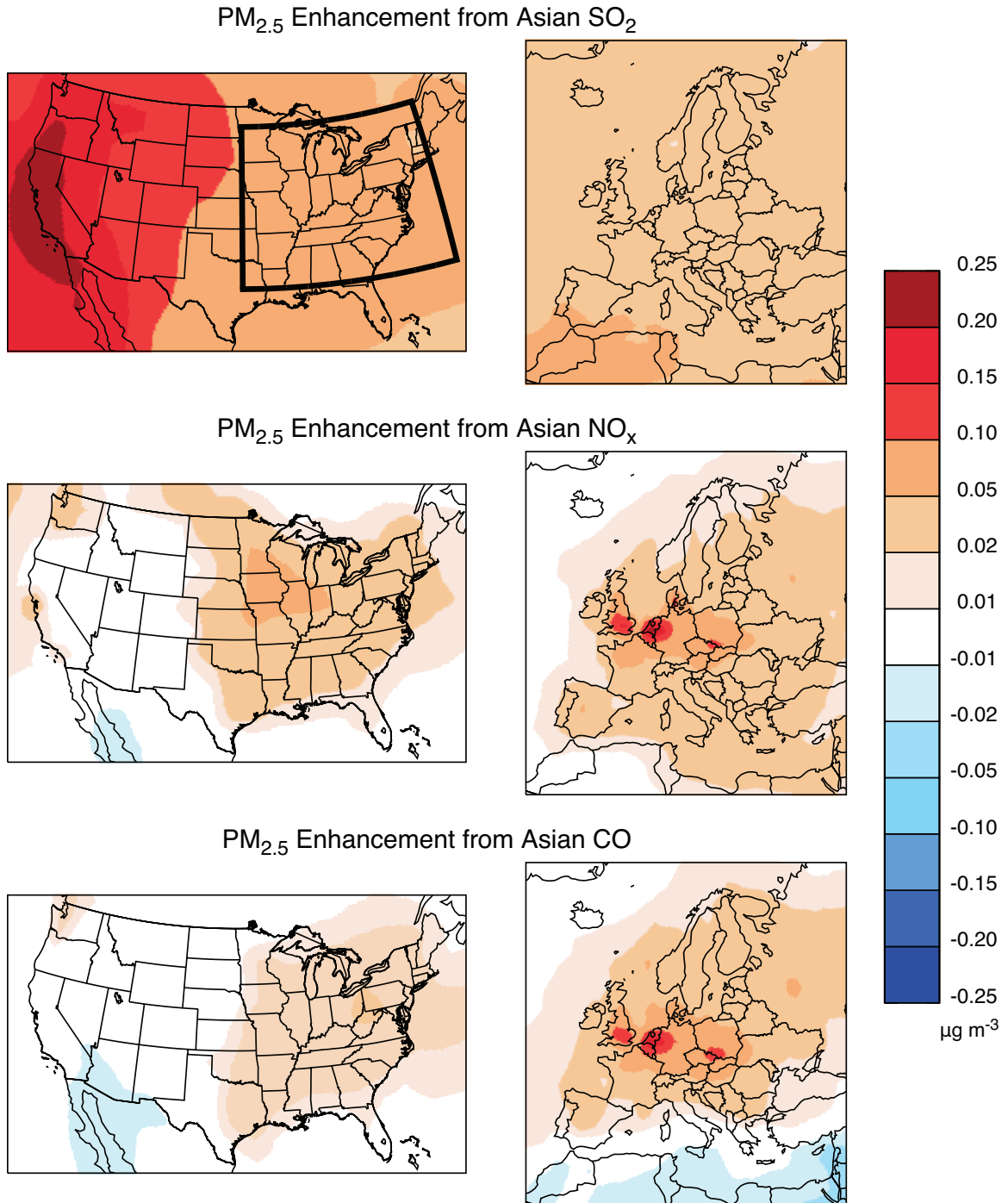


Figure 3.3: Annual mean enhancements of surface PM concentrations in Europe and the United States from Asian anthropogenic emissions of SO₂ (top), NO_x (middle), and CO (bottom). Values are differences between the control GEOS-Chem simulation and a sensitivity simulation with Asian anthropogenic sources shut off. Boxes in the top panels outline the receptor region in the United States for which speciation and seasonality are shown in Fig. 3.4.

OH , which is a major H_2O_2 sink.

Asian CO emissions decrease annual mean tropospheric OH by 5.6% and increase ozone by 3.1% and H_2O_2 by 9.4%. Figures 3.3 and 3.4 show that Asian CO affects northern European PM in a very similar manner to US CO emissions (Figs. 3.1 and 3.2) and with a similar magnitude as Asian NO_x . Similar to the effect of US CO emissions, Asian CO emissions increase in-cloud sulfate production by H_2O_2 over Europe causing sulfate enhancements in all seasons. Changes in sulfate in the US are largely driven by increased production by H_2O_2 . A reduction in gas-phase production of sulfate by OH detracts from

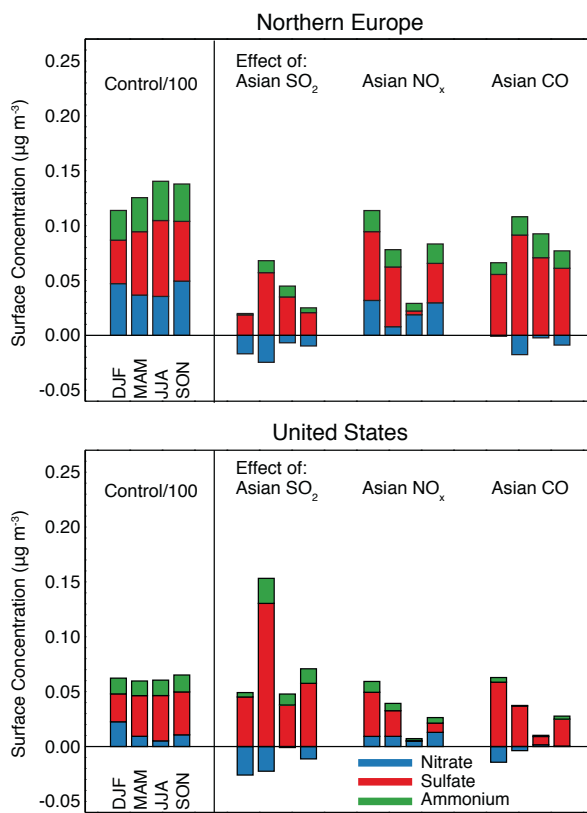


Figure 3.4: Speciation of sulfate-nitrate-ammonium (SNA) PM concentrations in surface air for the receptor regions of Figs. 3.1 and 3.3 (left panels) and corresponding intercontinental enhancements from Asian anthropogenic emissions of SO_2 , NO_x , and CO (right panels). Values are seasonal means from the GEOS-Chem model. Seasonal concentrations have been divided by 100 to fit on scale.

increased aqueous production. Nitrate concentrations decrease in both northern Europe and the US because of the lower OH concentrations.

3.4 Discussion

Anthropogenic emissions of NO_x and CO perturb sulfate and nitrate PM concentrations on intercontinental scales by affecting the background concentrations of oxidants and hence the oxidation rates of SO₂ and NO_x emitted in receptor regions. NO_x emissions cause OH, ozone, and H₂O₂ to increase on the hemispheric scale although H₂O₂ can decrease in some regions and seasons. CO emissions cause OH to decrease, but ozone and H₂O₂ concentrations to increase. CO increases H₂O₂ formation in part by decreasing OH, a major sink of H₂O₂ and in part by decreasing the OH/HO₂ ratio and thus promoting H₂O₂ formation. Most of the intercontinental effect on sulfate is through increases in ozone and H₂O₂, which drive faster SO₂ in-cloud oxidation under H₂O₂-limited conditions. Most of the effect of nitrate is through the increase in ozone in winter and the shoulder seasons, when NO_x oxidation is otherwise slow and the cold temperatures promote nitrate fractionation into the aerosol.

The intercontinental PM enhancement from NO_x and CO emissions tends to peak in receptor regions with the highest domestic sources of SO₂, NO_x, and NH₃, and hence with the highest PM concentrations. It is thus of particular policy relevance. US emissions of NO_x and CO increase PM by over 0.25 $\mu\text{g m}^{-3}$ (annual mean) in polluted regions of northern Europe and eastern China, a much larger effect than that of US SO₂ emissions. PM concentrations in the US are less sensitive to intercontinental NO_x and CO emissions because domestic PM sources are lower. The effect of Asian NO_x and CO on PM in the eastern US is still 0.1 $\mu\text{g m}^{-3}$, comparable to the effect of Asian SO₂ emissions. Northern

Europe is more sensitive to US than to Asian emissions of NO_x and CO because of the greater upwind proximity.

Our study used emission inventories for 2000. Emissions have changed over the past decade and also have some uncertainty. The more recent EPA NEI 2005 inventory for the US (<http://www.epa.gov/ttnchie1/net/2005inventory.html>) includes 2% more NO_x, 20% less CO, and 57% less SO₂ than used in this work, while the East Asian 2006 inventory of Zhang et al. (2009b) include 12% more NO_x, 19% more CO, and 14% less SO₂. These differences arise from both actual trends and improved emission accounting. The emission changes would tend to increase the importance of NO_x and CO vs. SO₂ in driving intercontinental influence on PM.

The intercontinental influence of NO_x and CO emissions on PM through changes in background oxidant fields depends in a complex way on the chemical environment in the receptor region including (1) the relative importance of OH, ozone, and H₂O₂ as oxidants for SO₂ and NO_x; (2) cloudiness; (3) H₂O₂ limitation of in-cloud SO₂ oxidation by H₂O₂; and (4) availability of ammonia for nitrate PM formation. All of these factors have substantial uncertainty in models, and the corresponding errors cannot easily be quantified using a single model. The intercontinental influence on oxidant levels is itself uncertain. The HTAP multi-model intercomparison of Fiore et al. (2009) shows good agreement between models for intercontinental influences on ozone, but no such evaluations have been conducted for OH and H₂O₂. In view of the potential for significant impacts presented in this paper, it would be of great interest to carry out a multi-model intercomparison of intercontinental influences of NO_x and CO emissions on PM.

Bibliography

- Alexander, B., Park, R., Jacob, D., Li, Q., Yantosca, R., Savarino, J., Lee, C., and Thiemens, M. (2005). Sulfate formation in sea-salt aerosols: Constraints from oxygen isotopes. *J Geophys Res-Atmos*, 110(D10):D10307.
- Barrett, S. R. H., Britter, R. E., and Waitz, I. A. (2010). Global mortality attributable to aircraft cruise emissions. *Environ Sci Technol*, 44(19):7736–7742.
- Binkowski, F. and Roselle, S. (2003). Models-3 Community Multiscale Air Quality (CMAQ) model aerosol component - 1. Model description. *J Geophys Res-Atmos*, 108(D6):4183.
- Bouwman, A. F., Lee, D. S., Asman, W. S. H., Dentener, F. J., Hoek, K. W. V. D., and Olivier, J. G. J. (1997). A global high-resolution emission inventory for ammonia. *Global Biogeochem Cy*, 11(4):561–587.
- Chin, M., Diehl, T., Ginoux, P., and Malm, W. (2007). Intercontinental transport of pollution and dust aerosols: Implications for regional air quality. *Atmos Chem Phys*, 7(21):5501–5517.
- Choi, Y.-S., Park, R. J., and Ho, C.-H. (2009). Estimates of ground-level aerosol mass concentrations using a chemical transport model with Moderate Resolution Imaging Spectroradiometer (MODIS) aerosol observations over East Asia. *J Geophys Res-Atmos*, 114(D4):D04204.
- Chung, S. and Seinfeld, J. (2002). Global distribution and climate forcing of carbonaceous aerosols. *J Geophys Res-Atmos*, 107(D19):4407.
- Dentener, F. J. and Crutzen, P. J. (1993). Reaction of N_2O_5 on tropospheric aerosols: Impact on the global distributions of NO_x , O_3 , and OH. *J Geophys Res-Atmos*, 98(D4):7149–7163.
- Donkelaar, A. V., Martin, R. V., Leaitch, W. R., Macdonald, A. M., Walker, T. W., Streets, D. G., Zhang, Q., Dunlea, E. J., Jimenez, J. L., Dibb, J. E., Huey, L. G., Weber, R., and Andreae, M. O. (2008). Analysis of aircraft and satellite measurements from the Intercontinental Chemical Transport Experiment (INTEX-B) to quantify long-range transport of East Asian sulfur to Canada. *Atmos Chem Phys*, 8(11):2999–3014.
- Evans, M. and Jacob, D. (2005). Impact of new laboratory studies of N_2O_5 hydrolysis on global model budgets of tropospheric nitrogen oxides, ozone, and OH. *Geophys Res Lett*, 32(9):L09813.
- Fairlie, T. D., Jacob, D. J., and Park, R. J. (2007). The impact of transpacific transport of mineral dust in the United States. *Atmos Environ*, 41(6):1251–1266.

- Fiore, A. M., Dentener, F. J., Wild, O., Cuvelier, C., Schultz, M. G., Hess, P., Textor, C., Schulz, M., Doherty, R. M., Horowitz, L. W., Mackenzie, I. A., Sanderson, M. G., Shindell, D. T., Stevenson, D. S., Szopa, S., Dingenen, R. V., Zeng, G., Atherton, C., Bergmann, D., Bey, I., Carmichael, G., Collins, W. J., Duncan, B. N., Faluvegi, G., Folberth, G., Gauss, M., Gong, S., Hauglustaine, D., Holloway, T., Isaksen, I. S. A., Jacob, D. J., Jonson, J. E., Kaminski, J. W., Keating, T. J., Lupu, A., Marmer, E., Montanaro, V., Park, R. J., Pitari, G., Pringle, K. J., Pyle, J. A., Schroeder, S., Vivanco, M. G., Wind, P., Wojcik, G., Wu, S., and Zuber, A. (2009). Multimodel estimates of intercontinental source-receptor relationships for ozone pollution. *J Geophys Res-Atmos*, 114:D04301.
- Forster, C., Wandinger, U., Wotawa, G., James, P., Mattis, I., Althausen, D., Simmonds, P., O'doherty, S., Jennings, S., Kleefeld, C., Schneider, J., Trickl, T., Kreipl, S., Jager, H., and Stohl, A. (2001). Transport of boreal forest fire emissions from Canada to Europe. *J Geophys Res-Atmos*, 106(D19):22887–22906.
- Heald, C. L., Jacob, D. J., Park, R. J., Alexander, B., Fairlie, T. D., Yantosca, R. M., and Chu, D. A. (2006). Transpacific transport of Asian anthropogenic aerosols and its impact on surface air quality in the United States. *J Geophys Res-Atmos*, 111(D14):D14310.
- Hudman, R. C., Jacob, D. J., Turquety, S., Leibensperger, E. M., Murray, L. T., Wu, S., Gilliland, A. B., Avery, M., Bertram, T. H., Brune, W., Cohen, R. C., Dibb, J. E., Flocke, F. M., Fried, A., Holloway, J., Neuman, J. A., Orville, R., Perring, A., Ren, X., Sachse, G. W., Singh, H. B., Swanson, A., and Wooldridge, P. J. (2007). Surface and lightning sources of nitrogen oxides over the United States: Magnitudes, chemical evolution, and outflow. *J Geophys Res-Atmos*, 112(D12):D12S05.
- Husar, R., Tratt, D., Schichtel, B., Falke, S., Li, F., Jaffe, D., Gasso, S., Gill, T., Laulainen, N., Lu, F., Reheis, M., Chun, Y., Westphal, D., Holben, B., Gueymard, C., McKendry, I., Kuring, N., Feldman, G., McClain, C., Frouin, R., Merrill, J., DuBois, D., Vignola, F., Murayama, T., Nickovic, S., Wilson, W., Sassen, K., Sugimoto, N., and Malm, W. (2001). Asian dust events of April 1998. *J Geophys Res-Atmos*, 106(D16):18317–18330.
- Jacob, D. (2000). Heterogeneous chemistry and tropospheric ozone. *Atmos Environ*, 34(12–14):2131–2159.
- Jaffe, D., Anderson, T., Covert, D., Kotchenruther, R., Trost, B., Danielson, J., Simpson, W., Berntsen, T., Karlsdottir, S., Blake, D., Harris, J., Carmichael, G., and Uno, I. (1999). Transport of Asian air pollution to North America. *Geophys Res Lett*, 26(6):711–714.
- Jaffe, D., McKendry, I., Anderson, T., and Price, H. (2003). Six 'new' episodes of trans-Pacific transport of air pollutants. *Atmos Environ*, 37(3):391–404.
- Kloster, S., Dentener, F., Feichter, J., Raes, F., van Aardenne, J., Roeckner, E., Lohmann, U., Stier, P., and Swart, R. (2008). Influence of future air pollution mitigation strategies on total aerosol radiative forcing. *Atmos Chem Phys*, 8(21):6405–6437.

- Kopacz, M., Jacob, D. J., Fisher, J. A., Logan, J. A., Zhang, L., Megretskiaia, I. A., Yantosca, R. M., Singh, K., Henze, D. K., Burrows, J. P., Buchwitz, M., Khlystova, I., McMillan, W. W., Gille, J. C., Edwards, D. P., Eldering, A., Thouret, V., and Nedelec, P. (2010). Global estimates of CO sources with high resolution by adjoint inversion of multiple satellite datasets (MOPITT, AIRS, SCIAMACHY, TES). *Atmos Chem Phys*, 10:855–876.
- Liao, H., Henze, D. K., Seinfeld, J. H., Wu, S., and Mickley, L. J. (2007). Biogenic secondary organic aerosol over the United States: Comparison of climatological simulations with observations. *J Geophys Res-Atmos*, 112(D6):D06201.
- Liu, J., Mauzerall, D. L., and Horowitz, L. W. (2009a). Evaluating inter-continental transport of fine aerosols:(2) Global health impact. *Atmos Environ*, 43(28):4339–4347.
- Liu, J., Mauzerall, D. L., Horowitz, L. W., Ginoux, P., and Fiore, A. M. (2009b). Evaluating inter-continental transport of fine aerosols: (1) Methodology, global aerosol distribution and optical depth. *Atmos Environ*, 43(28):4327–4338.
- Mao, J., Jacob, D. J., Evans, M. J., Olson, J. R., Ren, X., Brune, W. H., Clair, J. M. S., Crounse, J. D., Spencer, K. M., Beaver, M. R., Wennberg, P. O., Cubison, M. J., Jimenez, J. L., Fried, A., Weibring, P., Walega, J. G., Hall, S. R., Weinheimer, A. J., Cohen, R. C., Chen, G., Crawford, J. H., McNaughton, C., Clarke, A. D., Jaegle, L., Fisher, J. A., Yantosca, R. M., Sager, P. L., and Carouge, C. (2010). Chemistry of hydrogen oxide radicals HO_x in the Arctic troposphere in spring. *Atmos Chem Phys*, 10(13):5823–5838.
- Martin, R., Jacob, D., Yantosca, R., Chin, M., and Ginoux, P. (2003). Global and regional decreases in tropospheric oxidants from photochemical effects of aerosols. *J Geophys Res-Atmos*, 108(D3):4097.
- Olivier, J. G. J. and Berdowski, J. J. M. (2001). *The Climate System*. A. A. Balkema Publishers/Swets and Zeitliner Publishers, Lisse, Netherlands.
- Park, R., Jacob, D., Chin, M., and Martin, R. (2003). Sources of carbonaceous aerosols over the United States and implications for natural visibility. *J Geophys Res-Atmos*, 108(D12):4355.
- Park, R., Jacob, D., Field, B., Yantosca, R., and Chin, M. (2004). Natural and transboundary pollution influences on sulfate-nitrate-ammonium aerosols in the United States: Implications for policy. *J Geophys Res-Atmos*, 109(D15):D15204.
- Park, R. J., Jacob, D. J., Kumar, N., and Yantosca, R. M. (2006). Regional visibility statistics in the United States: Natural and transboundary pollution influences, and implications for the Regional Haze Rule. *Atmos Environ*, 40(28):5405–5423.

- Peltier, R. E., Hecobian, A. H., Weber, R. J., Stohl, A., Atlas, E. L., Riemer, D. D., Blake, D. R., Apel, E., Campos, T., and Karl, T. (2008). Investigating the sources and atmospheric processing of fine particles from Asia and the Northwestern United States measured during INTEX B. *Atmos Chem Phys*, 8(6):1835–1853.
- Prospero, J. (1999). Long-term measurements of the transport of African mineral dust to the southeastern United States: Implications for regional air quality. *J Geophys Res-Atmos*, 104(D13):15917–15927.
- Rae, J. G. L., Johnson, C. E., Bellouin, N., Boucher, O., Haywood, J. M., and Jones, A. (2007). Sensitivity of global sulphate aerosol production to changes in oxidant concentrations and climate. *J Geophys Res-Atmos*, 112(D10):D10312.
- Shindell, D., Lamarque, J. F., Unger, N., Koch, D., Faluvegi, G., Bauer, S., Ammann, M., Cofala, J., and Teich, H. (2008). Climate forcing and air quality change due to regional emissions reductions by economic sector. *Atmos Chem Phys*, 8(23):7101–7113.
- Shindell, D. T., Faluvegi, G., Koch, D. M., Schmidt, G. A., Unger, N., and Bauer, S. E. (2009). Improved attribution of climate forcing to emissions. *Science*, 326(5953):716–718.
- Streets, D., Bond, T., Carmichael, G., Fernandes, S., Fu, Q., He, D., Klimont, Z., Nelson, S., Tsai, N., Wang, M., Woo, J., and Yarber, K. (2003). An inventory of gaseous and primary aerosol emissions in Asia in the year 2000. *J Geophys Res-Atmos*, 108(D21):8809.
- Streets, D. G., Zhang, Q., Wang, L., He, K., Hao, J., Wu, Y., Tang, Y., and Carmichael, G. R. (2006). Revisiting China's CO emissions after the Transport and Chemical Evolution over the Pacific (TRACE-P) mission: Synthesis of inventories, atmospheric modeling, and observations. *J Geophys Res-Atmos*, 111(D14):D14306.
- Task Force on Hemispheric Transport of Air Pollution (2007). *Hemispheric transport of air pollution*. Air Pollut. Stud. 16. U.N. Econ. Comm. for Europe.
- Unger, N., Shindell, D. T., Koch, D. M., and Streets, D. G. (2006). Cross influences of ozone and sulfate precursor emissions changes on air quality and climate. *P Natl Acad Sci USA*, 103(12):4377–4380.
- van Donkelaar, A., Martin, R. V., Brauer, M., Kahn, R., Levy, R., Verduzco, C., and Vileneuve, P. J. (2010). Global estimates of ambient fine particulate matter concentrations from satellite-based aerosol optical depth: Development and application. *Environ Health Persp*, 118(6):847–855.
- Wang, Y., Hao, J., McElroy, M. B., Munger, J. W., Ma, H., Chen, D., and Nielsen, C. P. (2009). Ozone air quality during the 2008 Beijing Olympics: Effectiveness of emission restrictions. *Atmos Chem Phys*, 9(14):5237–5251.

- West, J., Ansari, A., and Pandis, S. (1999). Marginal PM_{2.5}: Nonlinear aerosol mass response to sulfate reductions in the eastern United States: Nonlinear aerosol mass response to sulfate reductions in the Eastern United States. *J Air Waste Manage*, 49(12):1415–1424.
- Yu, H., Remer, L. A., Chin, M., Bian, H., Kleidman, R. G., and Diehl, T. (2008). A satellite-based assessment of transpacific transport of pollution aerosol. *J Geophys Res-Atmos*, 113(D14):D14S12.
- Zhang, L., Jacob, D. J., Kopacz, M., Henze, D. K., Singh, K., and Jaffe, D. A. (2009a). Intercontinental source attribution of ozone pollution at western U.S. sites using an adjoint method. *Geophys Res Lett*, 36(11):L11810.
- Zhang, L., Jacob, D. J., Liu, X., Logan, J. A., Chance, K., Eldering, A., and Bojkov, B. R. (2010). Intercomparison methods for satellite measurements of atmospheric composition: application to tropospheric ozone from TES and OMI. *Atmos Chem Phys*, 10(10):4725–4739.
- Zhang, Q., Streets, D. G., Carmichael, G. R., He, K. B., Huo, H., Kannari, A., Klimont, Z., Park, I. S., Reddy, S., Fu, J. S., Chen, D., Duan, L., Lei, Y., Wang, L. T., and Yao, Z. L. (2009b). Asian emissions in 2006 for the NASA INTEX-B mission. *Atmos Chem Phys*, 9(14):5131–5153.

Chapter 4

Climatic effects of 1950-2050 changes in US anthropogenic aerosols

Part 1: Aerosol trends and radiative forcing

Abstract

We use the GEOS-Chem chemical transport model combined with the GISS general circulation model to calculate the aerosol direct and indirect (cloud) radiative forcings from US anthropogenic sources over the 1950-2050 period, based on historical emission inventories and future projections from the IPCC A1B scenario. The aerosol simulation is evaluated with observed spatial distributions and 1980-2010 trends of aerosol concentrations and wet deposition in the contiguous US. The radiative forcing from US anthropogenic aerosols is strongly localized over the eastern US. We find that it peaked in 1970-1990, with values over the eastern US (east of 100°W) of -2.0 W m^{-2} for direct forcing including contributions from sulfate (-2.0 W m^{-2}), nitrate (-0.2 W m^{-2}), organic carbon (-0.2 W m^{-2}), and black carbon ($+0.4 \text{ W m}^{-2}$). The aerosol indirect effect is of comparable magnitude to the direct forcing. We find that the forcing declined sharply from 1990 to 2010 (by 0.8 W m^{-2} direct and 1.0 W m^{-2} indirect), mainly reflecting decreases in SO₂ emissions, and project that it will continue declining post-2010 but at a much slower rate since US SO₂ emissions have already declined by almost 60% from their peak. This suggests that much of the warming effect from reducing US anthropogenic aerosol sources may have already been realized. The small positive radiative forcing from US BC emissions ($+0.3 \text{ W m}^{-2}$ over the eastern US in 2010) suggests that an emission control strategy focused on BC would have only limited climate benefit.

4.1 Introduction

Growth in population and energy demand over the past 100 years has greatly increased the anthropogenic source of atmospheric aerosols in the United States. This has caused public health, visibility, and deposition concerns (US Environmental Protection Agency (US EPA), 2009; 2010). Increasingly strict regulations on aerosol sources have been enacted by US air quality agencies over the past decades. However, aerosols also exert a negative radiative forcing on climate and reductions in their abundance aggravate greenhouse-driven climate change (Raes and Seinfeld, 2009). We quantify in this paper the changes in radiative forcing arising from historical and projected trends of US anthropogenic aerosol sources for the 1950-2050 period. In Chapter 5, we use a general circulation model (GCM) to analyze the resulting climate response.

Anthropogenic aerosols mainly consist of sulfate, nitrate, ammonium, black carbon (BC), and organic carbon (OC). Sulfate and nitrate aerosols are formed by oxidation of SO_2 and nitrogen oxides ($\text{NO}_x \equiv \text{NO} + \text{NO}_2$). Coal combustion is the dominant source of SO_2 in the US. SO_2 emissions grew until 1980 and then decreased by 56% between 1980 and 2008 (US EPA, 2010). Anthropogenic NO_x is emitted by fuel combustion in general and US emissions decreased by 36% between 1990 and 2008 (US EPA, 2010). Ammonia originates mainly from agriculture (Park et al., 2004) and has not been subjected to regulation. BC is emitted from combustion. Organic aerosol is traditionally partitioned by models into a primary component (POA) from combustion and a secondary component (SOA) of dominant biogenic origin (Chung and Seinfeld, 2002). According to Bond et al. (2007), US anthropogenic emissions of BC and POA decreased from 1925 to 1970 due to decline in residential coal use, but increased from 1970 to 1990 due to increase in broader

fuel use.

Aerosols directly affect climate by scattering and absorbing solar radiation. The Intergovernmental Panel on Climate Change (IPCC) estimates the aerosol direct effect to presently exert a global mean negative radiative forcing of $-0.5 \pm 0.4 \text{ W m}^{-2}$, partly offsetting the positive radiative forcing of $+2.6 \pm 0.3 \text{ W m}^{-2}$ from the long-lived greenhouse gases (Forster et al., 2007). Additionally, aerosols indirectly affect climate by acting as cloud condensation nuclei (CCN) and altering cloud properties. An increase in CCN generates more and smaller cloud droplets for the same cloud liquid water content, making clouds brighter (cloud albedo effect; Twomey, 1974) and longer lived (cloud lifetime effect; Albrecht, 1989). The IPCC best estimate for the global indirect radiative forcing from the cloud albedo effect is -0.7 W m^{-2} , with a range of uncertainty from -0.3 to -1.8 W m^{-2} (Forster et al., 2007). The cloud lifetime effect is even more uncertain, but could be comparable in magnitude to the cloud albedo effect with additional effects on the hydrological cycle (Denman et al., 2007). Additional aerosol indirect radiative effects involving cloud absorption, height, or glaciation could also be significant (Denman et al., 2007).

The need to integrate air quality and climate change mitigation objectives in environmental policymaking is increasingly recognized (National Research Council, 2005; Raes and Seinfeld, 2009; Penner et al., 2010). This is particularly the case for aerosols since air quality improvements come at the cost of climate warming. The US is an interesting testbed to analyze the climate implications of environmental regulations since the historical period from 1950 to present has witnessed a reversal of aerosol trends, increasing until 1980 and then decreasing, with regulations in place to enforce continued decrease in the future. Recent GCM simulations by Mickley et al. (submitted) suggest that completely removing US anthropogenic aerosol sources would increase temperatures in the eastern US by 0.4-

0.6°C on an annual mean basis and as much as by 1-2°C during summer heat waves. It has been argued that decreasing BC emissions (and hence aerosol absorption) could provide a win-win strategy for air quality and climate change mitigation (Jacobson, 2002; Bond, 2007; Grieshop et al., 2009). However, it is not clear how such a strategy could be implemented since BC sources cannot be controlled in isolation from other aerosol components, in particular POA (Chen et al., 2010a; Unger et al., 2010).

We use here a global chemical transport model (GEOS-Chem CTM) to reconstruct historical aerosol trends from 1950 to present and project future trends to 2050, with focus on the US aerosol loadings and including evaluation with observed trends. We then use the results in the Goddard Institute for Space Studies (GISS) GCM 3 to construct a 1950-2050 timeline of aerosol direct and indirect radiative forcing with decadal resolution, resolving the contributions from the different aerosol components. These decadal forcings for the 1950-2050 period are used in Chapter 5 to determine the sensitivity of US climate to anthropogenic aerosol sources in the past and in the future.

4.2 Methods

4.2.1 Global aerosol simulation

We use GEOS-Chem CTM simulations of coupled tropospheric ozone- NO_x -VOC-aerosol chemistry (version 8.01.01; <http://geos-chem.org/>) to describe the global evolution of aerosol concentrations resulting from changes in anthropogenic emissions from 1950 to 2050. The simulations are conducted for a series of 2-year decadal time slices from 1950 to 2050. The first year is used for initialization and the second year for analysis. All simulations use the same 2000-2001 meteorological data from the NASA Goddard Earth Observing System (GEOS-4). Using the same meteorological year isolates the effects of emission changes.

The GEOS-4 data are available with $1^\circ \times 1.25^\circ$ horizontal resolution, 55 levels in the vertical, and a temporal resolution of 6 hours (3 hours for surface variables). The data are regridged here to $2^\circ \times 2.5^\circ$ horizontal resolution for input to GEOS-Chem.

GEOS-Chem simulates the aerosol mass concentrations of sulfate-nitrate-ammonium (SNA), POA, SOA, and BC (Park et al., 2006; Liao et al., 2007). Gas-phase and aerosol chemistry are coupled by in-cloud SO_2 oxidation, gas-aerosol thermodynamic partitioning of SNA and SOA, aerosol effects on photolysis rates (Martin et al., 2003), and heterogeneous chemistry (Jacob, 2000; Evans and Jacob, 2005). Water-soluble gases and aerosols are scavenged in convective updrafts as well as by rainout and washout from convective anvils and large-scale precipitation (Liu et al., 2001). The model allows for species to return to the atmosphere if falling precipitation evaporates. Dry deposition is modeled using a resistance in series scheme (Wesely, 1989) as described in Wang et al. (1998).

Sulfate is formed by gas-phase reaction of SO_2 with OH and aqueous-phase reaction of SO_2 with H_2O_2 and ozone in clouds and sea-salt aerosols (Alexander et al., 2005). The global mean tropospheric lifetime of sulfate in the model is 4.0 days, comparable to other sulfate models (Schulz et al., 2006). Formation of SNA aerosol is computed locally with the MARS-A aerosol thermodynamic equilibrium model (Binkowski and Roselle, 2003). Following Park et al. (2005), we assume that 20% of BC and 50% of POA emitted from anthropogenic sources is hydrophilic and thus available for in-cloud scavenging. The remaining portions of BC and POA are emitted as hydrophobic and become hydrophilic in the atmosphere with an *e*-folding time of 1.2 days. Formation of SOA involves gas-aerosol partitioning of semi-volatile VOC oxidation products (Odum et al., 1997). It follows the work of Chung and Seinfeld (2002) as implemented in GEOS-Chem (Heald et al., 2006; Liao et al., 2007) and extended by Henze and Seinfeld (2006).

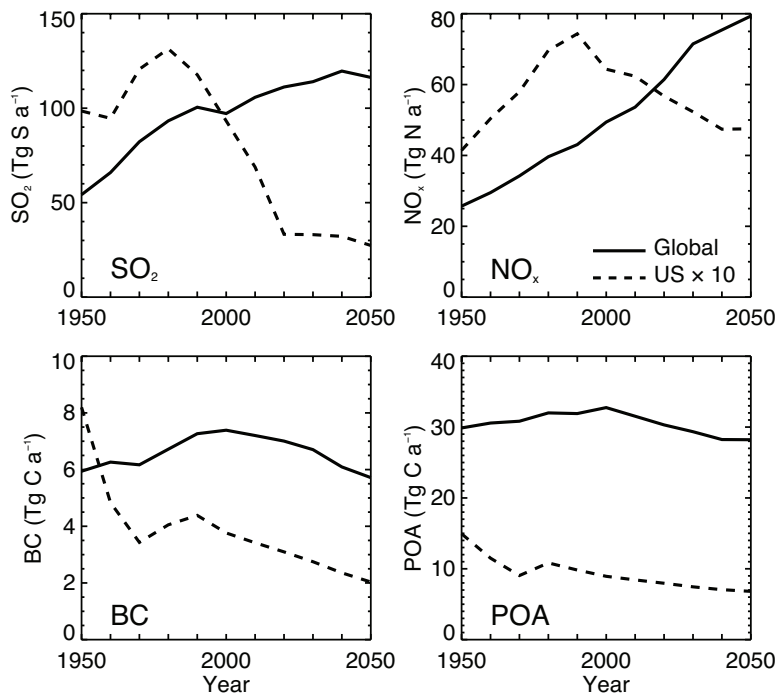


Figure 4.1: Global (solid) and US (dashed) trends in emissions of SO_2 , NO_x , BC, and POA for 1950-2050.

Figure 4.1 shows the 1950-2050 trends of global and US aerosol sources. Emissions of SO_2 and NO_x are from EDGAR Hyde 1.3 (van Aardenne et al., 2001) for 1950-1990 and EDGAR 3.2 FT (Olivier and Berdowski, 2001) for the year 2000. Emissions of BC and POA are from Bond et al. (2007). 2010-2050 decadal emissions are calculated by applying growth factors to year 2000 emissions. Similar to Fiore et al. (2002) and Wu et al. (2008), growth factors for different categories of anthropogenic emissions (biofuel and fossil fuel) and countries are derived from the Integrated Model to Assess the Greenhouse Effect (IMAGE; Streets et al., 2004) following the IPCC A1B scenario (Nakićenović and Swart, 2000). We do not consider trends in global emissions from aircraft (0.07 Tg S a^{-1} ; Chin et al., 2000) and ships (4.2 Tg S a^{-1} ; Corbett et al., 1999).

Natural sources of SO_2 , NO_x , and VOCs are held constant for the 1950-2050 period.

Volcanic emissions of SO_2 (non-eruptive and continuously eruptive only) are from Andres and Kasgnoc (1998) and amount to 5.5 Tg S a^{-1} . Oceanic dimethylsulfide (DMS) in GEOS-Chem has a global source of 21 Tg S a^{-1} and produces 19 Tg S a^{-1} of SO_2 following oxidation by OH and NO_3 (Park et al., 2004). Lightning NO_x emissions are calculated from a parameterization based on cloud top height (Price and Rind, 1992) and then scaled locally to match satellite observations from the Optical Transient Detector/Lightning Imaging Sensor (Sauvage et al., 2007; Murray et al., in prep). The global emission of lightning NO_x is 5.6 Tg N a^{-1} . Soil NO_x emissions follow the algorithm of Yienger and Levy (1995) as implemented by Wang et al. (1998); this amounts globally to 6.6 Tg N a^{-1} including 0.7 Tg N a^{-1} from fertilizer application (also held constant over 1950-2050). Biogenic emissions of isoprene and monoterpenes are calculated using the Model of Emissions of Gases and Aerosols from Nature (MEGAN; Guenther et al., 2006), which yields globally 380 Tg C a^{-1} isoprene and 98 Tg C a^{-1} monoterpenes. We use the climatological biomass burning inventory from Duncan et al. (2003), which yields 1.2 Tg S a^{-1} of SO_2 , 6.5 Tg N a^{-1} of NO_x , 2.9 Tg C a^{-1} of BC, and 23 Tg C a^{-1} of POA.

Ammonia emissions are also held constant over the 1950-2050 period for lack of better information. We use the global inventory of Bouwman et al. (1997) overwritten in southeastern Asia by Streets et al. (2003). Seasonal variations of ammonia emissions are described by Park et al. (2004). Global emissions total 60 Tg N a^{-1} including 40 Tg N a^{-1} from anthropogenic sources (mainly agriculture), 14 Tg N a^{-1} from natural biogenic activity, and 5.9 Tg N a^{-1} from biomass burning. US emissions total 2.2 Tg N a^{-1} from anthropogenic sources, 0.6 Tg N a^{-1} from natural biogenic activity, and 0.04 Tg N a^{-1} from biomass burning. As in Park et al. (2004), we reduce US ammonia emissions by 10% to match inverse model results of Gilliland et al. (2003).

4.2.2 Direct aerosol radiative forcing

We use the GISS GCM 3 (Rind et al., 2007) as modified by (Chen et al., 2010b) to calculate all-sky aerosol direct and indirect radiative forcing. The GCM uses monthly mean tropospheric aerosol distributions from GEOS-Chem, including sulfate, nitrate, BC, and OC ($OC \equiv POA + SOA$). OC is multiplied by 1.4 to convert from the simulated mass of organic carbon to total organic matter (Malm et al., 1994). These aerosol components are incorporated in a climate equilibrium simulation with resolution of 4° latitude \times 5° longitude, 23 vertical levels extending from the surface to 0.002 hPa, and fixed present-day sea surface temperatures (SST) and sea ice (Rayner et al., 2003). All-sky aerosol direct radiative forcing is determined within the GCM through parallel radiative calculations including and excluding anthropogenic aerosols. “Anthropogenic” includes contributions from fuel use and industry, but not open biomass burning. Sea salt and soil dust concentrations are from Hansen et al. (2002) but play no role in the radiative forcing.

Radiative forcing calculations are conducted for both external and internal aerosol mixtures. In the external mixture case, radiative forcing is calculated for the individual aerosol components and then summed to obtain the total anthropogenic aerosol radiative forcing. Externally mixed aerosol components are assumed to have a standard gamma size distribution with an area-weighted effective variance of 0.2 and an effective dry radius of 0.3 μm for sulfate and nitrate, 0.5 μm for OC, and 0.1 μm for BC (Chung and Seinfeld, 2002; Liao et al., 2004). Refractive indices are from Toon et al. (1976) for sulfate and nitrate, and from d’Almeida et al. (1991) for BC and OC. As in Chung and Seinfeld (2002) and (Liao et al., 2004), we determine the aerosol extinction efficiency, single scattering albedo, and asymmetry parameter from a lookup table generated by offline Mie calculations as a

function of aerosol size and refractive index.

Internally mixed aerosols are composed of sulfate, nitrate, OC, and BC. These particles are assumed to have a standard gamma size distribution with an effective dry radius of 0.3 μm and area-weighted variance of 0.2 (Chung and Seinfeld, 2002; Liao et al., 2004; Chen et al., 2007). Optical properties of the internal mixture are calculated using the volume-weighted mean of the refractive indices of the individual components. The radiative forcing of an individual aerosol component is calculated by removing it while holding the remaining components fixed.

4.2.3 Indirect aerosol radiative forcing

Chen et al. (2010b) previously applied the GISS GCM 3 to calculate the aerosol indirect effects initiated by aerosol particles acting as CCN and thus altering the number concentration N_c of cloud droplets. We follow their approach here using the gridded monthly aerosol concentration fields of SNA and carbonaceous aerosols from GEOS-Chem, together with their sea salt aerosol concentrations. N_c is related to the concentration of dissolved aerosol ions, m_i , by a standard power law dependence (Boucher and Lohmann, 1995; Penner et al., 2006):

$$\log N_c = A + B \log m_i \quad (4.1)$$

We calculate N_c from the archived GEOS-Chem aerosol distributions. Gridded 3-D fields of A and B were obtained by Chen et al. (2010b) from detailed simulations of aerosol microphysics and activation within the GCM (Adams and Seinfeld, 2002; Nenes and Seinfeld, 2003; Fountoukis and Nenes, 2005; Pierce and Adams, 2006). We use these fields here.

Following Chen et al. (2010b), we consider the first and second indirect effects applied to liquid stratiform clouds only. The first indirect effect arises from the enhancement of cloud optical depth from smaller cloud droplets. The cloud optical depth scales as the inverse of the area-weighted mean effective radius r_e of the cloud droplet size distribution (Del Genio et al., 1996). r_e is related to N_c by

$$r_e = \kappa^{-\frac{1}{3}} \left[\frac{3L}{4\pi N_c} \right]^{\frac{1}{3}} \quad (4.2)$$

where L is the liquid water content of the cloud (cm^3 water per cm^3 air), and κ is a constant (0.67 over land, 0.80 over ocean; Martin et al., 1994) that relates the volume mean droplet radius and r_e . We restrict r_e to be greater than $2 \mu\text{m}$ and less than $20 \mu\text{m}$.

The second aerosol indirect effect involves the effect of N_c on the rate of autoconversion of cloud droplets to precipitation. Chen et al. (2010b) introduced a dependence of the autoconversion rate on N_c based on the work of Khairoutdinov and Kogan (2000) that fitted results from an explicit microphysical model:

$$\frac{dq_l}{dt} = -1350 \gamma q_l^{2.47} N_c^{-1.79} \quad (4.3)$$

where q_l is the cloudwater mass content (kg water per kg of air), γ is a tuning parameter added by Hoose et al. (2008) and Chen et al. (2010b) to the original Khairoutdinov and Kogan (2000) equation ($\gamma = 1$) in order to retain GCM climate equilibrium. We achieve this here by using for $\gamma = 12$.

The first aerosol indirect radiative forcing (cloud albedo) is calculated for each decade between 1950 and 2050 using parallel radiative calculations, similar to the calculation of the aerosol direct radiative forcing. The parallel radiative calculations are conducted us-

ing cloud optical properties determined from N_c distributions with and without US anthropogenic aerosols. The second aerosol indirect effect (cloud lifetime) cannot be calculated in this manner due to coupling with the hydrological cycle. Instead, multi-year climate equilibrium simulations are required to account for the effects of feedback processes on cloud distributions (Denman et al., 2007; Forster et al., 2007). We thus calculate the total aerosol indirect radiative forcing (first and second effects) for each decade between 1950 and 2050 by conducting two 60-year climate equilibrium simulations, one with and one without US anthropogenic aerosol sources. Both simulations use fixed greenhouse gases, SST, and sea ice for year 2000. The first 10 years are used for initialization and the following 50 years (representing climate equilibrium conditions) are used for analysis. Comparison to the first aerosol indirect radiative forcing calculated independently as described above allows separate assessment of the first and second indirect effects. In order to test the significance of our results, we perform a Students t-test accounting for autocorrelation as described by Zwiers and von Storch (1995).

4.3 Evaluation of 1980-2010 US aerosol trends

We evaluate our simulation of aerosol sources, concentrations, and related long-term trends over the US with 1980-2009 wet deposition flux data available from the National Atmospheric Deposition Program/National Trend Network (NADP/NTN; <http://nadp.sws.uiuc.edu/NTN>), and 1990-2009 surface air concentrations available from the US Interagency Monitoring of Protected Visual Environments (IMPROVE; <http://vista.cira.colostate.edu/IMPROVE>) and the Clean Air Status and Trends Network (CASTNET; <http://java.epa.gov/castnet>). The wet deposition flux data provide constraints on aerosol sources considering that most of SO_2 , NO_x , and ammonia emitted in the US is deposited within the country by

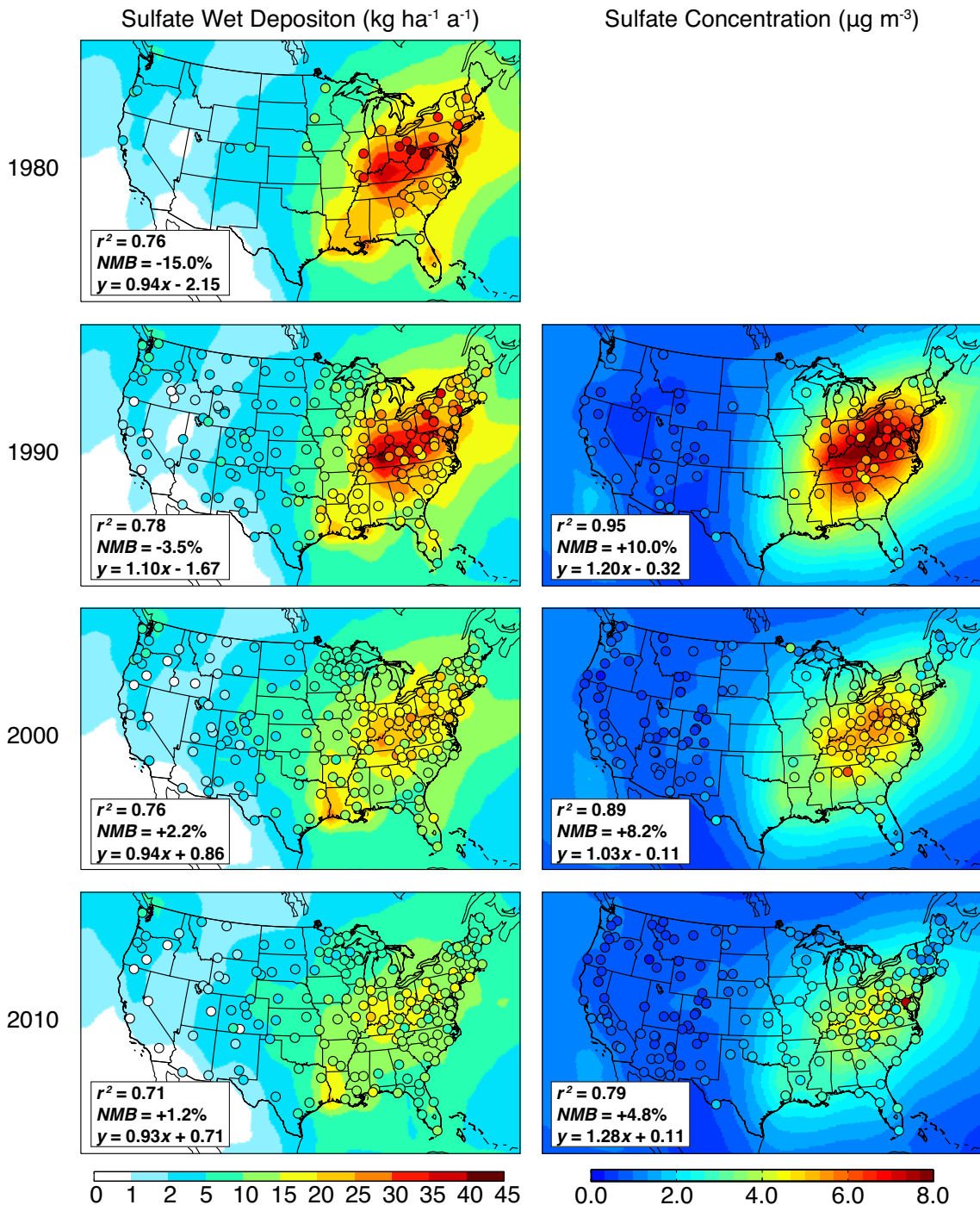


Figure 4.2: Sulfate wet deposition fluxes ($\text{kg ha}^{-1} \text{a}^{-1}$, left) and sulfate concentrations in surface air ($\mu\text{g m}^{-3}$, right). Observations (circles) are 3-year averages for 1979-1981 (wet deposition only), 1989-1991, 1999-2001, and 2008-2009. GEOS-Chem model values (background contours) are from decadal time slice simulations with 1980, 1990, 2000, and 2010 emissions. Reduced major axis linear regressions between model and observations are shown inset for each map along with the coefficient of determination (r^2) and normalized mean bias (NMB).

wet and dry processes (Chin and Jacob, 1996; Li et al., 2004; Zhang et al., in prep.).

Figure 4.2 compares the simulated and observed annual wet deposition fluxes and surface concentrations of sulfate, nitrate, and ammonium across the US for the years 1980, 1990, 2000, and 2010. Observations are three-year average values centered on the decadal year except 2010, which is a two-year average for 2008-2009. All observation sites meeting the NADP/NTN data completion criterion for at least two of the three years are included. Observations of surface air concentrations are not continuous and some records have substantial gaps. To address this, we first aggregate the observations as seasonal means (DJF, MAM, JJA, SON) for each year, requiring for each season a minimum of 10 data points for IMPROVE (3-day averages) and 5 data points for CASTNET (weekly averages). The seasonal means for the three years are then averaged, with the additional requirement that data be available for at least two of the years.

We assemble comparison statistics between the model (M) and observations (O) using the coefficient of determination (r^2), the corresponding reduced-major-axis linear regression, and the normalized mean bias (NMB) calculated for all N sites containing valid data:

$$NMB = \frac{\sum_{i=1}^N (M_i - O_i)}{\sum_{i=1}^N O_i} \quad (4.4)$$

Figure 4.2 shows that the model has excellent agreement with observed sulfate wet deposition across the US, capturing the spatial variability ($r^2 = 0.71 - 0.78$) and magnitude. The normalized mean bias is less than 4% for all available decades except 1980 (-15%). Simulated surface concentrations of sulfate have similar success, capturing spatial variability ($r^2 = 0.79 - 0.95$) with low bias (10% or less).

Figure 4.3 shows the simulated and observed trends in sulfate wet deposition and air

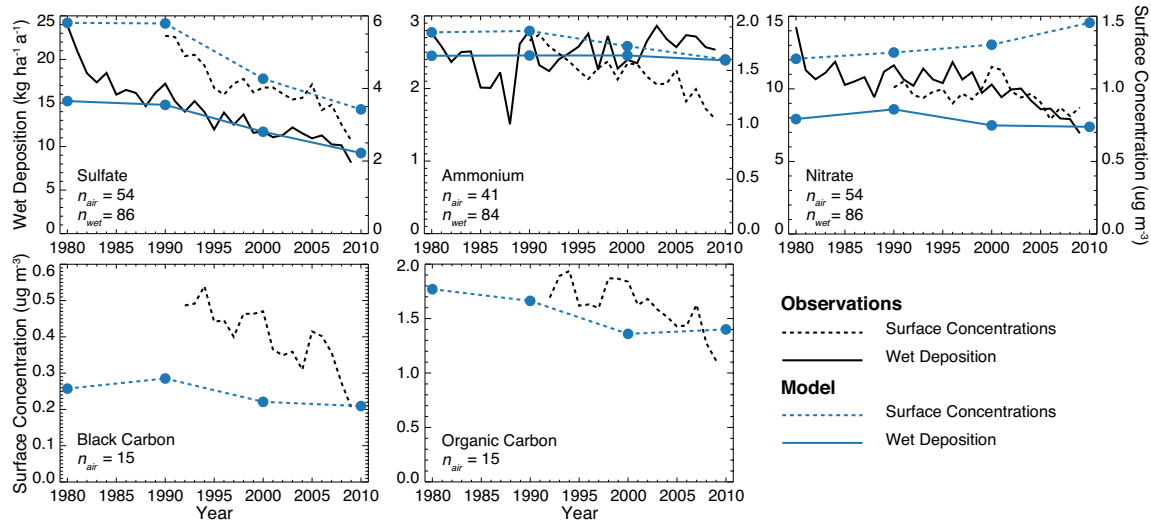


Figure 4.3: 1980-2010 trends in wet deposition fluxes (solid) and surface aerosol concentrations (dashed) in the eastern US (east of 100°W). Values are annual means. Model trends (blue) are compared to observations (black). The numbers of sites averaged in the trend analysis are given inset. Model values are sampled at the site locations and then averaged.

concentrations over the 1980-2010 period for the eastern US (east of 100°W). Values are averaged over all sites (n , shown inset) with observations available for more than 25 years (deposition) and more than 17 years (concentrations). Observed wet deposition of sulfate decreased by 58% between 1980 and 2010, consistent with the 56% reduction in SO₂ emissions reported by US EPA (2010). Sulfate aerosol concentrations show a parallel decreasing trend for 1990-2010. Modeled deposition and surface concentrations both decrease by 40% over 1980-2010, less than observed because of an apparent underestimate of 1980 emissions. The simulated decreases of sulfate deposition and surface concentrations are in better agreement with observations after 1990.

Figure 4.4 compares model and observations for ammonium wet deposition fluxes and aerosol concentrations. The model successfully captures the distribution ($r^2 = 0.63 - 0.75$) and magnitude ($NMB < 7\%$) of ammonium deposition between 1980 and 2010. The largest deposition is in the agricultural Midwest where emissions are highest. In that region the

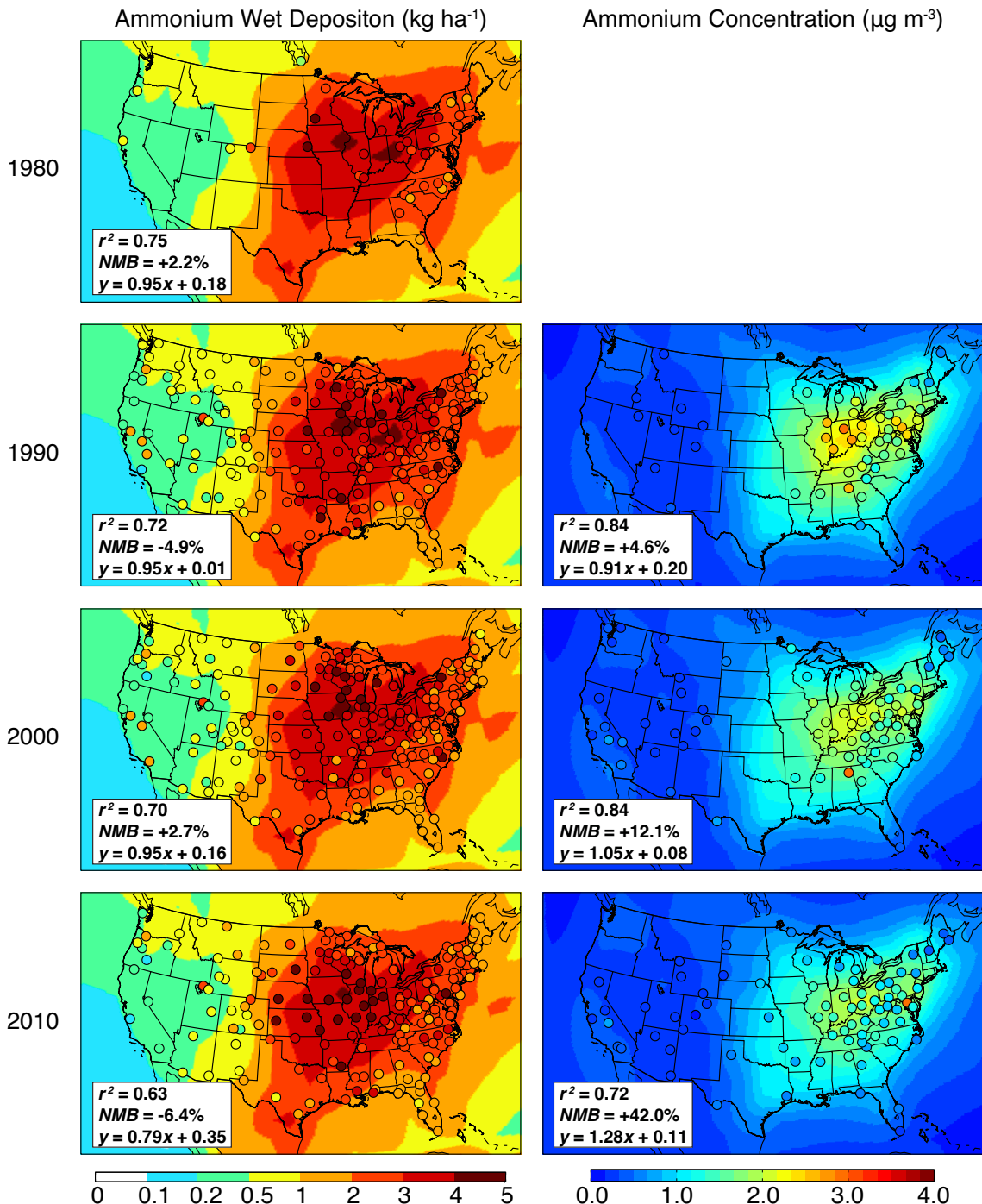


Figure 4.4: Same as Fig. 4.2 but for ammonium.

model is lower than observed. Aerosol ammonium concentrations peak in the industrial Midwest, reflecting the combination of high ammonia emissions and high concentrations of sulfate and nitrate that promote the fractionation of ammonia into the aerosol as ammonium. The model captures this spatial distribution ($r^2 = 0.72\text{-}0.84$), but is biased high, particularly in 2010 (+42%).

Figure 4.3 shows observed and simulated 1980-2010 trends in ammonium wet deposition and surface concentrations in the eastern US. The wet deposition data show no significant trend, consistent with the model (which assumes constant ammonia emissions). However, the observed surface concentrations show a large decreasing trend that is only weakly reproduced in the model. This decrease can be explained by decreases in sulfate and nitrate under conditions when the aerosol is neutralized. The inability of the model to capture the decrease in ammonium concentrations reflects a problem with the nitrate trend, as discussed below.

Figure 4.5 shows the wet deposition and surface air concentrations of nitrate. The model captures the spatial distribution of nitrate deposition ($r^2 = 0.71\text{-}0.81$), but underpredicts total nitrate wet deposition by 20-33% in 1980-2000. The low bias vanishes in 2010, following a decade of large reductions of NO_x from the energy generation sector (US EPA, 2010). Aerosol nitrate in the model is exclusively ammonium nitrate, and its formation is contingent on ammonia availability (since formation of ammonium sulfate is favored thermodynamically over ammonium nitrate). As such, its simulation tends to compound errors in sulfate and ammonium (Park et al., 2006). Our simulation shows relatively little bias and is improved compared to previous versions (Park et al., 2004, 2006). The observed maximum over the Midwest is well captured by the model where it reflects a balance between ammonia, NO_x , and SO_2 source influences.

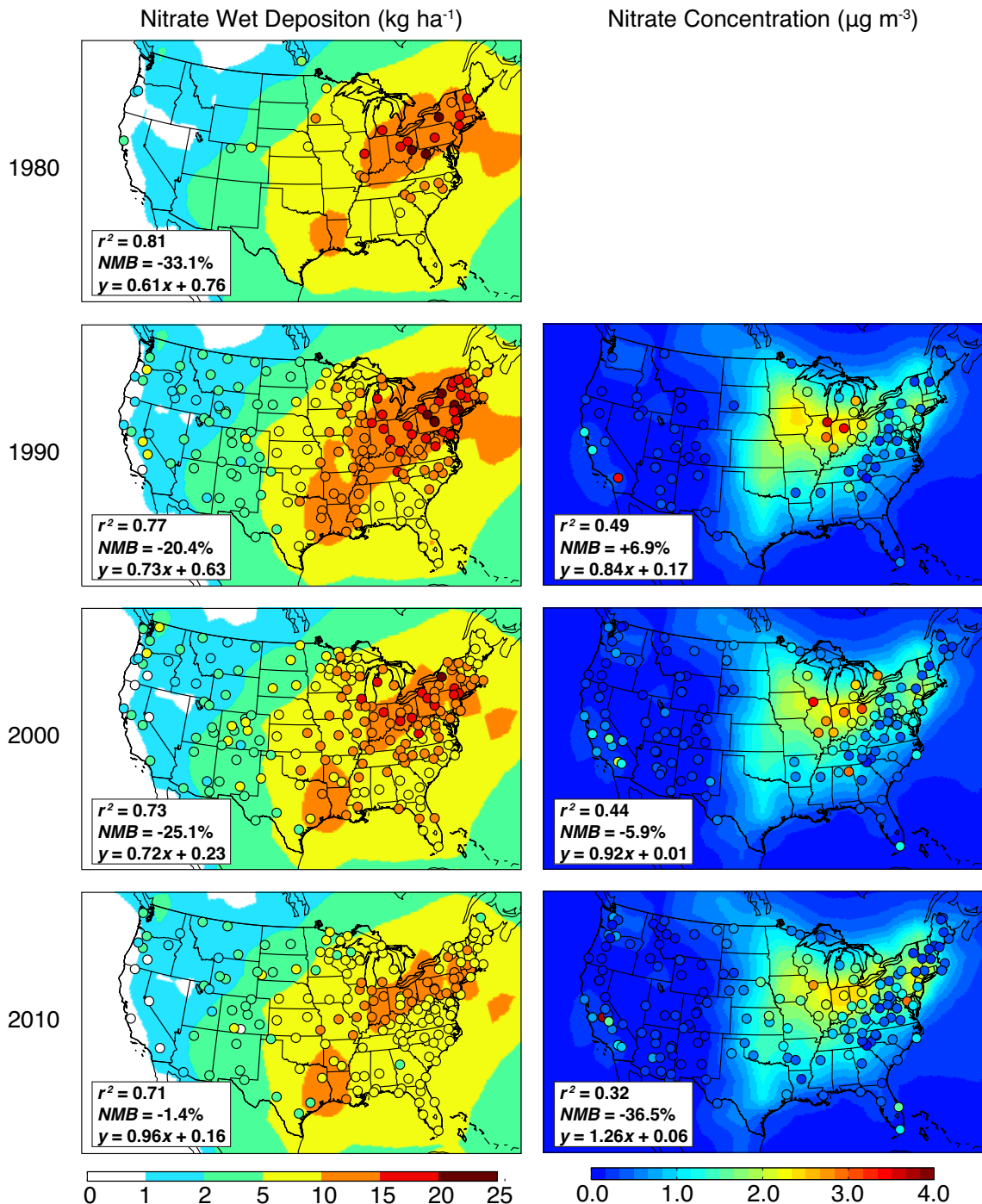


Figure 4.5: Same as Fig. 4.2 but for nitrate.

Observations of nitrate wet deposition show a 33% decrease from 1980 to 2009, consistent with the reported 36% reduction of NO_x emissions (US EPA, 2010). Most of this reduction was realized between 2000 and 2009 through the NO_x State Implementation Plan (SIP) Call. However, the model is largely flat over 1980-2010. The EDGAR emissions used for 1980-2000 are apparently too low. The IMAGE A1B projection used for 2000-2010 does not account for the NO_x SIP Call, and this fortuitously produces a good match to the 2008-2009 observations.

Observed aerosol nitrate concentrations were flat from 1990 to 2000 but then decreased by 23% between 2000 and 2009. In contrast, model concentrations increased weakly during this period because of the decrease in sulfate, resulting in more ammonium being available for ammonium nitrate formation (West et al., 1989). It seems from the observations that nitrate is less sensitive to changes in sulfate than would be expected from SNA thermodynamics.

Figure 4.6 compares simulated and observed surface concentrations of BC and OC for 1990-2010. Biogenic VOCs are a major source of OC in the Southeast. Open fires are an important component of observed variability for BC and OC in the West and in the Southeast (Park et al., 2007). These fires are not well reproduced by the model on an event basis, explaining in part the relatively low correlations between model and observed concentrations. The model is also biased low by 15-40% on average. Previous GEOS-Chem studies did not show as severe a bias because the BC and OC sources were fitted to reproduce the observations (Park et al., 2003) and included significantly higher biomass burning emissions (Park et al., 2003, 2006). Previous models using the Bond et al. (2004) inventory (similar to Bond et al. (2007) used here) also underestimate BC in North America (Koch et al., 2007, 2009)

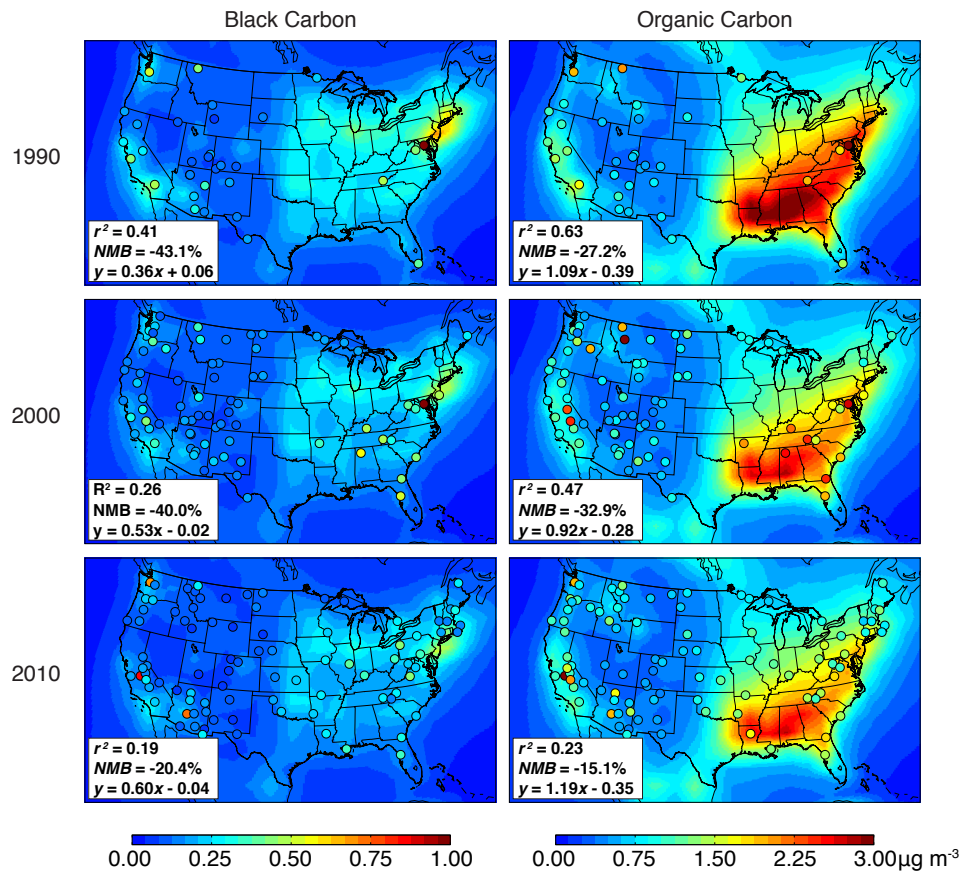


Figure 4.6: Black carbon (left) and organic carbon (right) concentration in surface air ($\mu\text{g m}^{-3}$). Observations (circles) are 3-year averages for 1989-1991, 1999-2001, and 2008-2009. GEOS-Chem model values (background contours) are from the decadal time slice simulations with 1990, 2000, and 2010 emissions. Reduced major axis linear regressions between model and observations are shown inset for each map along with the coefficient of determination (r^2) and normalized mean bias (NMB).

Figure 4.3 shows that observed BC and OC concentrations over the US decreased by 50% and 34% respectively between 1990 and 2009. The model trends are much weaker, with BC and OC concentrations decreasing by 27% and 16% respectively, as driven by the trends in the Bond et al. (2007) emission inventory and the IMAGE A1B projection. The mismatch between simulated and observed trends reduces the model low bias in 2010 to 20% for BC and 15% for OC.

4.4 Aerosol direct radiative forcing from US anthropogenic sources

Figure 4.7 (top) shows the annual mean aerosol direct radiative forcing for the peak in US anthropogenic aerosols in year 1980, assuming an internal aerosol mixture (the forcing increases by 10% for an external mixture, due to lesser effect from BC absorption). The forcing is strongly localized over the eastern US, where it reaches -4.9 W m^{-2} . This more than offsets for that region the 1980 radiative forcing from the long-lived greenhouse gases ($+1.8 \text{ W m}^{-2}$). On a global scale the aerosol direct radiative forcing from US anthropogenic aerosol sources in 1980 is -0.07 W m^{-2} , 25% of our computed global aerosol direct radiative forcing of -0.27 W m^{-2} from anthropogenic sources worldwide in 1980. By 2010 we find that the radiative forcing from anthropogenic US aerosol sources has decreased to -0.03 W m^{-2} globally, amounting to just 8% of the total from worldwide anthropogenic sources, reflecting the rapid decline of emissions in the US and growth in Asia (Figure 4.1). We show in Chapter 5 that even though the aerosol radiative forcing from US anthropogenic sources is very small on a global scale, the large regional forcing elicits a strong regional climate response over the eastern US.

Figure 4.8 (top) shows the 1950-2050 evolution of the annual mean aerosol direct radiative forcing averaged over the eastern US (east of 100°W). The aerosol direct radiative forcing peaks in 1970-1990 at -2.0 W m^{-2} (internally mixed). This value increases to -2.2 W m^{-2} if aerosols are treated as an external mixture. When externally mixed, BC radiative forcing is 40% lower than shown in Fig. 4.8 and the radiative forcing of sulfate and nitrate is 5-7% higher. OC shares common sources with BC, which makes it more sensitive to mixing; it has 30% higher radiative forcing in an external mixture than an internal mixture.

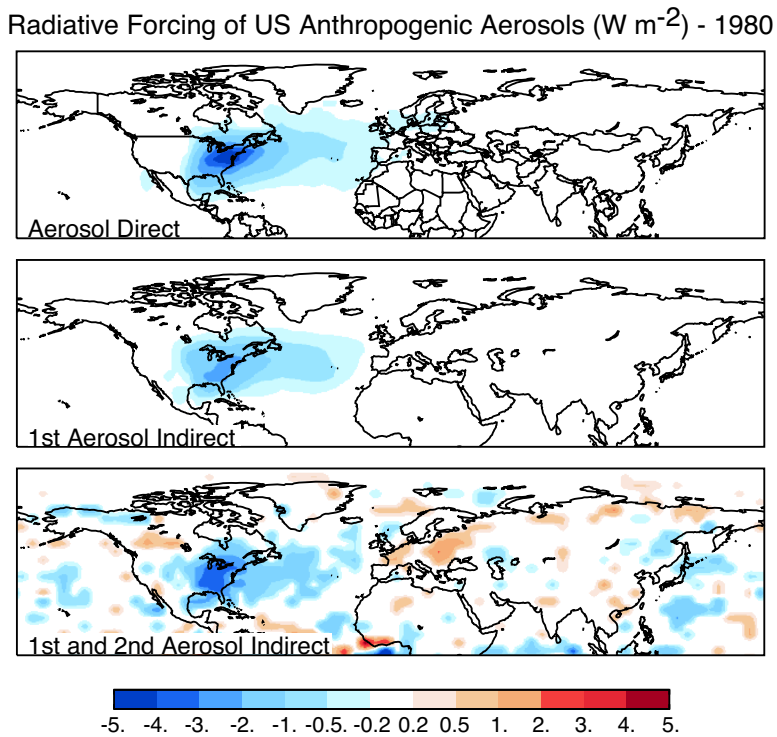


Figure 4.7: Annual mean aerosol direct (top), first indirect (middle), and total indirect (bottom) radiative forcing from US anthropogenic sources for year 1980. The aerosol direct effect is calculated assuming an internal mixture. Assuming an external mixture would increase the radiative forcing over the US by 10%. The direct and first indirect effects are calculated by parallel radiative calculations using perturbed aerosol abundances (direct) and cloud optical properties (first indirect). The total aerosol indirect effect is calculated by difference between 50-year climate equilibrium simulations with and without US anthropogenic aerosols. White areas show no significant change at the 95th percentile of confidence. The global mean values are -0.07 W m^{-2} for the direct effect, -0.05 W m^{-2} for the first indirect effect, and -0.08 W m^{-2} for the total indirect effect.

The radiative forcing trends in Fig. 4.8 mirror the model US emission trends in Fig. 4.1. We previously evaluated the model trends for 1980-2010 using observed records of wet deposition and aerosol concentrations (Fig. 4.3). For sulfate, which is the dominant radiative forcing agent, the model closely reproduces the observed trends for 1990-2010, but is 15% too low in 1980, suggesting a corresponding error in the aerosol radiative forcing estimate for 1980. For BC, the model is 40% too low in 1990 and 2000 but there is much less bias in 2010, reflecting a steep decline in the observations. For OC and nitrate, the

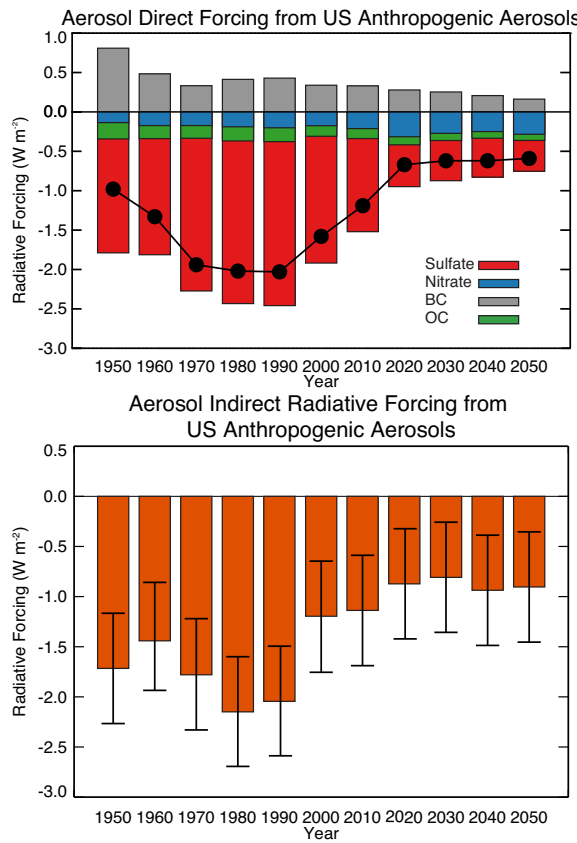


Figure 4.8: 1950-2050 evolution of aerosol direct (top) and total (first + second) indirect radiative forcing (bottom) from US anthropogenic sources over the eastern US (east of 100°W). Circles represent the net direct radiative forcing and the bars give the contributions from the different components. The direct radiative forcing calculations are for an internal aerosol mixture. Aerosol indirect radiative forcing is calculated as the difference between two 50-year equilibrium climate simulations with vs. without US anthropogenic aerosols. The error bars represent the 95% confidence interval of the forcing based on model interannual variability.

model has relatively little bias and the radiative forcing is small (nitrate is most abundant in winter when radiation is weak).

We can use the data in Fig. 4.3 to estimate the model error in computing the change in aerosol direct radiative forcing from 1980 to 2010. The model value for this change (adding the contribution from the different aerosol components, black line in Fig. 4.8) is $+0.78 \text{ W m}^{-2}$. Applying scaling factors for the individual components based on Fig. 4.3, and assuming that the model bias for BC in 1990 applies also to 1980, we obtain a change

Table 4.1: Global mean cloud properties^a

	This Work	Chen et al. (2010b)	Other Studies ^b
Total column N_c (10^{10} m^{-2})	3.8	6.2	2.1 - 7.6 ^c
N_c at 850 hPa (cm^{-3})	83.0	122.2	75.0 - 135.0 ^d
r_e at cloud top (μm) ^e	12.9	12.2	6.8 - 11.3 ^f
LWP (g m^{-2})	111.3	111.5	41.5 - 110.0 ^g
TOA SW CF (W m^{-2})	-55.2	-53.8	-49.9 - -61.0 ^h

^a Cloud droplet number concentration (N_c), effective area-weighted mean cloud droplet radius (r_e), liquid water path (LWP), top-of-atmosphere shortwave cloud forcing (TOA SW CF)

^b Survey of values from models and observation analyses reported by Chen et al. (2010b)

^c Menon et al. (2002) and Hoose et al. (2008)

^d Penner et al. (2006)

^e Modeled values of r_e are multiplied by $2^{1/3}$ to approximate the cloud top conditions of satellite retrievals (Meskhidze et al., 2007)

^f Menon et al. (2002), Kristjánsson et al. (2005), Penner et al. (2006)

^g Kristjánsson et al. (2005), Penner et al. (2006), and Hoose et al. (2008)

^h Menon et al. (2002), Kristjánsson et al. (2005), and Penner et al. (2006)

in radiative forcing constrained by observations of $+0.87 \text{ W m}^{-2}$, about 10% larger.

Future projection of US emissions from the IMAGE model applied to the IPCC A1B scenario (Fig. 4.1) indicates a continued decrease in aerosol direct radiative forcing, as shown in Fig. 4.8, but with little change past 2020. Aerosol radiative forcing will have decreased by almost a factor of 4 from its peak in 1970-1990.

Two policy-relevant implications can be drawn from the trends in US aerosol direct radiative forcing in Fig. 4.8. First, future decrease in aerosol radiative forcing due to reductions in anthropogenic emissions will likely be smaller than the decrease that has already been realized over 1980-2010. Thus most of the climate response from controlling US anthropogenic sources should have already been realized. Second, the present-day radiative forcing from BC is small (and even less if external forcing is assumed), weakening the argument of a win-win scenario for public health and climate from controlling BC emissions. We elaborate further on these two implications in Chapter 5.

4.5 Aerosol indirect radiative forcing from US anthropogenic sources

Estimating the aerosol indirect radiative forcing from cloud albedo and lifetime effects is far more uncertain than the direct radiative forcing. Uncertainties relate to the conversion from aerosol mass concentration to cloud droplet number concentration (N_c) and from there to cloud optical properties, including the effective cloud droplet radius (r_e) and the liquid water path (vertical column of liquid water amount, g m^{-2}). Table 4.1 compares the global mean cloud properties computed from our model to Chen et al. (2010b) (same GCM and parameterization, but different aerosol concentrations) and to other values in the literature. Our values are consistent with the published ranges.

Figure 4.9 shows the change in liquid stratiform cloud properties due to US anthropogenic aerosols in 1980 including column N_c , effective cloud droplet radius r_e , and cloud optical depth. US anthropogenic aerosols increase column integrated N_c by up to $8 \times 10^{10} \text{ m}^{-2}$, which reduces the effective cloud droplet radius of liquid stratiform clouds by up to $4.5 \mu\text{m}$, and increases the warm cloud optical depth by more than 3. The resulting first indirect radiative forcing (cloud albedo effect) amounts to 67% of the direct forcing (1.3 W m^{-2} averaged over the US east of 100°W) on an annual basis (Fig. 4.7 middle) and reaches up to -3.0 W m^{-2} in the Southeast. Similar to the aerosol direct effect, radiative forcing from the cloud albedo effect is largely confined to the US and the downwind North Atlantic.

Figure 4.7 (bottom) shows the radiative forcing from the total aerosol indirect effect (cloud albedo and lifetime effects) of US anthropogenic aerosols for 1980. The indirect forcing is calculated as the mean difference in net top of the atmosphere radiation between

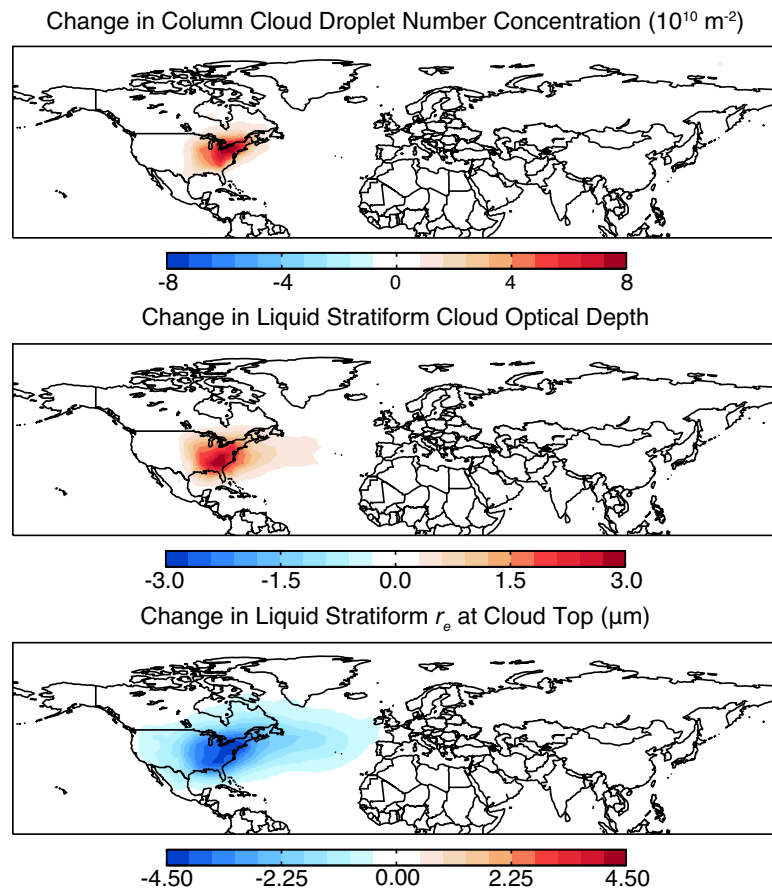


Figure 4.9: Effect of US anthropogenic aerosols on column integrated cloud droplet number concentration, liquid stratiform cloud droplet effective radius at cloud top (r_e), and liquid stratiform cloud optical depth. Values are annual model means for 1980.

50-year simulations with and without US anthropogenic aerosol sources, as described in Section 4.2.3. It is noisier than the direct radiative forcing, largely reflecting the cloud lifetime effect, but is similarly concentrated over the eastern US and the North Atlantic downwind. The annual mean total indirect forcing (cloud albedo + cloud lifetime effects) in the eastern US (east of 100°W) is -2.2 W m^{-2} for 1980, 10% larger than the direct effect and 70% larger than the first indirect effect alone. The total indirect effect is similarly larger globally (-0.08 W m^{-2} total indirect vs. -0.07 W m^{-2} direct).

Figure 4.8 (bottom) shows our computed 1950-2050 trend in aerosol indirect radiative

forcing over the eastern US (east of 100°W) from US anthropogenic sources. The error bars indicate the 95% confidence interval of this difference based on model interannual variability. The trend in indirect forcing is consistent with the evolution of SO₂ emissions (Fig. 4.1) and aerosol direct forcing (Fig. 4.8 top). Indirect forcing peaks in 1970-1990 at a value of -2.0 W m⁻², the same magnitude as the aerosol direct effect. SO₂ regulations cause a sharp decrease in forcing with a change of +1.0 W m⁻² between 1990 and 2010, and little change afterward.

4.6 Conclusions

Efforts to improve air quality through aerosol source reductions could have significant regional climate implications due to the strong and localized radiative forcing exerted by aerosols. The US is of particular interest for investigating this effect as aerosol concentrations peaked in the 1970-1990 period, have decreased rapidly since then, and are projected to continue decreasing in the future. We used here the GEOS-Chem CTM applied to historical emission inventories and future projections (IPCC A1B scenario) to simulate global trends in aerosol concentrations over the 1950-2050 period, and we applied those in the GISS GCM to calculate the direct and indirect radiative forcings from US anthropogenic aerosol sources. Chapter 5 examines the resulting climate effects over the US and globally.

A prominent feature of the aerosol radiative forcing history from US sources is the rapid 1980-2010 decline driven by air quality regulations. We tested our reconstruction of this history with observed spatial distributions and long-term trends in wet deposition (1980-2010) and aerosol concentrations (1990-2010). We reproduce successfully the observed 45% decline of sulfate wet deposition and concentrations between 1990 and 2010, but underestimate the earlier 1980 to 1990 decline. Ammonium wet deposition fluxes show

no long-term trend in the observations or in the model (where ammonia emissions are assumed constant). The combination of decreasing SO₂ emissions and constant ammonia emissions leads to a weak increasing trend of nitrate in the model, but observations show a decrease. Observations of BC and OC show stronger 1980-2010 declines than simulated by the model, implying a faster decline of emissions than is represented in current inventories.

We calculated a global direct radiative forcing from US anthropogenic aerosol sources of -0.07 W m⁻² in 1980 when the sources were at their peak. This forcing is strongly localized over the eastern US and downwind North Atlantic. It averages -2.0 W m⁻² over the eastern US (east of 100°W), including -2.0 W m⁻² from sulfate, +0.4 W m⁻² from BC, -0.2 W m⁻² from nitrate, and -0.2 W m⁻² from OC. These values assume an internal aerosol mixture; an external mixture would increase the overall negative radiative forcing by 10% due to decreased absorption by BC.

The direct radiative forcing from US anthropogenic aerosols declined strongly between 1970-1990 and 2010, largely reflecting the decline in SO₂ emissions. The global forcing declined to -0.03 W m⁻² by 2010, amounting to only 8% of the forcing from global anthropogenic aerosol sources (as compared to 25% in 1980). The forcing over the eastern US declined by 0.78 W m⁻² in the model between 1990 and 2010. Correction to this model estimate based on the observed trends of wet deposition fluxes and concentrations would imply a decline of 0.87 W m⁻².

We calculated the aerosol indirect forcing including the first and second indirect effects (cloud albedo and cloud lifetime) applied to warm stratiform clouds. We found that the indirect radiative forcing from US anthropogenic aerosol sources is mainly localized over the eastern US and North Atlantic, similarly to the direct forcing, and shows similar temporal trends over the 1950-2050 period. 1980 values over the eastern US average -2.2 W m⁻²,

similar in magnitude to the direct radiative forcing. About 60% of the indirect radiative forcing comes from the first (cloud albedo) effect.

We project that by 2050 the direct and indirect radiative forcings over the eastern US from US anthropogenic sources will have decreased to -0.6 W m^{-2} and -0.9 W m^{-2} respectively, 71% and 55% weaker than the 1980 peak. Nitrate is expected to become a major component of the aerosol radiative forcing in 2050 as NO_x emissions decrease more slowly than SO_2 emissions. However, we also find that essentially all of the 1980-2050 decrease in radiative forcing occurs over the 1990-2020 period, and that 62% has already been realized by 2010. US anthropogenic emissions are sufficiently weak by now that little additional reduction in forcing is expected in the future even with the projected continued decrease in emissions. In addition, the positive radiative forcing from the BC aerosol component is presently too small to provide significant climate leverage from future emission controls targeted at BC.

The current period is witnessing a dramatic decrease in US anthropogenic aerosol forcing as a result of air quality improvements. Combined with the sustained increase in greenhouse radiative forcing, this has the potential for particularly strong warming over the US. The extent to which regional radiative forcing translates into regional climate response is uncertain. We explore this climate response in Chapter 5.

Bibliography

- Adams, P. and Seinfeld, J. (2002). Predicting global aerosol size distributions in general circulation models. *J Geophys Res-Atmos*, 107(D19):4370.
- Albrecht, B. (1989). Aerosols, cloud microphysics, and fractional cloudiness. *Science*, 245(4923):1227.
- Alexander, B., Park, R. J., Jacob, D. J., Li, Q., Yantosca, R. M., Savarino, J., Lee, C. C. W.,

- and Thiemens, M. H. (2005). Sulfate formation in sea-salt aerosols: Constraints from oxygen isotopes. *J Geophys Res-Atmos*, 110(D10):D10307.
- Andres, R. and Kasgnoc, A. (1998). A time-averaged inventory of subaerial volcanic sulfur emissions. *J Geophys Res-Atmos*, 103(D19):25251–25261.
- Binkowski, F. and Roselle, S. (2003). Models-3 community multiscale air quality (CMAQ) model aerosol component - 1. Model description. *J Geophys Res-Atmos*, 108(D6):4183.
- Bond, T., Streets, D., Yarber, K., Nelson, S., Woo, J., and Klimont, Z. (2004). A technology-based global inventory of black and organic carbon emissions from combustion. *J Geophys Res-Atmos*, 109(D14):D14203.
- Bond, T. C. (2007). Can warming particles enter global climate discussions? *Environ Res Lett*, 2(4):045030.
- Bond, T. C., Bhardwaj, E., Dong, R., Jogani, R., Jung, S., Roden, C., Streets, D. G., and Trautmann, N. M. (2007). Historical emissions of black and organic carbon aerosol from energy-related combustion, 1850–2000. *Global Biogeochem Cy*, 21(2):1–16.
- Boucher, O. and Lohmann, U. (1995). The sulfate-CCN-cloud albedo effect - a sensitivity study with 2 general circulation models. *Tellus B*, 47(3):281–300.
- Bouwman, A., Lee, D., Asman, W., Dentener, F., Van Der Hoek, K., and Olivier, J. (1997). A global high-resolution emission inventory for ammonia. *Global Biogeochem Cy*, 11(4):561–587.
- Chen, W. T., Lee, Y. H., Adams, P. J., Nenes, A., and Seinfeld, J. H. (2010a). Will black carbon mitigation dampen aerosol indirect forcing? *Geophys Res Lett*, 37:L09801.
- Chen, W.-T., Liao, H., and Seinfeld, J. H. (2007). Future climate impacts of direct radiative forcing of anthropogenic aerosols, tropospheric ozone, and long-lived greenhouse gases. *J Geophys Res-Atmos*, 112(D14):D14209.
- Chen, W.-T., Nenes, A., Liao, H., Adams, P. J., Li, J.-L. F., and Seinfeld, J. H. (2010b). Global climate response to anthropogenic aerosol indirect effects: Present day and year 2100. *J Geophys Res-Atmos*, 115(D12):D12207.
- Chin, M., Rood, R., Lin, S., Muller, J., and Thompson, A. (2000). Atmospheric sulfur cycle simulated in the global model GOCART: Model description and global properties. *J Geophys Res-Atmos*, 105(D20):24671–24687.
- Chung, S. and Seinfeld, J. (2002). Global distribution and climate forcing of carbonaceous aerosols. *J Geophys Res-Atmos*, 107(D19):4407.
- Corbett, J., Fischbeck, P., and Pandis, S. (1999). Global nitrogen and sulfur inventories for oceangoing ships. *J Geophys Res-Atmos*, 104(D3):3457–3470.

- d'Almeida, G., Koepke, P., and Shettle, E. (1991). *Atmospheric Aerosols: Global Climatology and Radiative Characteristics*. A Deepak, Hampton, VA.
- Del Genio, A., Yao, M., Kovari, W., and Lo, K. (1996). A prognostic cloud water parameterization for global climate models. *J Climate*, 9(2):270–304.
- Denman, K. L., Brasseur, G., Chidthaisong, A., Ciais, P., Cox, P. M., Dickenson, R. E., Hauglustaine, D., Heinze, C., Holland, E., Jacob, D., Lohmann, U., Ramachandran, S., da Silva Dias, P. L., Wofsy, S. C., and Zhang, X. (2007). *Climate Change 2007: The Physical Science Basis*, chapter Couplings Between Changes in the Climate System and Biogeochemistry. Cambridge University Press.
- Duncan, B., Martin, R., Staudt, A., Yevich, R., and Logan, J. (2003). Interannual and seasonal variability of biomass burning emissions constrained by satellite observations. *J Geophys Res-Atmos*, 108(D2):4100.
- Evans, M. and Jacob, D. (2005). Impact of new laboratory studies of N_2O_5 hydrolysis on global model budgets of tropospheric nitrogen oxides, ozone, and OH. *Geophys Res Lett*, 32(9):L09813.
- Fiore, A. M., Jacob, D. J., Field, B. D., Streets, D. G., Fernandes, S. D., and Jang, C. (2002). Linking global to regional models to assess future climate impacts on surface ozone levels in the United States. *Geophys Res Lett*, 29(19):1919.
- Forster, P., Ramaswamy, V., Artaxo, P., Berntsen, T., Betts, R., Fahey, D. W., Haywood, J., Lean, J., Lowe, D. C., Myhre, G., Nganga, J., Prinn, R., Raga, G., Schulz, M., and Dorland, R. V. (2007). *Climate Change 2007: The Physical Science Basis*, chapter Changes in Atmospheric Constituents and in Radiative Forcing. Cambridge University Press.
- Fountoukis, C. and Nenes, A. (2005). Continued development of a cloud droplet formation parameterization for global climate models. *J Geophys Res-Atmos*, 110(D11):D11212.
- Gilliland, A. B., Dennis, R. L., Roselle, S. J., and Pierce, T. E. (2003). Seasonal NH_3 emission estimates for the eastern United States based on ammonium wet concentrations and an inverse modeling method. *J Geophys Res-Atmos*, 108(D15):4477.
- Grieshop, A. P., Reynolds, C. C. O., Kandlikar, M., and Dowlatabadi, H. (2009). A black-carbon mitigation wedge. *Nat Geosci*, 2:533–534.
- Guenther, A., Karl, T., Harley, P., Wiedinmyer, C., Palmer, P. I., and Geron, C. (2006). Estimates of global terrestrial isoprene emissions using MEGAN (Model of Emissions of Gases and Aerosols from Nature). *Atmos Chem Phys*, 6:3181–3210.

- Hansen, J., Sato, M., Nazarenko, L., Ruedy, R., Lacis, A., Koch, D., Tegen, I., Hall, T., Shindell, D., Santer, B., Stone, P., Novakov, T., Thomason, L., Wang, R., Wang, Y., Jacob, D., Hollandsworth, S., Bishop, L., Logan, J., Thompson, A., Stolarski, R., Lean, J., Willson, R., Levitus, S., Antonov, J., Rayner, N., Parker, D., and Christy, J. (2002). Climate forcings in Goddard Institute for Space Studies SI2000 simulations. *J Geophys Res-Atmos*, 107(D18):37.
- Heald, C. L., Jacob, D. J., Turquety, S., Hudman, R. C., Weber, R. J., Sullivan, A. P., Peltier, R. E., Atlas, E. L., De Gouw, J. A., Warneke, C., Holloway, J. S., Neuman, J. A., Flocke, F. M., and Seinfeld, J. H. (2006). Concentrations and sources of organic carbon aerosols in the free troposphere over north america. *J Geophys Res-Atmos*, 111(D23):1–12.
- Henze, D. K. and Seinfeld, J. H. (2006). Global secondary organic aerosol from isoprene oxidation. *Geophys Res Lett*, 33(9):L09812.
- Hoosse, C., Lohmann, U., Bennartz, R., Croft, B., and Lesins, G. (2008). Global simulations of aerosol processing in clouds. *Atmos Chem Phys*, 8(23):6939–6963.
- Jacob, D. (2000). Heterogeneous chemistry and tropospheric ozone. *Atmos Environ*, 34(12–14):2131–2159.
- Jacobson, M. Z. (2002). Control of fossil-fuel particulate black carbon and organic matter, possibly the most effective method of slowing global warming. *J Geophys Res-Atmos*, 107(D19):4410.
- Khairoutdinov, M. and Kogan, Y. (2000). A new cloud physics parameterization in a large-eddy simulation model of marine stratocumulus. *Mon Weather Rev*, 128(1):229–243.
- Koch, D., Bond, T. C., Streets, D., Unger, N., and van der Werf, G. R. (2007). Global impacts of aerosols from particular source regions and sectors. *J Geophys Res-Atmos*, 112(D2):D02205.
- Koch, D., Schulz, M., Kinne, S., McNaughton, C., Spackman, J. R., Balkanski, Y., Bauer, S., Berntsen, T., Bond, T. C., Boucher, O., Chin, M., Clarke, A., De Luca, N., Dentener, F., Diehl, T., Dubovik, O., Easter, R., Fahey, D. W., Feichter, J., Fillmore, D., Freitag, S., Ghan, S., Ginoux, P., Gong, S., Horowitz, L., Iversen, T., Kirkevag, A., Klimont, Z., Kondo, Y., Krol, M., Liu, X., Miller, R., Montanaro, V., Moteki, N., Myhre, G., Penner, J. E., Perlitz, J., Pitari, G., Reddy, S., Sahu, L., Sakamoto, H., Schuster, G., Schwarz, J. P., Seland, O., Stier, P., Takegawa, N., Takemura, T., Textor, C., van Aardenne, J. A., and Zhao, Y. (2009). Evaluation of black carbon estimations in global aerosol models. *Atmos Chem Phys*, 9(22):9001–9026.
- Kristjánsson, J. E., Iversen, T., Kirkevag, A., Seland, O., and Debernard, J. (2005). Response of the climate system to aerosol direct and indirect forcing: Role of cloud feedbacks. *J Geophys Res-Atmos*, 110(D24):D24206.

- Li, Q., Jacob, D. J., Munger, J. W., Yantosca, R. M., and Parrish, D. D. (2004). Export of NO_y from the North American boundary layer: Reconciling aircraft observations and global model budgets. *J Geophys Res-Atmos*, 109:D02313.
- Liao, H., Henze, D. K., Seinfeld, J. H., Wu, S., and Mickley, L. J. (2007). Biogenic secondary organic aerosol over the United States: Comparison of climatological simulations with observations. *J Geophys Res-Atmos*, 112(D06):D06201.
- Liao, H., Seinfeld, J., Adams, P., and Mickley, L. (2004). Global radiative forcing of coupled tropospheric ozone and aerosols in a unified general circulation model. *J Geophys Res-Atmos*, 109(D16):D16207.
- Liu, H., Jacob, D., Bey, I., and Yantosca, R. (2001). Constraints from Pb-210 and Be-7 on wet deposition and transport in a global three-dimensional chemical tracer model driven by assimilated meteorological fields. *J Geophys Res-Atmos*, 106(D11):12109–12128.
- Malm, W. C., Sisler, J. F., Huffman, D., Eldred, R. A., and Cahill, T. A. (1994). Spatial and seasonal trends in particle concentration and optical extinction in the United States. *J Geophys Res*, 99:1347–1370.
- Martin, G. M., Johnson, D. W., and Spice, A. (1994). The measurement and parameterization of effective radius of droplets in warm stratocumulus clouds. *J Atmos Sci*, 51(1823-1842).
- Martin, R., Jacob, D., Yantosca, R., Chin, M., and Ginoux, P. (2003). Global and regional decreases in tropospheric oxidants from photochemical effects of aerosols. *J Geophys Res-Atmos*, 108(D3):4097.
- Menon, S., Del Genio, A., Koch, D., and Tselioudis, G. (2002). GCM Simulations of the aerosol indirect effect: Sensitivity to cloud parameterization and aerosol burden. *J Atmos Sci*, 59(3):692–713.
- Meskjidze, N., Sotiropoulou, R. E. P., Nenes, A., Kouactchou, J., Das, B., and Rodriguez, J. M. (2007). Aerosol-cloud interactions in the nasa gmi: Model development and indirect forcing assessments for sulfate aerosol. *Atmos Chem Phys Discuss*, 7:14295–14300.
- Mickley, L. J., Leibensperger, E. M., Jacob, D. J., and Rind, D. (submitted). Regional warming from aerosol removal over the United States: Results from a transient 2010–2050 climate simulation. *Atmos Environ*.
- Murray, L. T. (in prep.). Spatial and interannual variability in lightning constrained by LIS/OTD satellite data fro 1980-2006: Implications for tropospheric ozone and OH.
- Nakićenović, N. and Swart, R. (2000). *Special Report on Emissions Scenarios: A Special Report of the Working Group III of the Intergovernmental Panel on Climate Change*. Cambridge University Press.

- National Research Council (2005). *Radiative Forcing of Climate Change: Expanding the Concept and Addressing Uncertainties*. National Academies Press, Washington, DC.
- Nenes, A. and Seinfeld, J. H. (2003). Parameterization of cloud droplet formation in global climate models. *J Geophys Res-Atmos*, 108(D14):4415.
- Odum, J., Jungkamp, T., Griffin, R., Forstner, H., Flagan, R., and Seinfeld, J. (1997). Aromatics, reformulated gasoline, and atmospheric organic aerosol formation. *Environ Sci Technol*, 31(7):1890–1897.
- Olivier, J. G. J. and Berdowski, J. J. M. (2001). *The Climate System*, chapter Global Emissions Sources and Sinks. A. A. Balkema Publishers/Swets and Zeitlinger Publishers, Lisse, Netherlands.
- Park, R., Jacob, D., Chin, M., and Martin, R. (2003). Sources of carbonaceous aerosols over the United States and implications for natural visibility. *J Geophys Res-Atmos*, 108(D12):4355.
- Park, R., Jacob, D., Field, B., Yantosca, R., and Chin, M. (2004). Natural and transboundary pollution influences on sulfate-nitrate-ammonium aerosols in the United States: Implications for policy. *J Geophys Res-Atmos*, 109:D15204.
- Park, R., Jacob, D., Kumar, N., and Yantosca, R. (2006). Regional visibility statistics in the United States: Natural and transboundary pollution influences, and implications for the Regional Haze Rule. *Atmos Environ*, 40(28):5405–5423.
- Park, R., Jacob, D., and Logan, J. (2007). Fire and biofuel contributions to annual mean aerosol mass concentrations in the United States. *Atmos Environ*, 41(35):7389–7400.
- Park, R. J., Jacob, D. J., Palmer, P. I., Clarke, A. D., Weber, R. J., Zondlo, M. A., Eisele, F. L., Bandy, A. R., Thornton, D. C., Sachse, G. W., and Bond, T. C. (2005). Export efficiency of black carbon aerosol in continental outflow: Global implications. *J Geophys Res-Atmos*, 110(D11):8.
- Penner, J. E., Prather, M. J., Isaksen, I. S. A., Fuglestvedt, J. S., Klimont, Z., and Stevenson, D. (2010). Short-lived uncertainty? *Nat Geosci*, 3:587–588.
- Penner, J. E., Quaas, J., Storelvmo, T., Takemura, T., Boucher, O., Guo, H., Kirkevag, A., Kristjansson, J. E., and Selander, O. (2006). Model intercomparison of indirect aerosol effects. *Atmos Chem Phys*, 6:3391–3405.
- Pierce, J. and Adams, P. (2006). Global evaluation of CCN formation by direct emission of sea salt and growth of ultrafine sea salt. *J Geophys Res-Atmos*, 111(D6):D06203.
- Price, C. and Rind, D. (1992). A simple lightning parameterization for calculating global lightning distributions. *J Geophys Res*, 97(D9):9919–9933.

- Raes, F. and Seinfeld, J. H. (2009). New directions: Climate change and air pollution abatement: A bumpy road. *Atmos Environ*, 43(32):5132–5133.
- Rayner, N., Parker, D., Horton, E., Folland, C., Alexander, L., Rowell, D., Kent, E., and Kaplan, A. (2003). Global analyses of sea surface temperature, sea ice, and night marine air temperature since the late nineteenth century. *J Geophys Res-Atmos*, 108(D14):4407.
- Rind, D., Lerner, J., Jonas, J., and Mclinden, C. (2007). Effects of resolution and model physics on tracer transports in the NASA Goddard Institute for Space Studies general circulation models. *J Geophys Res-Atmos*, 112(D9):D09315.
- Sauvage, B., Martin, R. V., Donkelaar, A. V., Liu, X., Chance, K., Jaeglé, L., Palmer, P. I., Wu, S., and Fu, T. M. (2007). Remote sensed and in situ constraints on processes affecting tropical tropospheric ozone. *Atmos Chem Phys*, 7:815–838.
- Schulz, M., Textor, C., Kinne, S., Balkanski, Y., Bauer, S., Berntsen, T., Berglen, T., Boucher, O., Dentener, F., and Guibert, S. (2006). Radiative forcing by aerosols as derived from the AeroCom present-day and pre-industrial simulations. *Atmos Chem Phys*, 6(12):5225–5246.
- Streets, D., Bond, T., Carmichael, G., Fernandes, S., Fu, Q., He, D., Klimont, Z., Nelson, S., Tsai, N., Wang, M., Woo, J., and Yarber, K. (2003). An inventory of gaseous and primary aerosol emissions in Asia in the year 2000. *J Geophys Res-Atmos*, 108(D21):8809.
- Streets, D., Bond, T., Lee, T., and Jang, C. (2004). On the future of carbonaceous aerosol emissions. *J Geophys Res-Atmos*, 109(D24):D24212.
- Toon, O. B., Pollack, J., and KHARE, B. (1976). The optical constants of several atmospheric aerosol species: ammonium sulfate, aluminum oxide, and sodium chloride. *J Geophys Res*, 81(33):5733–5748.
- Twomey, S. (1974). Pollution and the planetary albedo. *Atmos Environ*, 8:1251–1256.
- Unger, N., Bond, T. C., Wang, J. S., Koch, D. M., Menon, S., Shindell, D. T., and Bauer, S. (2010). Attribution of climate forcing to economic sectors. *P Natl Acad Sci USA*, 107(8):3382–3387.
- US Environmental Protection Agency (2009). *Acid Rain and Related Programs - 2007 Progress Report*. Washington, DC.
- US Environmental Protection Agency (2010). *Our Nation's Air - Status and Trends Through 2008*. Washington, DC.
- van Aardenne, J., Dentener, F., and Olivier, J. (2001). A $1^\circ \times 1^\circ$ resolution data set of historical anthropogenic trace gas emissions for the period 1890–1990. *Global Biogeochem Cy*, 15(4):909–928.

- Wang, Y., Jacob, D., and Logan, J. (1998). Global simulation of tropospheric O₃-NO_x-hydrocarbon chemistry 1. Model formulation. *J Geophys Res-Atmos*, 103(D9):10713–10725.
- Wesely, M. L. (1989). Parameterization of surface resistances to gaseous dry deposition in regional scale numerical models. *Atmos Environ*, 23:1293–1304.
- West, J. J., Ansari, A. S., and Pandis, S. N. (1989). Marginal PM_{2.5}: Nonlinear aerosol mass response to sulfate reductions in the eastern United States. *J Air & Wast Magage Assoc*, 49:1415–1424.
- Wu, S., Mickley, L. J., Leibensperger, E. M., Jacob, D. J., Rind, D., and Streets, D. G. (2008). Effects of 2000-2050 global change on ozone air quality in the United States. *J Geophys Res-Atmos*, 113(D6):D06302.
- Yienger, J. and Levy, H. (1995). Empirical model of global soil-biogenic NO_x emissions. *J Geophys Res-Atmos*, 100(D6):11447–11464.
- Zhang, L. (in prep.). Patterns and mechanisms of reactive nitrogen deposition over the United States.
- Zwiers, F. and von Storch, H. (1995). Taking serial correlation into account in tests of the mean. *J Climate*, 8(2):336–351.

Chapter 5

Climatic effects of 1950-2050 changes in US anthropogenic aerosols

Part 2: Climate Response

Abstract

We investigate the climate response to US anthropogenic aerosol sources over the 1950 to 2050 period by using the NASA GISS general circulation model (GCM) and comparing to observed US temperature trends. Time-dependent aerosol distributions are generated from the GEOS-Chem chemical transport model applied to historical emission inventories and future projections. Radiative forcing from US anthropogenic aerosols peaked in 1970-1990 and has strongly declined since due to air quality regulations. We find that the regional radiative forcing from US anthropogenic aerosols elicits a strong regional climate response, cooling the central and eastern US by 0.5-1.0°C on average during 1970-1990, with the strongest effects on maximum daytime temperatures in summer and fall. Aerosol cooling reflects comparable contributions from direct and indirect (cloud-mediated) radiative effects. Absorbing aerosol (mainly black carbon) has negligible warming effect. Aerosol cooling reduces surface evaporation and thus decreases precipitation along the US east coast, but also increases the southerly flow of moisture from the Gulf of Mexico resulting in increased cloud cover and precipitation in the central US. Observations over the eastern US show a lack of warming in 1960-1980 followed by very rapid warming since, which we reproduce in the GCM and attribute to trends in US anthropogenic aerosol sources. Present US aerosol concentrations are sufficiently low that future air quality regulations are projected to cause little further warming (0.1°C over 2010-2050). We find that most of the potential warming from aerosol source controls in the US has already been realized over the 1980-2010 period.

5.1 Introduction

Global mean surface temperatures increased by $0.74 \pm 0.18^\circ\text{C}$ between 1906 and 2005 due to increasing greenhouse gases (Trenberth et al., 2007), but regional temperature trends are more complicated. For example, the eastern US experienced a cooling between 1930 and 1990 (Fig. 5.1). Anthropogenic aerosols are known to have mitigated some of the global warming from greenhouse gases (Hegerl et al., 2007), but the importance of aerosol cooling on temperature trends in the US has received little attention. As US aerosol sources are increasingly controlled to improve air quality, the associated cooling is undone resulting in accelerated warming (Andreae et al., 2005; Brasseur and Roeckner, 2005; Kloster et al., 2009; Mickley et al., submitted). Air quality improvement thus comes with climate consequences (Raes and Seinfeld, 2009). In Chapter 4, we reconstructed and projected the aerosol trends and associated radiative forcing from US anthropogenic sources over the 1950-2050 period. US aerosol concentrations peaked in 1970-1990 and have decreased rapidly since. We use here a general circulation model (GCM) to study the associated climate response.

Aerosols directly affect the climate system by scattering and absorbing solar radiation, and indirectly by altering cloud microphysical properties. Scattering cools and absorption warms the atmosphere, but both cause a reduction in surface solar radiation. Observations of surface solar radiation over the US show a widespread decrease over the 1950-1990 period followed by more recent increase (Liepert and Tegen, 2002; Long et al., 2009). These trends have been identified in clear and all-sky scenes, suggesting a role for both direct and indirect aerosol effects. These trends in surface solar radiation are qualitatively consistent with changes in aerosol sources (Streets et al., 2009), but cannot be fully explained by

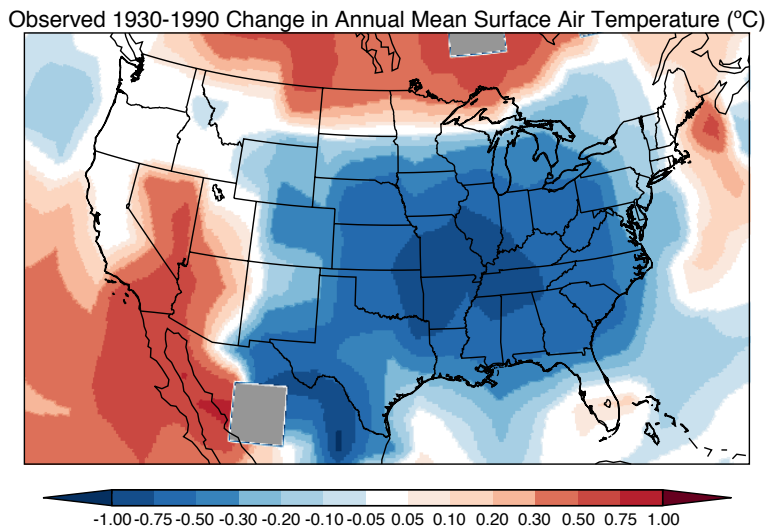


Figure 5.1: Observed change in surface air temperature between 1930 and 1990. Temperature change based on the linear trend as in Hansen et al. (2001). Observations are from the NASA GISS Surface Temperature Analysis (GISTEMP; <http://data.giss.nasa.gov/gistemp/>).

anthropogenic aerosols (Liepert and Tegen, 2002; Long et al., 2009; Wild, 2009a).

Aerosols are scavenged from the atmosphere by precipitation on a time scale of days, so that their radiative forcing is strongly localized over source regions (Schulz et al., 2006). A critical issue is whether the regional radiative forcing of aerosols elicits a correspondingly regional climate response. Observation-based studies have related changes in surface solar radiation with other climate variables as a method of deducing the local effects of aerosol forcing. They show evidence that aerosols have lowered surface air temperature and temporarily offset greenhouse warming (Qian and Giorgi, 2000; Wild et al., 2007; Ruckstuhl et al., 2008; Philipona et al., 2009), reduced the diurnal temperature range by dampening daily maximum temperatures (Liu et al., 2004b; Wild et al., 2007; Makowski et al., 2009), lowered evaporation rates (Peterson et al., 1995; Liu et al., 2004a; Roderick et al., 2007), and increased soil moisture (Robock et al., 2005).

Some GCM studies have found strong regional climate sensitivity to aerosols including

in India (Menon et al., 2002; Wang et al., 2009a), southeast Asia (Chang et al., 2009; Zhang et al., 2009; Lee and Kim, 2010), the North Atlantic (Fischer-Bruns et al., 2009), and California (Jacobson, 2008). However, other studies have found that aerosol radiative forcing elicits little regional climate response, and produces instead a global climate effect with patterns similar (but opposite in sign) to greenhouse gas forcing (Mitchell et al., 1995; Shindell et al., 2007; Levy et al., 2008; Shindell et al., 2008; Kloster et al., 2009). Mickley et al. (submitted) used a GCM to simulate the climate response of completely removing aerosols over the US and found a 0.4-0.6°C regional warming in the US with little effect elsewhere. Fischer-Bruns et al. (2010) investigated the climate impacts of removing North American aerosols and found a 1.0-1.5°C summer warming in surface air over the US and North Atlantic Ocean. They also found a 1.5-2.0°C warming of the Arctic in winter.

There is strong motivation for air quality agencies to decrease aerosol concentrations to improve public health. Better understanding of the associated climate response is necessary. The US is of particular interest in this regard because aerosol concentrations rose in the 20th century, peaked in the 1980s, and have been decreasing rapidly since due in large part to a 56% reduction of SO₂ emissions between 1980 and 2008 (US Environmental Protection Agency (US EPA), 2010). Here we use the 1950-2050 time series of US aerosol trends and radiative forcing from Chapter 4 to conduct 1950-2050 transient-climate simulations with the NASA Goddard Institute for Space Studies (GISS) GCM 3 (Rind et al., 2007). Our objective is to investigate the regional climate effects of historical and projected changes in US anthropogenic aerosol sources. An important advance compared to previous work is the use of a realistic evolution of aerosol sources.

5.2 Methods

We conduct sensitivity simulations with the GISS GCM 3 to study the evolving 1950-2050 climate response to changing US anthropogenic aerosol sources. The GCM uses archived global 3-D monthly mean concentrations of different aerosol components from the GEOS-Chem chemical transport model (CTM) with time-dependent emissions based on historical data and future projections. The CTM simulations are described in Chapter 4 and a brief summary is given below.

5.2.1 Aerosol simulations

We conduct a 2-year GEOS-Chem simulation of coupled ozone- NO_x -VOC-aerosol chemistry (<http://geos-chem.org>; Bey et al., 2001; Park et al., 2004) for each decade between 1950 and 2050. The first year is used as model initialization. Monthly mean fine aerosol concentrations are archived from the second year for use in the GCM including sulfate-nitrate-ammonium (SNA), primary organic aerosol (POA), secondary organic aerosol (SOA), and black carbon (BC) (Park et al., 2006; Liao et al., 2007). Simulations for all years use the same assimilated meteorological data from 2000-2001 so that changes in concentrations over the 1950-2050 period are due to emissions only. The meteorological data are from the NASA Goddard Earth Observing System (GEOS)-4 with $1^\circ \times 1.25^\circ$ horizontal resolution, 55 vertical levels, and 6-hour temporal resolution (3-hour for surface variables and mixing depths). The horizontal resolution is degraded to $2^\circ \times 2.5^\circ$ for input to GEOS-Chem. The effect of US anthropogenic sources is determined by a parallel sensitivity simulation with zero US anthropogenic emissions of SO_2 , NO_x , POA, and BC for each decade. “Anthropogenic” here includes fuel and industrial sources but not open fires.

We use 1950-1990 global anthropogenic emissions of SO₂ and NO_x from EDGAR Hyde 1.3 (van Aardenne et al., 2001) and 2000 emissions from EDGAR 3.2 FT (Olivier and Berdowski, 2001). Historical emissions of BC and POA are from Bond et al. (2007). Emissions past 2000 are calculated using growth factors derived from the Integrated Model to Assess the Greenhouse Effect (IMAGE; Streets et al., 2004) following the IPCC A1B scenario (Nakićenović and Swart, 2000). As in Fiore et al. (2002) and Wu et al. (2008), growth factors are calculated for different countries and fuel types (fossil fuel and biofuel). Ammonia emissions are from Bouwman et al. (1997) as modified by Park et al. (2004), except for East Asia (Streets et al., 2003). Additional sources include climatological biomass burning (Duncan et al., 2003), fertilizer (Wang et al., 1998), aircraft (Chin et al., 2000), the biosphere, volcanoes, and lightning. See Chapter 4 for more detail.

5.2.2 Climate simulations

We conduct transient climate simulations with the GISS GCM 3 using a horizontal resolution of 4° × 5° and 23 vertical levels that extend from the surface to 0.002 hPa. GISS GCM 3 shares a common history with another NASA GISS GCM, Model E (Schmidt et al., 2006), but the two differ in their parameterizations of gravity wave drag, convection, and the boundary layer (Rind et al., 2007). GISS GCM 3 has been previously used in studies investigating air quality-climate interactions (Leibensperger et al., 2008; Wu et al., 2008; Pye et al., 2009; Chen et al., 2010), tracer transport (Rind et al., 2007), climate response to solar forcing (Rind et al., 2008), and stratospheric ozone-climate interactions (Rind et al., 2009b,a). The model contains a Q-flux ocean, in which monthly oceanic heat transports are held constant but sea surface temperature and sea ice coverage are allowed to respond to energy exchange with the atmosphere (Hansen et al., 1988). We calculate ocean heat trans-

port using equilibrium climate simulations forced with observed sea surface temperature (SST) and sea ice distributions for 1946-1955 (Rayner et al., 2003), following the method outlined by Hansen et al. (1988).

Archived 3-D monthly mean aerosol concentrations are imported from GEOS-Chem to compute the aerosol direct effect. Concentrations are interpolated between decadal time slices. Aerosol optical properties are calculated assuming an internal mixture. Following Chung and Seinfeld (2002) and Liao et al. (2004), we assume a standard gamma aerosol size distribution with an effective dry radius of $0.3 \mu\text{m}$ and area-weighted variance of 0.2. Optical properties of the internal mixture are calculated using the volume-weighted mean of the refractive indices of the individual components. The resulting direct forcing from US anthropogenic aerosol sources in 1980 (peak aerosol loading) is -0.05 W m^{-2} globally but -2.0 W m^{-2} over the eastern US. Dust and sea salt aerosols are considered externally mixed and held constant for 1950-2050 at the climatological values of Hansen et al. (2002).

Aerosol indirect radiative effects are computed following the approach previously implemented by Chen et al. (2010) in the GISS GCM 3. This includes the first indirect effect (cloud albedo) and the second indirect effect (cloud lifetime) on liquid stratiform clouds only. Aerosol mass concentrations affect the cloud droplet number concentration $N_c (\text{m}^{-3})$, which in turn determines the effective radius of cloud droplets and the rate of autoconversion to precipitation. We calculate N_c locally from the archived GEOS-Chem aerosol distributions using the method of Chen et al. (2010):

$$\log N_c = A + B \log m_i \quad (5.1)$$

where m_i is the molar concentration of dissolved aerosol ions (mol m^{-3}) and A and B

are gridded 3-D monthly mean coefficients derived from detailed simulations of aerosol microphysics and activation within the GCM (Adams and Seinfeld, 2002; Nenes and Seinfeld, 2003; Fountoukis and Nenes, 2005; Pierce and Adams, 2006). Cloud optical depth scales as the inverse of the area-weighted mean effective radius r_e of the cloud droplet size distribution (Del Genio et al., 1996). We obtain r_e from:

$$r_e = \kappa^{-\frac{1}{3}} \left[\frac{3L}{4\pi N_c} \right]^{\frac{1}{3}} \quad (5.2)$$

where L is the liquid water content of the cloud (cm^3 water per cm^{-3} air), and κ is a constant (0.67 over land, 0.80 over ocean; Martin et al., 1994) that relates the volume-weighted mean and area-weighted mean radii. Autoconversion rates are calculated using the parameterization of (Khairoutdinov and Kogan, 2000), which fits results from an explicit microphysical model:

$$\frac{dq_l}{dt} = -1350 \gamma q_l^{2.47} N_c^{-1.79} \quad (5.3)$$

where q_l is the cloudwater mass content (kg kg^{-1}). Hoose et al. (2008) and Chen et al. (2010) added the tuning parameter γ in order to retain GCM climate equilibrium. We find that a γ value of 12 retains top-of-atmosphere (TOA) radiative balance in a climate equilibrium simulation for 1950 conditions including fixed SST and sea ice (Chapter 4).

Two sets of control simulations were conducted. The first includes only the direct radiative forcing from aerosols, using the imported aerosol concentrations from GEOS-Chem. The second additionally imports N_c to account for the aerosol indirect effects. Sensitivity simulations were conducted relative to each of these controls using aerosol and N_c fields from the GEOS-Chem simulations with US anthropogenic sources of SO_2 , NO_x , POA, and

BC shut off. Differences between the control and sensitivity simulations then measure the climate response to US anthropogenic sources through the direct and indirect effects of aerosols.

Each set of simulations consists of a five-member ensemble conducted from 1950 to 2050 using the natural and greenhouse gas forcing described by Hansen et al. (2002). Future greenhouse gas concentrations follow the IPCC SRES A1B scenario with CO₂, N₂O, and CH₄ reaching 522, 0.350, and 2.40 ppm, respectively, by 2050. Initiating climate simulations from 1950 equilibrium conditions neglects the small radiative imbalance that occurred at that time. A previous study with the GISS GCM using the same climate forcing as here (except for tropospheric aerosols) found the Earth to be out of radiative balance by +0.18 W m⁻² for 1951 conditions (Sun and Hansen, 2003). This suggests that our simulations underestimate post-1950 global warming by approximately 0.1°C, a small effect that does not impact our assessment of the climate response to US anthropogenic aerosols since it is common to both the control and sensitivity simulations.

We conducted an additional sensitivity simulation to isolate the climate effects of US anthropogenic sources of BC. This simulation uses the sulfate, nitrate, POA, and SOA distributions from the control simulation, but no BC emission from US anthropogenic sources. Results indicate that the climate effects of US anthropogenic BC are small and indistinguishable from interannual variability. This is consistent with the weak radiative forcing from US anthropogenic BC (+0.4 W m⁻² over the eastern US for 1970-1990). We do not discuss this simulation further.

We test the statistical significance of our results using a version of Students t-test accounting for serial correlation (Zwiers and von Storch, 1995). Presented results are significant at the 95th percentile and represent the mean of ensemble members unless specified.

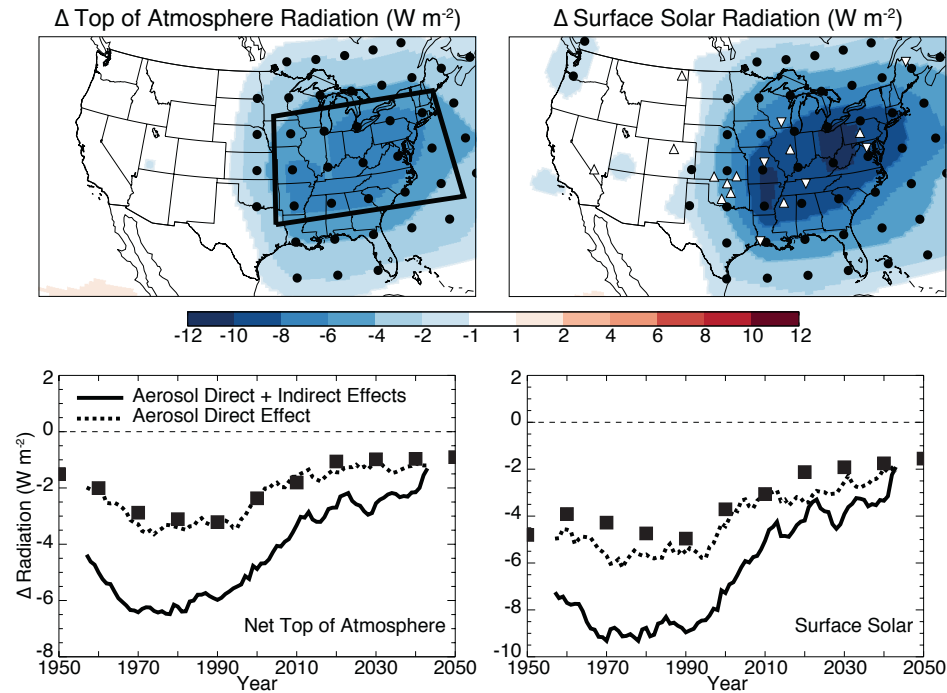


Figure 5.2: Changes in net top-of-atmosphere (TOA) radiation (left) and surface solar radiation (right) due to US anthropogenic aerosol sources. The top panels show the annual mean aerosol effect (direct and indirect) averaged over 1970-1990. The bottom panels show the 1950-2050 evolution of the direct effect only (dashed) and the sum of direct and indirect effects (solid) averaged over the mid-Atlantic US (boxed region). Values are differences between the control simulation and a simulation with US anthropogenic aerosol sources shut off. In the top panels, dots indicate differences significant at the 95th percentile, downward triangles indicate observation sites used by Liepert and Tegen (2002), and upward triangles indicate observation sites used by Long et al. (2009). In the lower panels, black squares indicate the annual mean aerosol direct radiative forcings over the mid-Atlantic US region from US anthropogenic sources derived from the results of Chapter 4. Time series have been filtered by a 15-year moving average.

5.3 Climate response to US anthropogenic aerosols

5.3.1 Radiation

Figure 5.2 shows the annual mean change in net TOA and surface solar radiation due to the direct and indirect radiative effects of US anthropogenic aerosols in 1970-1990, the period when US aerosol loadings were at their peak. These differ from the radiative forcings reported in Chapter 4 in that they include the effects of climate response, such as changes

in cloud cover. We find that the radiative effect is strongly concentrated over the eastern US, and define a mid-Atlantic US region boxed in Fig. 5.2 where the effect is maximum. The annual mean TOA radiative effect averages -6 W m^{-2} over that region, whereas the global TOA radiative effect is only -0.08 W m^{-2} .

The bottom panels of Fig. 5.2 show the 1950-2050 time series of the TOA and surface radiative effects from US anthropogenic aerosol sources over the mid-Atlantic region. Results are shown for the direct effect only and for the sum of direct and indirect effects. The magnitudes and trends of the direct effect match closely the corresponding direct radiative forcings computed in Chapter 4 (squares in Fig. 5.2). The indirect effect is comparable in magnitude to the direct effect. Sulfate is the largest contributor to US anthropogenic aerosol forcing (Chapter 4). We see from Fig. 5.2 that the radiative perturbations largely follow the evolution of SO_2 sources: increase until 1980 and rapid decrease afterward. Changes level off after 2020, by which time SO_2 emissions are 80% lower than their 1980 peak.

The surface radiative effects in Fig. 5.2 are about 50% larger than the TOA effects due to aerosol absorption. Liepert and Tegen (2002) used six observation sites east of 95°W (downward triangles in Fig. 5.2) from the National Solar Radiation Database (NSRDB; http://rredc.nrel.gov/solar/old_data/nsrdb/) to estimate a clear-sky trend in surface solar radiation of -7 W m^{-2} between 1961 and 1990 that they attributed to the aerosol direct effect. Long et al. (2009) calculated an observed 1996-2007 increase in surface solar radiation of $+5 \text{ W m}^{-2}$ (clear sky) and $+8 \text{ W m}^{-2}$ (all sky) averaged over 11 Department of Energy Atmospheric Radiation Measurement (ARM) and National Oceanic and Atmospheric Administration (NOAA) US Surface Radiation Budget (SURFRAD) sites (upward triangles in Fig. 5.2). However, and as previously noted (Liepert and Tegen, 2002; Long et al., 2009; Wild, 2009a,b), we find that anthropogenic aerosols cannot explain the magnitude of the

observed surface radiation trends. Sampling our control simulation at the six sites analyzed by Liepert and Tegen (2002), we find a simulated all-sky decrease of surface solar radiation of 1.1 W m^{-2} between 1961 and 1990 due to the aerosol direct effect, much smaller than the observed value. Conversion of our all-sky trend to the clear-sky value would not reconcile the difference. Similarly, our control simulation underestimates the 1996-2007 all-sky increase of Long et al. (2009) ($+2.4 \text{ W m}^{-2}$ vs. $+8 \text{ W m}^{-2}$).

We previously showed that our simulated aerosol trends over the US are in good agreement with observations, at least for 1980-present when data are available (Chapter 4). The observed surface solar radiation trends thus seem much larger than can be explained from aerosol trends. The 1961-1990 NSRDB surface solar radiation data suffer from inconsistent data quality, but the more recent measurements presented by Long et al. (2009) have consistent annual calibration and daily performance monitoring. The cause of the model-observation discrepancy is unclear but points to the danger of interpreting observed trends in surface radiation as driven by aerosols.

5.3.2 Temperature

Figure 5.3 shows the annual mean temperature changes in surface air and at 500 hPa due to the direct and indirect effects of US anthropogenic aerosol sources over the 1970-1990 period when US anthropogenic aerosol forcing was at its peak. Changes in surface air temperature peak in the eastern US ($0.5\text{-}1.0^\circ\text{C}$), collocated with the maximum radiative effect (Fig. 5.2). The cooling influence of US anthropogenic aerosols extends over much of the Northern Hemisphere, but beyond the US and North Atlantic Ocean it is only marginally significant against interannual variability. The annual mean cooling averages 0.1°C for the Northern Hemisphere and 0.05°C for the Southern Hemisphere.

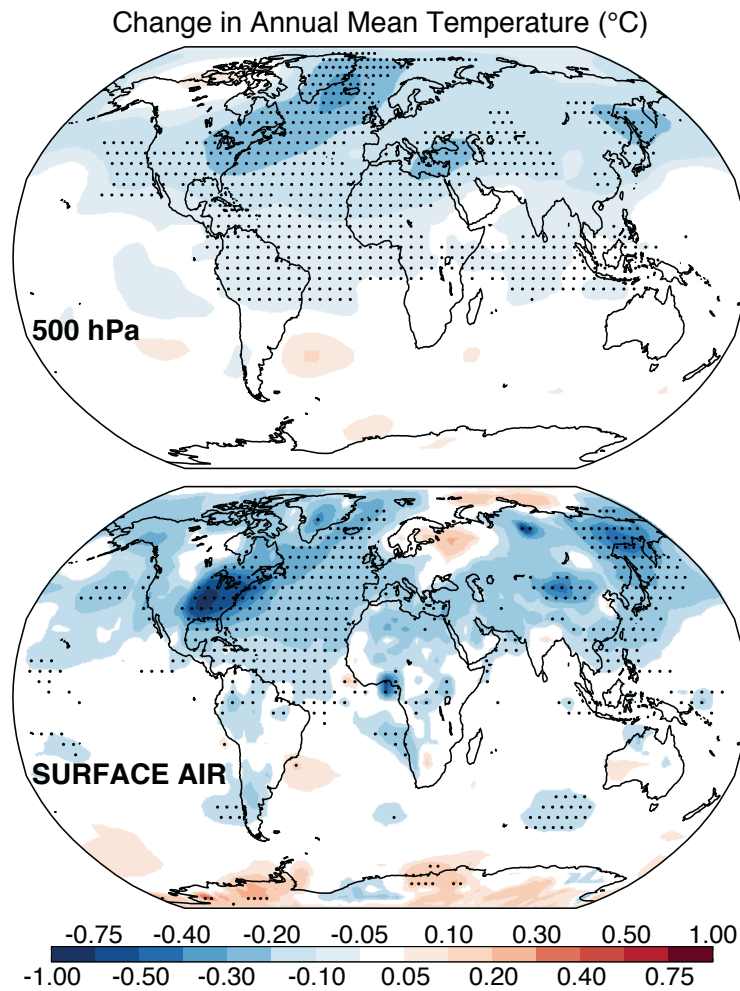


Figure 5.3: Effect of US anthropogenic aerosol sources on annual mean temperatures ($^{\circ}\text{C}$) for the 1970-1990 period (when US aerosol loading was at its peak). Values are shown for surface air (bottom) and 500 hPa (top) temperatures. They represent the mean difference between 5-member ensemble GCM simulations including vs. excluding US anthropogenic aerosol sources, and considering both aerosol direct and indirect effects. Dots indicate differences significant at the 95th percentile.

As pointed out in the Section 5.1, some GCM studies find a strong spatial correlation between regional radiative forcing and climate response (as is shown here) while others do not. The reason is not clear and warrants a dedicated GCM intercomparison in the future. A contributing factor may be the magnitude and spatial distribution of the forcing. Larger, more distributed forcings may elicit a more non-localized response. A recent study by

Fischer-Bruns et al. (2010) of climate sensitivity to North American anthropogenic aerosol finds a strong Arctic climate response that is not apparent in our work.

Cooling is more diffuse at higher altitudes, reflecting the faster transport of heat (Fig. 5.3, top). At 500 hPa, the largest cooling is 0.3°C over the eastern US and North Atlantic Ocean. Statistically significant cooling covers more of the Northern Hemisphere at 500 hPa than at the surface. Annual mean cooling at 500 hPa averages 0.1°C for the Northern Hemisphere and 0.02°C for the Southern Hemisphere, similar to the hemispheric changes in surface air temperature. Cooling is even more diffuse at 300 hPa (not shown), but Northern Hemisphere cooling is similarly 0.1°C.

Figure 5.4 shows the surface air cooling due to US anthropogenic aerosols for the 1970–1990 period for the simulations including only the aerosol direct effect (top) and the combination of direct and indirect effects (bottom), focusing on the US. The bottom panel is a zoomed version of the bottom panel of Fig. 5.3. Significant cooling extends over much of the US even when the aerosol direct effect alone is considered. The magnitude of the cooling doubles when the indirect effects are included but the spatial patterns are similar. Thus the significance and localization of the US cooling due to US anthropogenic aerosol sources is not contingent on the indirect effects, which are far more uncertain than the direct effect. Cooling is strongest in the Midwest, shifted westward relative to the region of peak aerosol abundance shown in Fig. 4.2. This is due to hydrological factors and is discussed further in Section 5.3.3.

Figure 5.5 shows seasonal statistics of the effects of US anthropogenic aerosols on surface air temperatures in the mid-Atlantic US (boxed region in Fig. 5.2). The change in surface air temperature is largest in JJA and SON, with regionally averaged cooling of more than 1.0°C in SON. Aerosol radiative forcing is largest in summer when solar radiation is

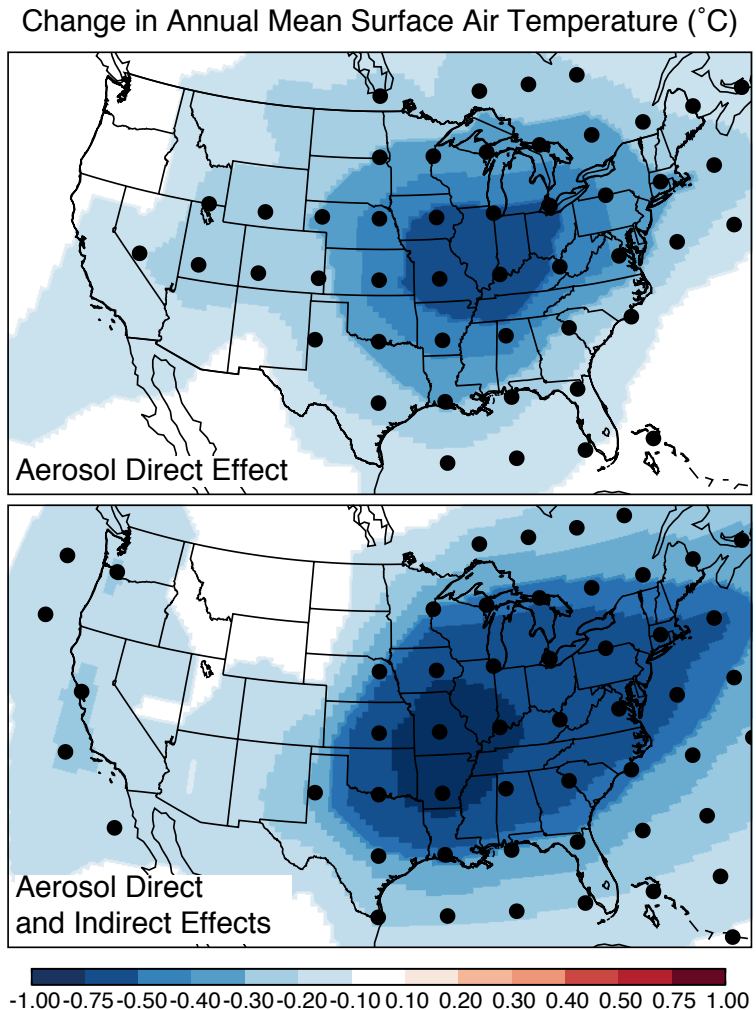


Figure 5.4: Effect of US anthropogenic aerosol sources on surface air temperatures for the 1970-1990 period when US aerosol loading was at its peak. Values represent the mean difference between 5-member ensemble GCM simulations including vs. excluding US anthropogenic aerosol sources, and considering the aerosol direct only (top) and the sum of direct and indirect effects (bottom). Dots indicate differences significant at the 95th percentile. The bottom panel contains the same information as the bottom panel of Figure 3 but zoomed over the US.

strongest. The larger surface air temperature changes in SON reflect the drier conditions so that less of the radiative effect is buffered by changes in surface evaporation (latent heat flux).

Figure 5.5 additionally shows the changes in extreme temperatures. We find that aerosol cooling has a larger effect on daily maximum than daily minimum temperatures, in all sea-

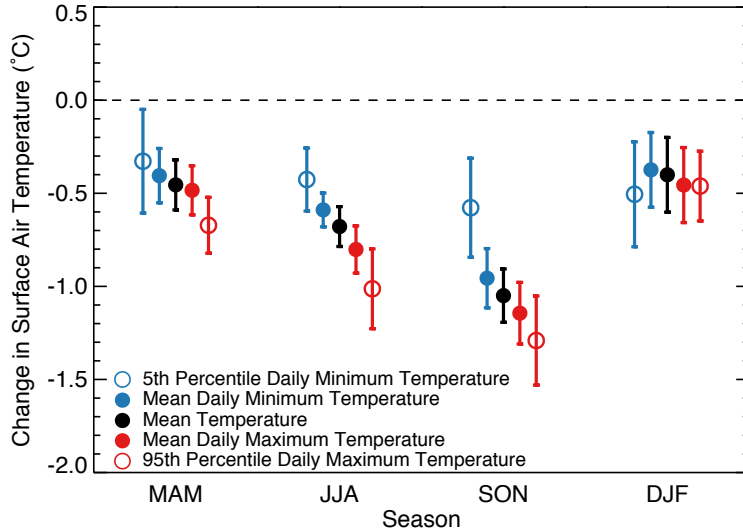


Figure 5.5: Effect of US anthropogenic aerosols on seasonal surface air temperature statistics over the mid-Atlantic US (boxed region in Fig. 5.2). Values are for 1970-1990, when US aerosol loads were at their peak. Statistics were obtained by difference between 5-member ensemble GCM simulations including vs. excluding US anthropogenic aerosol sources, and considering both the aerosol direct and indirect effects. Error bars indicate 95% confidence intervals.

sons, as expected since the forcing is due to scattering of solar radiation. The cooling is largest during heat waves of JJA and SON (95th percentile daily maximum temperatures, corresponding to the 5 hottest days of each season). These heat waves occur under cloud free conditions when the aerosol direct effect is especially effective. We find that the warmest days are cooler by 1.0°C in JJA and 1.3°C in SON. The coldest nights of each season (5th percentile daily minimum temperatures) are least sensitive to aerosols except in winter when they are typically associated with synoptic-scale clear-sky conditions.

The model pattern of aerosol-driven cooling over the US in Fig. 5.4 is remarkably similar to the observed 1930-1990 trend in surface air temperature shown in Fig. 5.1. The largest area of cooling in the central US has previously been referred to as a warming hole (Pan et al., 2004; Kunkel et al., 2006). Previous GCM studies have associated this warming hole with variations in SSTs in the tropical Pacific (Robinson et al., 2002; Kunkel

et al., 2006; Wang et al., 2009b). Kunkel et al. (2006) additionally point out a strong association between the observed variability of North Atlantic SSTs and central US surface temperatures. Our results indicate that the warming hole could be due to US anthropogenic aerosols, as SO₂ anthropogenic emissions in 1930 were only 60% of those in 1980. We find that US anthropogenic aerosols lower SSTs in the North Atlantic region outlined by Kunkel et al. (2006) by up to 0.3°C. Lower SSTs over the North Atlantic enhance the anticyclonic transport of marine air over the Gulf Coast of the US, magnifying the cooling as discussed below.

5.3.3 Hydrology and dynamics

Aerosols affect the hydrological cycle by reducing evaporation (due to reduced surface solar radiation) and by altering cloud cover and precipitation. Figure 5.6 shows the annual mean response of evaporation, precipitation, soil moisture availability, and cloud cover to US anthropogenic aerosols for the 1970-1990 period. The changes shown in Fig. 5.6 are for the total aerosol effect (direct + indirect), but similar responses with less statistical significance are found when only the aerosol direct effect is considered.

Reduced solar radiation at the surface decreases annual mean evaporation rates in the eastern US and the North Atlantic (Fig. 5.6a). The change is greatest in summer, when evaporation along the eastern seaboard decreases by up to 0.4 mm day⁻¹. As mentioned in Section 5.3.2, the decrease in latent heat flux associated with lower evaporation rates acts as a buffer to surface temperature changes, reducing the magnitude of aerosol cooling. We find that US anthropogenic aerosols decrease latent heat fluxes much more in summer (6.6 W m⁻² for 1970-1990 averaged over mid-Atlantic US) than in autumn (0.6 W m⁻²), reflecting the greater availability of soil moisture in summer. In contrast to the general

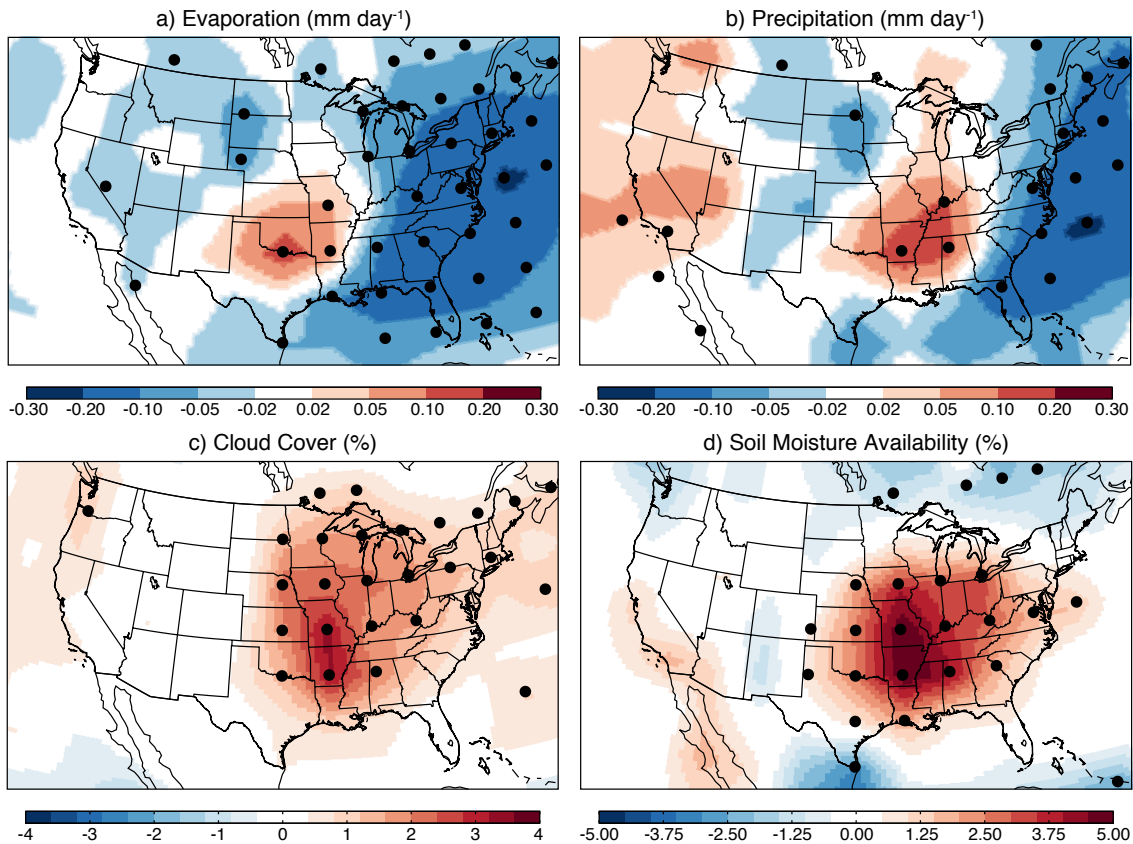


Figure 5.6: Effect of US anthropogenic aerosols on annual mean evaporation, precipitation, cloud cover, and soil moisture availability for the 1970-1990 period. Values represent the mean differences between 5-member ensemble GCM simulations including vs. excluding US anthropogenic aerosol sources, and considering both the aerosol direct and indirect effects. Cloud cover and soil moisture availability changes are shown as absolute percentages. Changes significant at the 95th percentile are marked with a dot.

decrease in evaporation rates over the US, we find an increase in the south-central region.

This is due to changes in soil moisture as discussed below.

The reduction in evaporation in the eastern US results in a decrease of downwind precipitation along the eastern seaboard (Fig. 5.6b). The decrease in precipitation is additionally promoted by the aerosol cloud lifetime effect (second aerosol indirect effect), which reduces the precipitation efficiency of clouds. The cloud lifetime effect is applied in the model to liquid stratiform clouds only, and this appears to be the dominant cause for the in-

crease in eastern US cloud cover in Fig. 5.6c. We find little net change in moist convective cloud cover.

In contrast to the general slowdown of the hydrological cycle over the US, we find that evaporation and precipitation increase in the south central US. This is mostly driven by a summertime aerosol-induced change in circulation. Figure 5.7 shows the effect of US anthropogenic aerosols on 850 hPa geopotential heights in summer. Aerosols cool the North Atlantic (Fig. 5.3), strengthening the Bermuda High and thus the onshore flow of marine air from the Gulf of Mexico that is the principal source of moisture for the central and eastern US in summer. This enhances cloud cover, precipitation, and soil moisture over the south-central US (Fig. 5.6). A similar increase in central US precipitation due to anthropogenic sulfate was presented but not discussed by Jones et al. (2007). Increased cloud cover in the central US due to anthropogenic aerosols explains the particularly strong

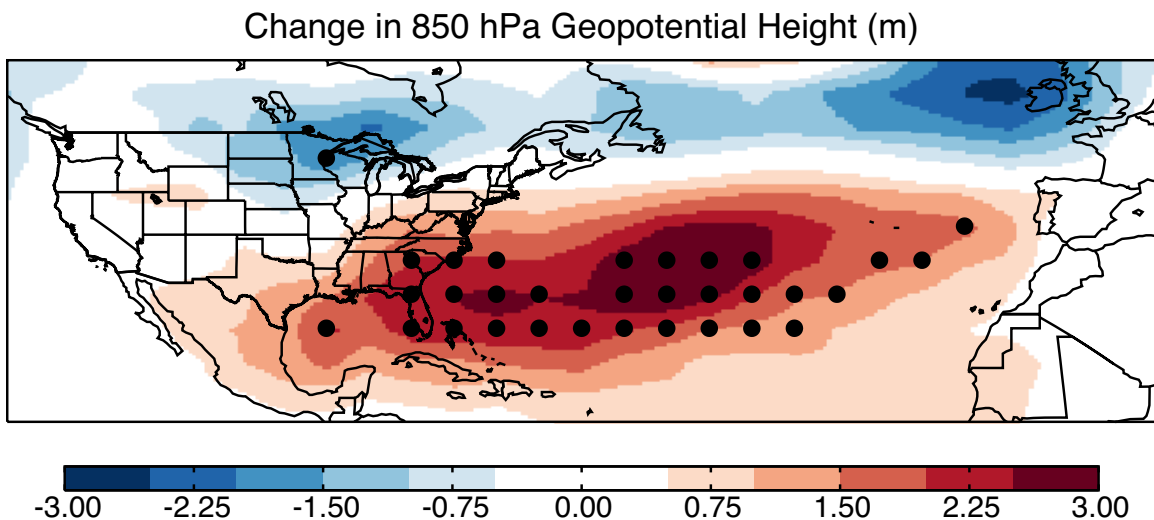


Figure 5.7: Change in the summer mean 850 hPa geopotential height due to US anthropogenic aerosols for the 1970-1990 period. Values represent the mean difference between 5-member ensemble GCM simulations including vs. excluding US anthropogenic aerosol sources, and considering both the aerosol direct and indirect effects. Changes significant at the 95th percentile are marked with a dot.

radiative and surface cooling effects in that region (Figs. 5.2 and 5.4). This is consistent with previous observational studies of the US warming hole which found it to be associated with additional moisture from the Gulf of Mexico causing enhanced evapotranspiration (Pan et al., 2004) and cloud cover (Robinson et al., 2002). Our work suggests that US anthropogenic aerosols may be the drivers of changes in circulation causing central US cooling.

5.4 Aerosol effects on 1950-2050 trends in US surface air temperature

Our analysis of the climate effects of US anthropogenic aerosols has focused so far on the 1970-1990 period when the US aerosol loading was the largest. Chapter 4 presented a detailed analysis of US anthropogenic aerosol trends for the 1950-2050 period. US aerosol loading (and corresponding radiative forcing) increased from 1950 to 1980, decreased since then, and is projected to continue decreasing in the future (Fig. 5.2). Most of the anthropogenic aerosol radiative forcing is due to sulfate produced by oxidation of SO₂. Emissions of SO₂ in the US decreased by 56% from their peak in 1980 to 2008 according to US EPA (2010) and this is verified by observed trends in sulfate wet deposition (Chapter 4). US sources of SO₂ and other aerosol precursors in the IPCC A1B scenario are projected to continue to decrease until 2020 and then level off.

Figure 5.8 shows the 1950-2050 simulated cooling trends over the mid-Atlantic US (region boxed in Fig. 5.2) due to US anthropogenic aerosol sources. Cooling increased from -0.3°C in the 1950s to -0.65°C in the 1970s, remained flat until 1995, and decreased back to -0.3°C by 2010. Further decrease in aerosol cooling is projected over the coming decades but at a much slower rate, to -0.2°C by 2030. This trend in cooling is well correlated with

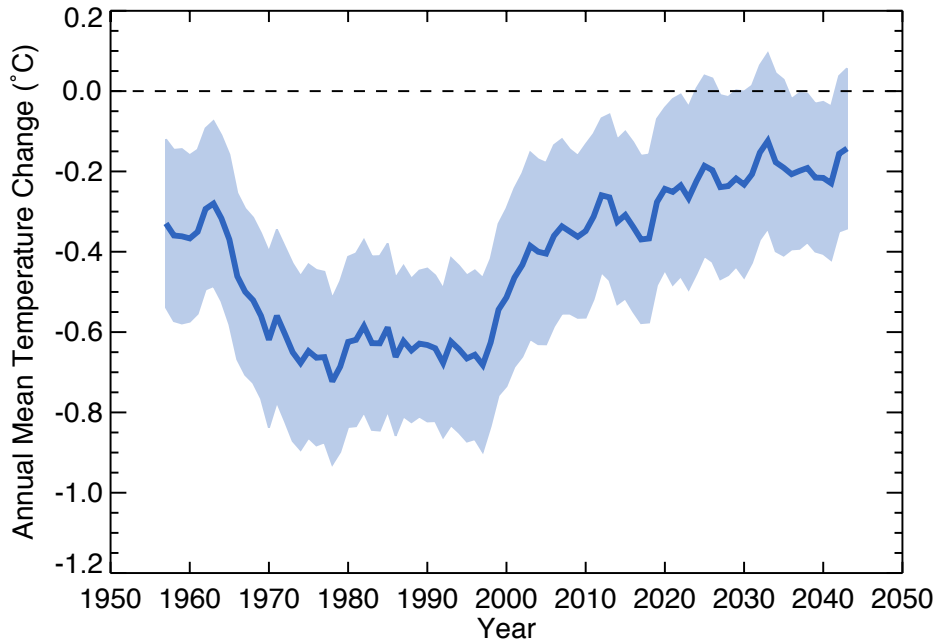


Figure 5.8: Change in annual mean surface air temperature over the mid-Atlantic US (boxed region in Fig. 5.2) due to US anthropogenic aerosol sources. Values are differences for 5-member ensembles between a 1950-2050 control simulation including radiative forcing from both greenhouse gases and aerosols (direct and indirect effects) and a sensitivity simulation with US anthropogenic aerosol sources shut off. The time series has been smoothed with a 15-year moving average. Shading indicates the 95% confidence interval.

the model trend in US aerosol sources (Chapter 4). The corresponding sensitivity of mid-Atlantic US surface air temperatures to regional aerosol forcing is $0.09^{\circ}\text{C} / \text{W m}^{-2}$. This is an order of magnitude smaller than the global climate sensitivity parameter of $0.76^{\circ}\text{C} / \text{W m}^{-2}$ for the GISS GCM 3 derived from doubled CO₂ simulations (Rind et al., 2007), as would be expected from the horizontal transport of heat. Still, we find that the large localized forcing elicits a strong regional climate response.

The trend of aerosol cooling over the mid-Atlantic US in Fig. 5.8 implies that most of the 0.5°C warming over the US expected between 1980 and 2050 from aerosol decreases has in fact already been realized by 2010. This 1980-2010 warming trend in the model can be compared to the observational record. Figure 5.9 shows the observed (GIS-

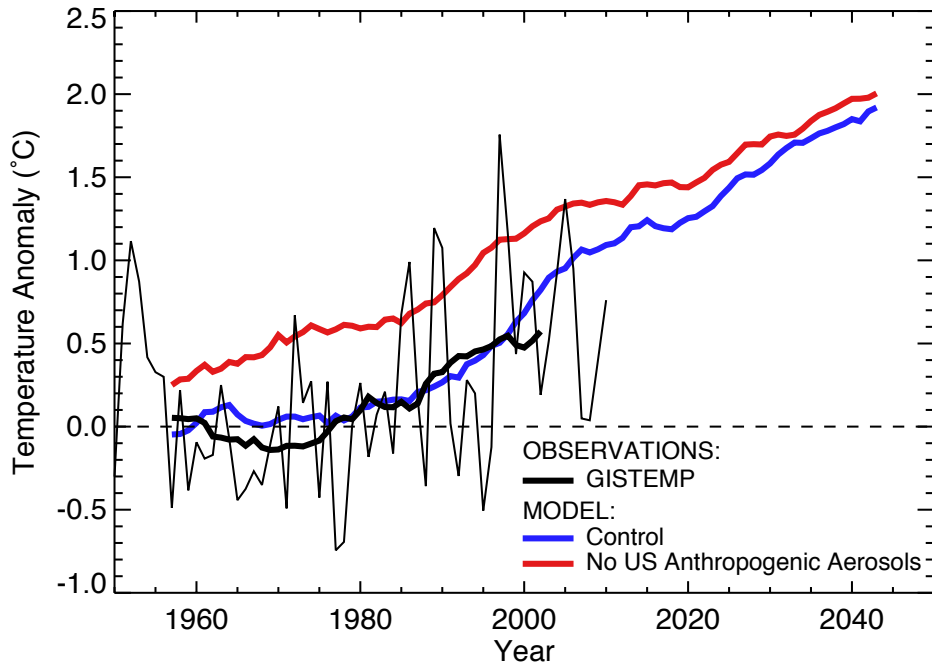


Figure 5.9: 1950-2050 trends in annual mean surface air temperatures over the mid-Atlantic US (boxed region in Fig. 2). Observations (GISTEMP) are compared to the control simulation including greenhouse and aerosol forcings and to the sensitivity simulation with no US anthropogenic aerosols. Observations are the anomaly relative to the observed 1951-1980 mean and are shown for individual years (thin line) and for a 15-year moving average (thick line). Model temperatures are the 5-member ensemble mean anomaly relative to the 1951-1980 mean of the control simulation, and are shown as 15-year moving averages.

TEMP; <http://data.giss.nasa.gov/gistemp/>) 1950-2010 time series of surface air temperature anomalies over the mid-Atlantic US in comparison to the control model simulation and to the sensitivity simulation with no US anthropogenic aerosol sources. Anomalies are relative to the 1951-1980 means in the observations and the control simulation and have been filtered by a 15-year moving average. Observed and simulated trends for different time periods are summarized in Table 5.1.

The observations show no significant warming between 1960 and 1979 ($+0.01 \pm 0.20^\circ\text{C decade}^{-1}$). Our control simulation, which incorporates US anthropogenic aerosols, reproduces this result ($-0.02 \pm 0.20^\circ\text{C decade}^{-1}$). The simulation without US anthropogenic

Table 5.1: Trends in surface air temperature ($^{\circ}\text{C decade}^{-1}$) in the mid-Atlantic US ^a

	1960 - 1979	1980 - 2010	2020 - 2050
Observations ^b	$+0.01 \pm 0.20^{\text{c}}$	$+0.21 \pm 0.18$	—
Model			
Control ^d	-0.02 ± 0.20	$+0.41 \pm 0.08$	$+0.29 \pm 0.07$
No US Anthropogenic Aerosols ^e	$+0.30 \pm 0.19$	$+0.30 \pm 0.10$	$+0.25 \pm 0.08$

^a Averages for the boxed region in Fig. 5.2^b Observations from the NASA GISS Surface Temperature Analysis (GISTEMP;
<http://data.giss.nasa.gov/gistemp/>)^c 95% confidence interval^d Control simulation including best estimates of greenhouse gas, aerosol, and natural radiative forcing^e Sensitivity simulation excluding US anthropogenic sources of SO₂, NO_x, black carbon (BC), and primary organic aerosol (POA)

aerosols, however, produces significant warming over the period ($+0.30 \pm 0.19^{\circ}\text{C decade}^{-1}$).

We conclude that the increasing abundance of US anthropogenic aerosols effectively offset greenhouse warming before 1980.

Anthropogenic aerosol sources in the US peaked in 1980 and declined afterward. Fig. 5.9 shows significant observed warming over the eastern US for the 1980-2009 period ($+0.21 \pm 0.20^{\circ}\text{C decade}^{-1}$), in contrast to the 1960-1979 period when aerosol concentrations were increasing. Our control simulation reproduces this result, with a warming rate of $+0.41 \pm 0.08^{\circ}\text{C decade}^{-1}$ for the 1980-2009 period. The sensitivity simulation without US anthropogenic aerosols shows slower warming ($+0.30 \pm 0.10^{\circ}\text{C decade}^{-1}$), which represents a continuation of the 1960-1979 trend due to greenhouse warming. The larger trend in the control simulation reflects the increasing trend of positive radiative forcing due to loss of the aerosol radiation shield. Beyond 2010 the rate of warming in the control simulation eases and eventually approaches that of the sensitivity simulation with no US anthropogenic aerosol sources.

5.5 Conclusions

Aerosol concentrations over the US peaked in the 1970-1990 period, have decreased rapidly since, and are projected to continue decreasing in the future as a result of air quality regulations to protect public health. We used a general circulation model (GISS GCM 3) in a 1950-2050 transient-climate simulation to study the regional climate response to this time-dependent regional aerosol radiative forcing. Our goal was to determine how aerosol trends have contributed to recent climate trends over the US and to examine the climate consequences of further US aerosol reductions in the future.

We computed aerosol trends over the 1950-2050 period by using the GEOS-Chem chemical transport model (CTM) applied to historical emission inventories (1950-2000) and to future emission projections from the IPCC A1B scenario. Historical trends were evaluated with wet deposition and aerosol concentration data over the US. This work was described in Chapter 4. Here we used the archived aerosol trends from GEOS-Chem to drive the transient-climate simulations in the GISS GCM 3. We conducted control simulations for 1950-2050 including our best estimates of greenhouse and aerosol radiative forcing, considering either the direct aerosol radiative forcing only or the combination of direct and indirect aerosol radiative forcings. Sensitivity simulations were conducted for both cases with US anthropogenic aerosol sources shut off. The climate response to US anthropogenic aerosol sources was diagnosed by difference between the control and sensitivity simulations. 5-member ensembles of simulations were conducted to test statistical significance.

We began by examining the climatic effects of US anthropogenic aerosol sources in 1970-1990, when these sources were at their peak. During that period, the direct and

indirect effects of US anthropogenic aerosols decreased top-of-atmosphere (TOA) radiation by up to 8 W m^{-2} over the eastern US (5 W m^{-2} from the direct effect alone). Surface radiation over the mid-Atlantic US (boxed region of Fig. 5.2) decreased by 2 W m^{-2} from 1950 to 1970 (dimming), remained flat from 1970 to 1990, and then increased by 4 W m^{-2} from 1990 to 2010 (brightening). These surface radiation trends in the model are qualitatively consistent with observed trends but much weaker. Considering that the model reproduces well the observed 1980-2010 aerosol trends in the US (Chapter 4), it appears that the observed dimming/brightening trends are much larger than can be explained from aerosols.

We find that US anthropogenic aerosols in 1970-1990 cooled the central and eastern US by $0.5\text{-}1.0^\circ\text{C}$ on an annual mean basis. Half of this cooling is from the direct aerosol radiative effect and half is from indirect effects. The cooling is strongest in summer and fall, and strongest during heat waves. Daily maximum temperatures on the hottest autumn days are lowered by 1.3°C . Our results are consistent with observations that show that the eastern US had a steady or cooling temperature trend from 1930 to 1980. This cooling anomaly in the observations has been reported previously as a warming hole (Pan et al., 2004; Kunkel et al., 2006). It has been attributed in these studies to sea surface temperature (SST) anomalies but we attribute it here to the effect of US anthropogenic aerosols.

We find that US anthropogenic aerosols generally slow down the hydrological cycle in the eastern US by reducing evaporation. This decreases precipitation along the east coast by up to 0.2 mm day^{-1} on an annual mean basis (0.4 mm day^{-1} in summer). However, the cooling of the western North Atlantic due to US anthropogenic aerosols also enhances the southerly flow of moist air from the Gulf of Mexico which increases cloud cover, precipitation, and soil moisture in the central US. The increase in cloud cover over the central

US magnifies in turn the aerosol cooling effect. This hydrological contribution to the central US warming hole has been previously identified from observations by Robinson et al. (2002) and Pan et al. (2004), and we show that it is consistent with the expected effect of US anthropogenic aerosols.

We went on to examine the effect of changing US anthropogenic aerosol sources on US surface air temperatures over the 1950-2050 period, comparing to observed trends over the mid-Atlantic US where the aerosol radiative effect is strongest. Without US anthropogenic aerosol sources, we find in the model a relatively constant rate of warming over the 1950-2050 period, driven by increasing greenhouse gases. In contrast, the observations show no warming trend from 1950 to 1980, followed by very rapid warming from 1980 to present. We show that this pattern can be explained by US anthropogenic aerosol sources. The lack of warming from 1950 to 1980 reflects an increasing US aerosol loading, offsetting the warming from greenhouse gases. As the aerosol sources level off in 1980 and then decrease, warming takes over and accelerates due to the loss of the aerosol cooling shield. We thus find that the observed warming from 1990 to 2010 is significantly greater than would have been expected from greenhouse gases alone. We project that future reductions in US aerosol sources will increase warming over the mid-Atlantic US by 0.1°C . However, we find that most of the warming due to reducing US aerosol sources for air quality objectives has in fact already been realized (0.35°C over the mid-Atlantic US in 1980-2010).

Our results have several implications for US air quality policy. We find that reductions in aerosol sources to improve air quality have elicited a strong regional warming response over the past 20 years. However, we also find that future aerosol reductions should have little climate impact because sources are already low. It has been suggested that future black carbon (BC) emission controls could provide relief from future warming (Bond, 2007;

Grieshop et al., 2009; Penner et al., 2010), but we find that BC sources in the US are too small for their climatic impact to be significant.

Although our results are specific to the US, they also warn of possibly strong regional warming over East Asia in the coming decades as China embarks on vigorous emission controls to address its pressing aerosol pollution problem. Climate response to anthropogenic aerosols in East Asia may be very different from the US because of the greater contribution of BC to the aerosol mix and because of specific meteorological features such as the monsoon. Application of our approach to that region would be of considerable interest.

Bibliography

- Adams, P. and Seinfeld, J. (2002). Predicting global aerosol size distributions in general circulation models. *J Geophys Res-Atmos*, 107(D19):4370.
- Andreae, M., Jones, C., and Cox, P. (2005). Strong present-day aerosol cooling implies a hot future. *Nature*, 435(7046):1187–1190.
- Bey, I., Jacob, D., Yantosca, R., Logan, J., Field, B., Fiore, A., Li, Q., Liu, H., Mickley, L., and Schultz, M. (2001). Global modeling of tropospheric chemistry with assimilated meteorology: Model description and evaluation. *J Geophys Res-Atmos*, 106(D19):23073–23095.
- Bond, T. C. (2007). Can warming particles enter global climate discussions? *Environ Res Lett*, 2(4):045030.
- Bond, T. C., Bhardwaj, E., Dong, R., Jogani, R., Jung, S., Roden, C., Streets, D. G., and Trautmann, N. M. (2007). Historical emissions of black and organic carbon aerosol from energy-related combustion, 1850–2000. *Global Biogeochem Cy*, 21(2):1–16.
- Bouwman, A., Lee, D., Asman, W., Dentener, F., Van Der Hoek, K., and Olivier, J. (1997). A global high-resolution emission inventory for ammonia. *Global Biogeochem Cy*, 11(4):561–587.
- Brasseur, G. and Roeckner, E. (2005). Impact of improved air quality on the future evolution of climate. *Geophys Res Lett*, 32(23):L23704.

- Chang, W., Liao, H., and Wang, H. (2009). Climate responses to direct radiative forcing of anthropogenic aerosols, tropospheric ozone, and long-lived greenhouse gases in eastern China over 1951–2000. *Adv Atmos Sci*, 26(4):748–762.
- Chen, W.-T., Nenes, A., Liao, H., Adams, P. J., Li, J.-L. F., and Seinfeld, J. H. (2010). Global climate response to anthropogenic aerosol indirect effects: Present day and year 2100. *J Geophys Res-Atmos*, 115(D12):D12207.
- Chin, M., Rood, R., Lin, S., Muller, J., and Thompson, A. (2000). Atmospheric sulfur cycle simulated in the global model GOCART: Model description and global properties. *J Geophys Res-Atmos*, 105(D20):24671–24687.
- Chung, S. and Seinfeld, J. (2002). Global distribution and climate forcing of carbonaceous aerosols. *J Geophys Res-Atmos*, 107(D19):4407.
- Del Genio, A., Yao, M., Kovari, W., and Lo, K. (1996). A prognostic cloud water parameterization for global climate models. *J Climate*, 9(2):270–304.
- Duncan, B., Martin, R., Staudt, A., Yevich, R., and Logan, J. (2003). Interannual and seasonal variability of biomass burning emissions constrained by satellite observations. *J Geophys Res-Atmos*, 108(D2):4100.
- Fiore, A. M., Jacob, D. J., Field, B. D., Streets, D. G., Fernandes, S. D., and Jang, C. (2002). Linking global to regional models to assess future climate impacts on surface ozone levels in the United States. *Geophy Res Lett*, 29(19):1919.
- Fischer-Brunns, I., Banse, D. F., and Feichter, J. (2009). Future impact of anthropogenic sulfate aerosol on North Atlantic climate. *Clim Dynam*, 32(4):511–524.
- Fischer-Brunns, I., Feichter, J., Kloster, S., and Schneidereit, A. (2010). How present aerosol pollution from North America impacts North Atlantic climate. *Tellus A*, pages 1–11.
- Fountoukis, C. and Nenes, A. (2005). Continued development of a cloud droplet formation parameterization for global climate models. *J Geophys Res-Atmos*, 110(D11):D11212.
- Grieshop, A. P., Reynolds, C. C. O., Kandlikar, M., and Dowlatabadi, H. (2009). A black-carbon mitigation wedge. *Nat Geosci*, 2:533–534.
- Hansen, J., Fung, I., Lacis, A., Rind, D., Lebedeff, S., Ruedy, R., Russell, G., and Stone, P. (1988). Global climate changes as forecast by Goddard Institute for Space Studies 3-dimensional model. *J Geophys Res-Atmos*, 93(D8):9341–9364.
- Hansen, J., Ruedy, R., Sato, M., Imhoff, M., Lawrence, W., Easterling, D., Peterson, T., and Karl, T. (2001). A closer look at United States and global surface temperature change. *J Geophys Res-Atmos*, 106(D20):23,947–23,963.

- Hansen, J., Sato, M., Nazarenko, L., Ruedy, R., Lacis, A., Koch, D., Tegen, I., Hall, T., Shindell, D., Santer, B., Stone, P., Novakov, T., Thomason, L., Wang, R., Wang, Y., Jacob, D., Hollandsworth, S., Bishop, L., Logan, J., Thompson, A., Stolarski, R., Lean, J., Willson, R., Levitus, S., Antonov, J., Rayner, N., Parker, D., and Christy, J. (2002). Climate forcings in Goddard Institute for Space Studies SI2000 simulations. *J Geophys Res-Atmos*, 107(D18):37.
- Hegerl, G. C., Zwiers, F. W., Braconnot, P., Gillett, N. P., Luo, Y., Orsini, J. A. M., Nicholls, N., Penner, J. E., and Stott, P. A. (2007). *Climate Change 2007: The Physical Science Basis*, chapter Understanding and Attributing Climate Change. Cambridge University Press.
- Hoose, C., Lohmann, U., Bennartz, R., Croft, B., and Lesins, G. (2008). Global simulations of aerosol processing in clouds. *Atmos Chem Phys*, 8(23):6939–6963.
- Jacobson, M. Z. (2008). Short-term effects of agriculture on air pollution and climate in California. *J Geophys Res-Atmos*, 113:D23101.
- Jones, A., Haywood, J. M., and Boucher, O. (2007). Aerosol forcing, climate response, and climate sensitivity in the Hadley Centre climate model. *J Geophys Res-Atmos*, 112(D20):D20211.
- Khairoutdinov, M. and Kogan, Y. (2000). A new cloud physics parameterization in a large-eddy simulation model of marine stratocumulus. *Mon Weather Rev*, 128(1):229–243.
- Kloster, S., Dentener, F., Feichter, J., Raes, F., Lohmann, U., Roeckner, E., and Fischer-Brunn, I. (2009). A GCM study of future climate response to aerosol pollution reductions. *Clim Dyn*, 34:1177–1194.
- Kunkel, K. E., Liang, X.-Z., Zhu, J., and Lin, Y. (2006). Can CGCMs simulate the twentieth-century “warming hole” in the central United States? *J Climate*, 19(17):4137–4153.
- Lee, W.-S. and Kim, M.-K. (2010). Effects of radiative forcing by black carbon aerosol on spring rainfall decrease over Southeast Asia. *Atmos Environ*, 44:3739–3744.
- Leibensperger, E. M., Mickley, L. J., and Jacob, D. J. (2008). Sensitivity of US air quality to mid-latitude cyclone frequency and implications of 1980-2006 climate change. *Atmos Chem Phys*, 8:12.
- Levy, H., Schwarzkopf, M. D., Horowitz, L., Ramaswamy, V., and Findell, K. L. (2008). Strong sensitivity of late 21st century climate to projected changes in short-lived air pollutants. *J Geophys Res-Atmos*, 113(D6):D06102.
- Liao, H., Henze, D. K., Seinfeld, J. H., Wu, S., and Mickley, L. J. (2007). Biogenic secondary organic aerosol over the United States: Comparison of climatological simulations with observations. *J Geophys Res-Atmos*, 112(D06):D06201.

- Liao, H., Seinfeld, J., Adams, P., and Mickley, L. (2004). Global radiative forcing of coupled tropospheric ozone and aerosols in a unified general circulation model. *J Geophys Res-Atmos*, 109(D16):D16207.
- Liepert, B. and Tegen, I. (2002). Multidecadal solar radiation trends in the United States and Germany and direct tropospheric aerosol forcing. *J Geophys Res-Atmos*, 107(D12):4153.
- Liu, B., Xu, M., Henderson, M., and Gong, W. (2004a). A spatial analysis of pan evaporation trends in China, 1955-2000. *J Geophys Res-Atmos*, 109(D15):D15102.
- Liu, B., Xu, M., Henderson, M., Qi, Y., and Li, Y. (2004b). Taking China's temperature: Daily range, warming trends, and regional variations, 1955-2000. *J Climate*, 17(22):4453–4462.
- Long, C. N., Dutton, E. G., Augustine, J. A., Wiscombe, W., Wild, M., Mcfarlane, S. A., and Flynn, C. J. (2009). Significant decadal brightening of downwelling shortwave in the continental United States. *J Geophys Res-Atmos*, 114:1–20.
- Makowski, K., Jaeger, E. B., Chiacchio, M., Wild, M., Ewen, T., and Ohmura, A. (2009). On the relationship between diurnal temperature range and surface solar radiation in Europe. *J Geophys Res-Atmos*, 114:D00D07.
- Martin, G. M., Johnson, D. W., and Spice, A. (1994). The measurement and parameterization of effective radius of droplets in warm stratocumulus clouds. *J Atmos Sci*, 51(1823–1842).
- Menon, S., Hansen, J., Nazarenko, L., and Luo, Y. (2002). Climate effects of black carbon aerosols in China and India. *Science*, 297(5590):2250–2253.
- Mickley, L. J., Leibensperger, E. M., Jacob, D. J., and Rind, D. (submitted). Regional warming from aerosol removal over the United States: Results from a transient 2010–2050 climate simulation. *Atmos Environ*.
- Mitchell, J., Davis, R., Ingram, W., and Senior, C. (1995). On surface temperature, greenhouse gases, and aerosols: Models and observations. *J Climate*, 8(10):2364–2386.
- Nakićenović, N. and Swart, R. (2000). *Special Report on Emissions Scenarios: A Special Report of Working Group III of the Intergovernmental Panel on Climate Change*. Cambridge University Press.
- Nenes, A. and Seinfeld, J. H. (2003). Parameterization of cloud droplet formation in global climate models. *J Geophys Res-Atmos*, 108(D14):4415.
- Olivier, J. G. J. and Berdowski, J. J. M. (2001). *The Climate System*, chapter Global Emissions Sources and Sinks. A. A. Balkema Publishers/Swets and Zeitlinger Publishers, Lisse, Netherlands.

- Pan, Z. T., Arritt, R. W., Takle, E. S., Gutowski, W. J., Anderson, C. J., and Segal, M. (2004). Altered hydrologic feedback in a warming climate introduces a “warming hole”. *Geophys Res Lett*, 31(17):L17109.
- Park, R., Jacob, D., Field, B., Yantosca, R., and Chin, M. (2004). Natural and transboundary pollution influences on sulfate-nitrate-ammonium aerosols in the United States: Implications for policy. *J Geophys Res-Atmos*, 109:D15204.
- Park, R., Jacob, D., Kumar, N., and Yantosca, R. (2006). Regional visibility statistics in the United States: Natural and transboundary pollution influences, and implications for the Regional Haze Rule. *Atmos Environ*, 40(28):5405–5423.
- Penner, J. E., Prather, M. J., Isaksen, I. S. A., Fugelstvedt, J. S., Klimont, Z., and Stevenson, D. (2010). Short-lived uncertainty? *Nat Geosci*, 3:587–588.
- Peterson, T., Golubev, V. S., and Groisman, P. Y. (1995). Evaporation losing its strength. *Nature*, 377(6551):687–688.
- Philipona, R., Behrens, K., and Ruckstuhl, C. (2009). How declining aerosols and rising greenhouse gases forced rapid warming in Europe since the 1980s. *Geophys Res Lett*, 36(2):5.
- Pierce, J. and Adams, P. (2006). Global evaluation of CCN formation by direct emission of sea salt and growth of ultrafine sea salt. *J Geophys Res-Atmos*, 111(D6):D06203.
- Pye, H. O. T., Liao, H., Wu, S., Mickley, L. J., Jacob, D. J., Henze, D. K., and Seinfeld, J. H. (2009). Effect of changes in climate and emissions on future sulfate-nitrate-ammonium aerosol levels in the United States. *J Geophys Res-Atmos*, 114(D1):18.
- Qian, Y. and Giorgi, F. (2000). Regional climatic effects of anthropogenic aerosols? The case of Southwestern China. *Geophys Res Lett*, 27(21):3521–3524.
- Raes, F. and Seinfeld, J. H. (2009). New directions: Climate change and air pollution abatement: A bumpy road. *Atmos Environ*, 43(32):5132–5133.
- Rayner, N., Parker, D., Horton, E., Folland, C., Alexander, L., Rowell, D., Kent, E., and Kaplan, A. (2003). Global analyses of sea surface temperature, sea ice, and night marine air temperature since the late nineteenth century. *J Geophys Res-Atmos*, 108(D14):4407.
- Rind, D., Jonas, J., Stammerjohn, S., and Lonergan, P. (2009a). The Antarctic ozone hole and the Northern Annular Mode: A stratospheric interhemispheric connection. *Geophys Res Lett*, 36(9):1–5.
- Rind, D., Lean, J., Lerner, J., Lonergan, P., and Leboissitier, A. (2008). Exploring the stratospheric/tropospheric response to solar forcing. *J Geophys Res-Atmos*, 113:D24103.

- Rind, D., Lerner, J., Jonas, J., and McLinden, C. (2007). Effects of resolution and model physics on tracer transports in the NASA Goddard Institute for Space Studies general circulation models. *J Geophys Res-Atmos*, 112(D9):D09315.
- Rind, D., Lerner, J., McLinden, C., and Perlitz, J. (2009b). Stratospheric ozone during the Last Glacial Maximum. *Geophys Res Lett*, 36(9):1–5.
- Robinson, W. A., Ruedy, R., and Hansen, J. E. (2002). General circulation model simulations of recent cooling in the east-central United States. *J Geophys Res-Atmos*, 107(D25):4748.
- Robock, A., Mu, M., Vinnikov, K., Trofimova, I., and Adamenko, T. (2005). Forty-five years of observed soil moisture in the Ukraine: No summer desiccation (yet). *Geophys Res Lett*, 32(3):L03401.
- Roderick, M. L., Rotstayn, L. D., Farquhar, G. D., and Hobbins, M. T. (2007). On the attribution of changing pan evaporation. *Geophys Res Lett*, 34(17):L17403.
- Ruckstuhl, C., Philipona, R., Behrens, K., Collaud Coen, M., Dürr, B., Heimo, A., Mätzler, C., Nyeki, S., Ohmura, A., Vuilleumier, L., Weller, M., Wehrli, C., and Zelenka, A. (2008). Aerosol and cloud effects on solar brightening and the recent rapid warming. *Geophys Res Lett*, 35(12):6.
- Schmidt, G., Ruedy, R., Hansen, J., Aleinov, I., Bell, N., Bauer, M., Bauer, S., Cairns, B., Canuto, V., Cheng, Y., Del Genio, A., Faluvegi, G., Friend, A., Hall, T., Hu, Y., Kelley, M., Kiang, N., Koch, D., Lacis, A., Lerner, J., Lo, K., Miller, R., Nazarenko, L., Oinas, V., Perlitz, J., Perlitz, J., Rind, D., Romanou, A., Russell, G., Sato, M., Shindell, D., Stone, P., Sun, S., Tausnev, N., Thresher, D., and Yao, M. (2006). Present-day atmospheric simulations using GISS ModelE: Comparison to in situ, satellite, and reanalysis data. *J Climate*, 19(2):153–192.
- Schulz, M., Textor, C., Kinne, S., Balkanski, Y., Bauer, S., Berntsen, T., Berglen, T., Boucher, O., Dentener, F., and Guibert, S. (2006). Radiative forcing by aerosols as derived from the AeroCom present-day and pre-industrial simulations. *Atmos Chem Phys*, 6(12):5225–5246.
- Shindell, D. T., Faluvegi, G., Bauer, S. E., Koch, D. M., Unger, N., Menon, S., Miller, R. L., Schmidt, G. A., and Streets, D. G. (2007). Climate response to projected changes in short-lived species under an A1B scenario from 2000–2050 in the GISS climate model. *J Geophys Res-Atmos*, 112(D20):D20103.
- Shindell, D. T., Levy, H., Schwarzkopf, M. D., Horowitz, L. W., Lamarque, J.-F., and Faluvegi, G. (2008). Multimodel projections of climate change from short-lived emissions due to human activities. *J Geophys Res-Atmos*, 113(D11):18.

- Streets, D., Bond, T., Carmichael, G., Fernandes, S., Fu, Q., He, D., Klimont, Z., Nelson, S., Tsai, N., Wang, M., Woo, J., and Yarber, K. (2003). An inventory of gaseous and primary aerosol emissions in Asia in the year 2000. *J Geophys Res-Atmos*, 108(D21):8809.
- Streets, D., Bond, T., Lee, T., and Jang, C. (2004). On the future of carbonaceous aerosol emissions. *J Geophys Res-Atmos*, 109(D24):D24212.
- Streets, D. G., Yan, F., Chin, M., Diehl, T., Mahowald, N., Schultz, M., Wild, M., Wu, Y., and Yu, C. (2009). Anthropogenic and natural contributions to regional trends in aerosol optical depth, 1980–2006. *J Geophys Res-Atmos*, 114:D00D18.
- Sun, S. and Hansen, J. E. (2003). Climate simulations for 1951–2050 with a coupled atmosphere-ocean model. *J Climate*, 16(17):2807–2826.
- Trenberth, K. E., Jones, P. D., Ambenje, P., Bojariu, R., Easterling, D., Tank, A. K., Parker, D., Rahimzadeh, F., Renwick, J. A., Rusticucci, M., Soden, B., and Zhai, P. (2007). *Climate Change 2007: The Physical Science Basis*, chapter Observations: Surface and Atmospheric Climate Change. Cambridge University Press.
- US Environmental Protection Agency (2010). *Our Nation's Air - Status and Trends Through 2008*. Washington, DC.
- van Aardenne, J., Dentener, F., and Olivier, J. (2001). A $1^\circ \times 1^\circ$ resolution data set of historical anthropogenic trace gas emissions for the period 1890–1990. *Global Biogeochem Cy*, 15(4):909–928.
- Wang, C., Kim, D., Ekman, A. M. L., Barth, M. C., and Rasch, P. J. (2009a). Impact of anthropogenic aerosols on Indian summer monsoon. *Geophys Res Lett*, 36:L21704.
- Wang, M., Penner, J. E., and Liu, X. (2009b). Coupled IMPACT aerosol and NCAR CAM3 model: Evaluation of predicted aerosol number and size distribution. *J Geophys Res-Atmos*, 114(D6):1–30.
- Wang, Y., Jacob, D., and Logan, J. (1998). Global simulation of tropospheric O₃-NO_x-hydrocarbon chemistry 1. Model formulation. *J Geophys Res-Atmos*, 103(D9):10713–10725.
- Wild, M. (2009a). Global dimming and brightening: A review. *J Geophys Res-Atmos*, 114:1–31.
- Wild, M. (2009b). How well do IPCC-AR4/CMIP3 climate models simulate global dimming/brightening and twentieth-century daytime and nighttime warming? *J Geophys Res-Atmos*, 114:D00D11.
- Wild, M., Ohmura, A., and Makowski, K. (2007). Impact of global dimming and brightening on global warming. *Geophys Res Lett*, 34(4):L04702.

- Wu, S., Mickley, L. J., Leibensperger, E. M., Jacob, D. J., Rind, D., and Streets, D. G. (2008). Effects of 2000-2050 global change on ozone air quality in the United States. *J Geophys Res-Atmos*, 113(D6):D06302.
- Zhang, Y., Sun, S., Olsen, S. C., Dubey, M. K., and He, J. (2009). CCSM3 simulated regional effects of anthropogenic aerosols for two contrasting scenarios: Rising Asian emissions and global reduction of aerosols. *Int. J. Climatol.*
- Zwiers, F. and von Storch, H. (1995). Taking serial correlation into account in tests of the mean. *J Climate*, 8(2):336–351.